Modelling Silver Transport

in

Spherical HTR Fuel

by

Jacobus Johannes van der Merwe

Submitted in partial fulfilment of the requirements for the degree

Doctor of Philosophy

in the Faculty of Natural & Agricultural Science

University of Pretoria

Pretoria

February 2009

Abstract

For direct cycle gas cooled high temperature reactor designs, operating conditions may be limited as a result of excessive maintenance dose rates caused by the ^{110m}Ag source term on the turbine. The accurate prediction of silver fission and activation products' release during normal operation is required to ensure regulatory compliance and economic viability of planned power plants. Fuel qualification programs should provide satisfactory results to ensure correct analyses, but will however not be available for many years. In the meantime data from the German fuel development program may be utilized. Traditionally diffusion models were used to derive transport parameters from limited irradiation testing of fuel materials and components. Best estimates for all applicable German fuel irradiation tests with defendable uncertainty ranges were never derived. However, diffusion theory and current parameters cannot account for all irradiation and heat-up test results, and for some tests, it appears unacceptably conservative. Other transport mechanisms have been suggested and alternative calculation models are being considered. In this thesis the relevant German material and irradiation tests were evaluated with the current PBMR metallic fission product release calculation model. Transport through all the fuel materials and components and from the sphere to the coolant gas was considered and best possible models and parameters were suggested. For the transport of silver through the SiC layer an alternative suggested model called the Molecular Vapour Transport Release (MVR) Model was evaluated against the traditional diffusion model. From this evaluation it was shown that classical diffusion modelling was still a viable model to predict silver transport in SiC. The MVR model was found to be a feasible model as well. However, due to the much larger verification and validation effort required, it was decided to use the diffusion model until such time that experimental results become available that might elucidate the exact physical transport model. The evaluation also showed that the diffusion model used must be quantified in a detailed evaluation of all applicable irradiation tests. A study of all German irradiation tests was previously performed and the applicable irradiation tests were identified. A detailed evaluation of these irradiation tests were performed with an updated diffusion model. New transport and material parameters were derived in this detailed evaluation and compared with existing values. An evaluation of some heat-up tests of irradiated fuel spheres was performed to assess the range for which the newly derived transport parameters are valid. The different models with their old and newly derived parameters were used to analyse sample PBMR cores. Recommendations were made to the suitability of the different models and parameters for future PBMR silver fission and activation product analyses.

Table of Contents

List of Figures

List of Tables

List of Acronyms and Terms

This list contains the abbreviations used in this document.

Abbreviation or Acronym	Definition
atm	atmosphere
AVR	Arbeitsgemeinschaft Versuchsreaktor
CP	Coated Particle
CVD	Chemical Vapour Deposition
DLOFC	Depressurized Loss of Forced Cooling
EFPD	Equivalent Full-power Days
FE	Fuel Element
FIMA	Fissions per Initial Metal Atoms
FIPREX	Fission Products Release under Extraordinary conditions
FZJ	Forschungszentrum Jülich GmbH
GA	General Atomics
GETTER	Software used to model fission product transport in spherical fuel
HBK	Hochtemperaturreaktor-Brennstoff-Kreislauf
HEU	Highly Enriched Uranium
HFR	High Flux Reactor
HRB	Hochtemperatur Reaktorbau
HTA	Hochtemperatur Anlage
HTR	High Temperature Reactor
HTR-Modul	High Temperature Reactor - Modular design
IAEA	International Atomic Energy Agency

Abbreviation or Acronym	Definition
IMGA	Irradiated Microsphere Gamma Analyzer
J	joule
K	kelvin
KFA	Kernforschungsanlage (Jülich)
KORA	Corrosion Apparatus
KÜFA	Cold finger apparatus
LEU	Low-enriched Uranium
LOFC	Loss of Forced Coolant
MCNP	Monte Carlo N-particle Transport Code
MPS	Main Power System
MVR	Molecular Vapour Transport Release
n/a	not applicable
NEA	Nuclear Engineering Analysis
NGNP	Next Generation Nuclear Plant
NTF	Nano-tube Failure
PBMR	Pebble Bed Modular Reactor
Pa	pascal
PIE	Post-irradiation Examination
ppm	parts per million
PyC	Pyrolytic Carbon or Pyrocarbon
R/B	Release-to-Birth
RDFM	Reactor Design and Fuel Management
SI	International System of Units
SiC	Silicon Carbide

Abbreviation or Acronym	Definition
SPN	Self-powered Neutron (detector)
TPD	Temperature Programmed Desorption
TRISO	Triple Coated Isotropic
V&V	Verification and Validation
VSOP	Very Superior Old Program

Acknowledgements

This work is dedicated to Dr Johan Venter, who has accepted the role as a father rather than a mentor to me at PBMR.

I also wish to extend my deepest gratitude to the following people:

- Jeetesh Keshaw who has been my friend rather than a colleague, who supported this work through many contributions.
- Dr Dirk Olivier who's interest in the problem and first evaluation of the problem has inspired me to do this work. His collaboration was essential to the success of this thesis.
- Coenie Stoker who has been a leader rather than a manager who had the patience to allow me to do this work.
- My German friends: Dr Heinz Nabielek who raised the silver source term originally and who was always ready to provide advice. Dr Karl Verfondern with his exceptional knowledge of fission product transport who always offered valuable advice. Prof Heiko Barnert who has provided invaluable support in obtaining all the German literature.
- Prof Johan Malherbe, my study leader for his willingness to undertake this study, and all his support and encouragement to write a scientifically correct thesis.
- Dr Johan Slabber, for allowing PBMR technology to be used for this thesis.

1. Introduction

For direct-cycle high-temperature reactors (HTRs) utilizing low-enriched uranium fuel, the production, release, transport and subsequent deposition of silver fission and activation products in the Main Power System (MPS) may pose maintenance problems due to excessive radiation levels to operating personnel [1]. For higher operating temperature designs, ^{110m}Ag release from fuel and deposition on high-maintenance MPS components may lead to more expensive maintenance concepts or limit planned power and outlet temperature. Accurate analyses of silver release from fuel under all expected normal operating conditions is therefore of paramount importance. Erroneous prediction of the silver source term or unnecessary uncertainties used in analyses could have serious implications for the economic case of a planned power plant. It is therefore critical that the best possible calculation model is derived from the available information.

In deriving a new, or evaluating an existing calculation model, it is important to understand the exact fuel design, fission product production, and transport through fuel materials. This could be done by considering HTR fuel sphere design, current transport models suggested, and evaluations against all available transport data. Since PBMR fuel is manufactured to be German-equivalent, PBMR may utilize German fuel programme irradiation tests as part of its fuel qualification programme to verify and validate fission product release models and parameters for its preliminary licence applications.

Historically, fission product transport through fuel materials has been considered to obey Fick's laws of diffusion through all fuel materials [2]. For silver, the limiting transport process was found to be through the SiC layer as the other fuel materials offer much less retention at reactor operating temperatures. Although it was found that SiC does not retain silver completely, it does slow down silver transport substantially [3]. Once transport behaviours through all materials have been quantified, further study was devoted to transport of silver through the SiC layer. It has been never shown that silver migrates through SiC by diffusion, but it has been assumed that the transport mechanism responsible could be approximated by a diffusion model. Various experimental studies resulted in different diffusion coefficients for silver in SiC (e.g. [1], [3] and [4]).

Due to a perceived independence on temperature, the diffusion model for silver transport through SiC has been questioned [5]. Further work led to a suggestion that silver is not transported through SiC by diffusion but by a vapour transport mechanism [6]. Although this model was questioned since it is primarily based on an absence of diffusion evidence [7], rather than on evidence of vapour transport; it does provide an alternative solution to

modelling the transport of silver in SiC. A calculation model and software were developed to perform silver release analyses from spherical fuel based on vapour transport [8]. The transport parameters required for vapour transport were derived from a first estimate evaluation of a limited set of German fuel irradiation data.

The exact transport mechanism of silver through SiC has not been resolved after 20 years of research during the German fuel development programme and now, after yet another 20 years, it is still not resolved. Other fuel qualification and characterization programmes are underway all over the world. However, it is unlikely that a solution to this problem will be found soon. In the meantime, accurate and defendable analyses of a typical PBMR core's ^{110m}Ag source term are required. This evaluation does not attempt to find the exact mechanism of silver transport, but to derive and defend a calculation model to predict the ^{110m}Ag source term under operating conditions, irrespective of the actual transport mechanisms.

1.1 Fuel Design

One of the fundamental safety requirements of modern HTRs is the ability of fuel spheres to retain fission and activation radionuclides within the fuel spheres under all expected reactor conditions. The reactor design must therefore ensure that fuel elements are never exposed to conditions in excess of their design qualification. Similarly, fuel design must make it possible for fuel elements to be manufactured economically in large volumes, while maintaining fuel quality and integrity during manufacture and subsequent irradiation.

The primary containment barrier is the Triple Coated Isotropic (TRISO) coated particle, which proved to be effective during various irradiation tests and experiments. Fission products formed in the fuel kernel either form stable oxides with oxygen released during the fission process, or have very long diffusion times through coating layers of the particle. The TRISO coated particles therefore retain fission products very effectively inside the fuel during normal operation.

Exceptions are silver and strontium fission and activation products, which do not form stable oxides at operating temperatures and have relatively fast diffusion times through coated particle layers. Fortunately, strontium has a very high sorption isotherm from graphite and is also delayed by the binder used in matrix material manufacture that significantly delays strontium release. Silver, on the other hand, has no such delaying mechanisms and is readily released from spherical fuel spheres at elevated temperatures.

Modern HTR fuel sphere design is shown in Figure 1. The design is based on the German fuel sphere design produced for the High-Temperature Reactor 500 (HTR-500) and HTR-Modul Proof Tests. This fuel type is generally regarded as state-of-the-art for German pebble fuel production [9]. It is designed for optimal performance under normal operating conditions and to withstand all design base accident conditions [10].

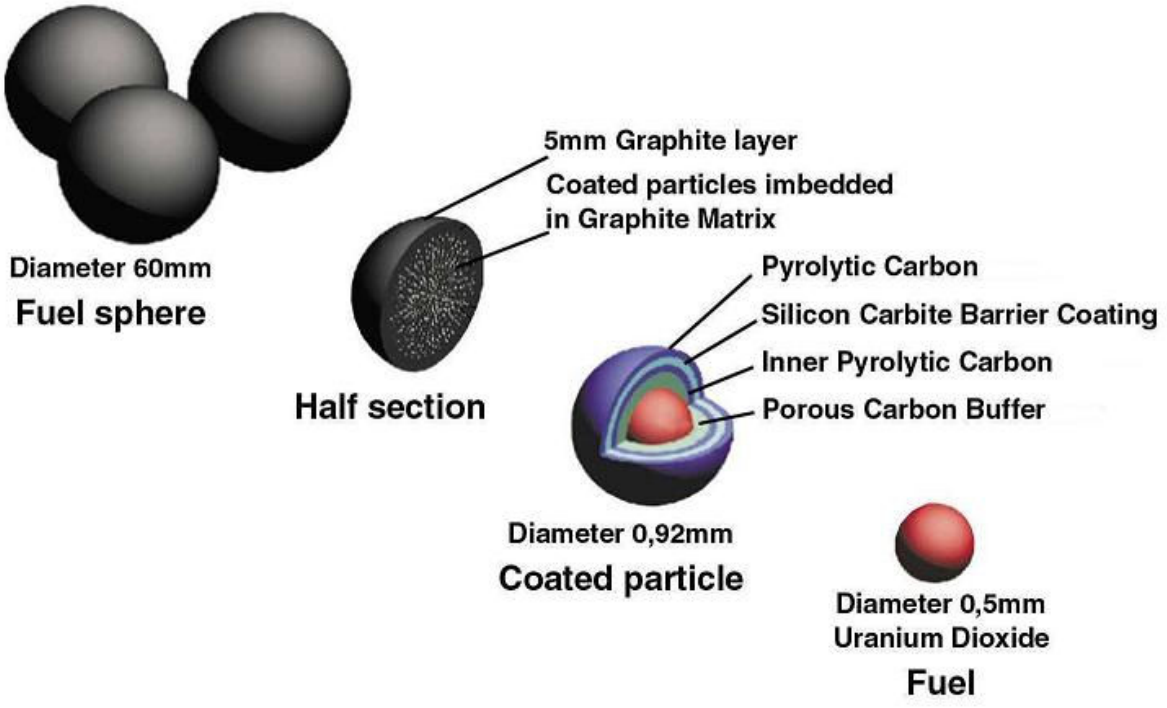

Figure 1: Fuel Element Design

Fuel spheres are manufactured from graphite matrix material (A3-3), in which TRISO coated particles are imbedded. The outer 5 mm layer contains no particles and is made up of matrix material only. The outer fuel-free zone protects the coated particles from damage from outside direct mechanical effects such as abrasion and shock. It further acts as a barrier layer against chemical corrosion in the case of water or air ingress in the core. The graphite matrix material functions as a good heat transfer medium and stabilizes the coated particles in the sphere. Good thermal contact is achieved between coated particles and matrix material, so that low temperature gradients occur in the fuel sphere.

The TRISO particle consists of a spherical UO_2-kernel, 500 micron in diameter, surrounded by four coating layers. UO_2 has a high melting point, therefore retaining its integrity under all reactor conditions. Oxygen released during fission binds with fission products to form immobile oxides. The majority of fission products are retained in the coated particle in this way. The kernel produces almost all the power of the reactor through nuclear fission. It acts as a retention barrier for gaseous fission products, thereby reducing internal pressure of the coated particle. Fission products that do not form stable oxides are released from the kernel through a diffusion process. All fission products are therefore retained or have their release reduced by the UO_2 kernel.

The kernel is surrounded by a 95-micron low-density pyrolitic carbon (PyC) layer, known as the buffer layer. This layer acts as a sacrificial layer, allowing the kernel to swell under irradiation, and providing void volume for fission gases released from the kernel. The rest of the layers are therefore protected from recoiling fission products and excessive internal pressure by the buffer layer.

The next layer is made up of dense pyrocarbon, 40 micron thick and known as the inner PyC layer. It forms an impenetrable barrier to gaseous fission products, and slows down the transport of metallic fission products to the SiC layer. During manufacture it provides a surface for the SiC to adhere to, and protects the kernel from chlorine in the form of hydrochloric acid during SiC deposition.

The SiC layer is the primary fission product barrier, being 35 micron thick. It retains all gaseous and metallic fission products to a very high extent, with the exception of silver and strontium. It provides the structural support required to contain internal gas pressure in the coated particle.

The final layer is again made of dense pyrocarbon, 40 micron thick and known as the outer PyC layer. It is under compressive stress, putting positive pressure on the SiC, helping to contain internal gas pressures. It protects the SiC layer during manufacture from chemical and mechanical damage.

To prevent coated particles from touching each other in the matrix material, which may lead to failures during the pressing stage, each coated particle is over-coated with a layer of matrix material graphite before being mixed with the bulk matrix material. Fuel spheres are pressed and machined to form perfect spheres, 60 mm in diameter.

1.2 Silver Fission and Activation Products

The main silver fission products are stable ^{109}Ag that activates to ^{110m}Ag (250 days half-life) and ^{111}Ag (7.45 days half-life). As can be seen from Figure 2, both are low-yield fission products, with cumulative fission yields from uranium of only 0.028% and 0.017% for ^{109}Ag and ^{111}Ag, respectively. For plutonium this picture changes drastically and fission yields of 1.4% and 0.30% are achieved for the two nuclides respectively. Silver release is therefore a bigger concern for high burn-up fuel where plutonium fission forms a significant fraction of the power produced in the plant. For the current PBMR design, equilibrium plutonium power fractions are in the order of 32%. For end-of-life fuel about 65% of fission power comes from plutonium fissions.

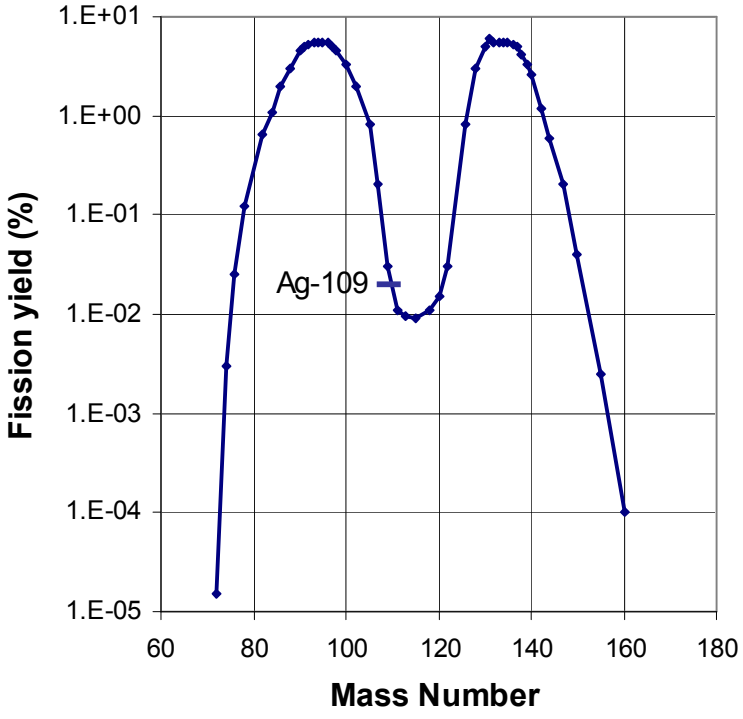

Figure 2: Thermal Neutron Fission Product Yields for ^{235}U

^{111}Ag has a relatively short half-life of only 7.45 days, and as such is only of importance during accident events. ^{109}Ag is a stable isotope, and in itself presents no danger. ^{109}Ag, however, has a large neutron capture cross section, and is activated in a neutron field to form ^{110m}Ag. Approximately 1% of the ^{109}Ag inventory is activated to ^{110m}Ag at the end of life of a fuel sphere. This includes corrections for decay and neutron capture. ^{110m}Ag is a strong γ-emitting activation product that presents a considerable radiation danger in large quantities if not shielded. With a half-life of 250 days it is released during normal operation as well as during accident events.

Most postulated accident events are dominated by ^{131}I, ^{133}I and ^{137}Cs, and to a lesser extent, ^{111}Ag and ^{90}Sr so that ^{110m}Ag is not a major contributor to public dose rates for postulated accident conditions. The main concern therefore is the production and release of ^{110m}Ag from spherical fuel elements in the reactor, and its subsequent deposition in cooler regions of the MPS, the turbine and recuperator in particular, during normal operation. Evaluation of tests and experiments conducted under conditions similar to PBMR normal operating conditions will therefore take precedence in evaluating silver release models and parameters.

1.3 Fission Production Sources

There are three distinct sources of fission products in fuel spheres:

- uranium and thorium contamination of the fuel materials;
- defective and failed coated particles; and
- intact TRISO coated particles.

These three sources and the phenomena that influence them are described below. Relative contributions to the total silver source term are based on calculations performed by a diffusion type calculation model and latest parameters suggested in the literature [2]. A fourth source also exists that is important only for activation products: The natural contamination of the activation product precursor in the fuel materials.

1.3.1 Uranium and thorium contamination of the fuel materials

Natural uranium and thorium contamination occurs in all natural materials and the raw materials used to manufacture the graphitic matrix material are no exception. This natural uranium and thorium breed fissionable plutonium and ^{233}U that in turn produce fission products. This contamination is primarily in the matrix material of the fuel sphere and release of fission products created by fissions of this contamination only have to diffuse through the matrix material before being released.

Contributions from contamination in fuel materials under normal operation conditions are only 0.2% for ^{110m}Ag and 27% for ^{111}Ag, and less than 1% for both nuclides for accident conditions. These very low relative contributions are because release from intact coated particles (that contains almost all the fissionable material) is significant. The almost negligible ^{110m}Ag contribution is due to the fact that the precursor ^{109}Ag is almost completely released from matrix material before it becomes activated to ^{110m}Ag. The only parameters that significantly influence these releases are the fuel quality specification (natural uranium, thorium and silver occurring in the matrix material) and silver diffusion coefficients in graphite. The tiny contribution to silver release under all expected conditions negates the necessity to investigate and better define this source term.

1.3.2 Defective and failed coated particles

Even under the best manufacturing conditions a small fraction of coated fuel particles will be defective. A particle is considered failed or defective if its coating layers are absent or are damaged sufficiently to allow the release of fission gases. The large-scale production experience in Germany has led to a high-quality spherical fuel element with a mean defect particle fraction of 3×10^{-5}. Furthermore, under abnormally high temperatures and power surges, coated fuel particles may start to fail. Statistical analyses of German production fuel were used to determine PBMR-manufactured fuel failure fractions. A one-sided upper 95% confidence level of 6×10^{-5} was determined. No coated particles ever failed during irradiation testing under normal operating conditions. However, due to relatively small sample sizes, failures cannot be excluded, and failure curves were derived from statistical evaluations. These expected curves and their uncertainty ranges were modelled and are used in design calculations [11]. Phenomena that may influence coated particle performance (amoeba effect, Palladium-SiC interactions, etc.) were investigated and considered where applicable [10].

Contributions from these defective and failed coated particles under normal operation conditions are 1.5% for ^{110m}Ag and 65% for ^{111}Ag. Under accident conditions contributions to ^{111}Ag release is less than 5%. The only parameters that significantly influence these releases are the fuel failure fraction and silver diffusion coefficients in UO_2 and graphite. Small contributions of ^{110m}Ag (normal operation) and ^{111}Ag (accident events) and the relative unimportance of ^{111}Ag during normal operation negate the necessity to investigate and better define this source term.

1.3.3 Intact TRISO coated particles

Whether diffusion or alternative transport models are considered, the biggest contributor to silver release from high-quality fuel is intact coated particles. Intact coated particles are defined as particles that have all their coating layers intact, are impervious to fission gas release, and release only a very small fraction of their ^{137}Cs inventory.

The contribution from intact coated particles under normal operation conditions are more than 98% for ^{110m}Ag and 8.5% for ^{111}Ag. Silver transport through SiC is the same, whether it is ^{110m}Ag or ^{111}Ag. The strong variation in ^{110m}Ag and ^{111}Ag release contribution has to do with the half-life of ^{111}Ag. The short half-life of ^{111}Ag does not allow this fission product formed in intact kernels to be released. The ^{111}Ag simply decays before it can complete its journey through the coating layers.

This is not the case during accident events, where higher temperatures reduce the breakthrough time to hours, and more than 90% of the total ^{111}Ag source term is released from intact particles.

It is therefore clear that only the diffusion coefficients and actual transport mechanisms of silver through the coating layers of an intact TRISO particle, its subsequent transport through the matrix material and desorption into the gas coolant need to be investigated and qualified in detail. The primary metallic fission product barrier layer in a TRISO particle is the SiC layer and should be the focus in modelling silver transport in and release from a fuel element. The secondary transport processes, diffusion through UO_2, PyC and matrix material and sorption on the fuel surface cannot be ignored though, and must be quantified to ensure that evaluations of SiC transport models are free from any unaccounted effects.

1.3.4 Natural contamination of activation product precursors

Some radiological important activation products have precursors that occur naturally and may be important contributors to the activation product source term. In the case of the activation product ^{110m}Ag, the precursor ^{109}Ag is a naturally occurring isotope of silver with an abundance of 48%. During low-temperature irradiation this natural contamination could dominate the ^{110m}Ag source term depending on the actual contamination level. It is difficult to measure extremely low levels of silver in fuel materials; therefore the detection limits are quite high. This causes high uncertainties of the ^{110m}Ag source terms at low irradiation temperatures. It is vital that actual silver contamination levels in fuel materials are quantified.

2. Modelling Options

2.1 Diffusion Calculation Model

The existing PBMR calculation model [12] is based on the HochTemperatur Reaktorbau (HRB) calculation model developed in Germany during the German fuel development programme. It is centred on the software product GETTER [13] and utilizes accepted transport parameters [2]. GETTER has been extensively analysed and mathematically verified to ensure that the activation product source term is calculated correctly.

2.1.1 Fission product recoil

Fission products produced during fission of fissionable isotopes recoil from their fission sites into neighbouring material. The recoil stopping range for each fission product nuclide is dependent on its mass, kinetic energy available to accelerate the nuclides from the fission site, and the material through which it penetrates. These stopping ranges determine the recoil fraction in each of the material components.

In HTR spherical fuel, the origin of this recoil is from the UO_2 kernels and natural contamination of the fuel material. Assuming a simplified isotropic geometric recoil model, the recoil release rate from a sphere of radius r_a is given by [14]:

$$R = S \cdot \pi \cdot \left(r_0 \cdot r_a^{\,2} - \frac{r_0^{\,3}}{12} \right), \qquad (1)$$

where

S is the source rate of fission products produced by fissions in material (atoms.cm^{-3}.s^{-1}) and

r_0 is the recoil range of fission product in material (cm).

Due to relatively large diffusion coefficients of silver in UO_2, the majority of ^{109}Ag formed during fission in the fuel kernel is released even at modest reactor temperatures. The contributions of recoil and knock-on effects, which are geometrical in nature, are only significant at low temperatures (< 700 °C). Under such conditions, transport through the matrix material is so slow that the silver source term is negligible in radiological terms. Recoil release is therefore included in the calculation model only for the sake of completeness.

2.1.2 Diffusion

After fission products have recoiled into neighbouring fuel materials, they are transported through the fuel materials to the surface of the fuel sphere. The calculation model assumes that fission products are primarily transported through fuel materials according to Fick's law of diffusion:

$$J_x = -D\frac{dN}{dx} \tag{2}$$

By taking into account fission product production (S) and decay terms (λc) in spherical geometry the diffusion equation becomes:

$$\frac{\partial c}{\partial t} = D\left(\frac{\partial^2 c}{\partial r^2} + \frac{2}{r}\frac{\partial c}{\partial r}\right) - \lambda c + S \tag{3}$$

The diffusion coefficient D is dependent on the temperature according to the Arrhenius equation:

$$D = D_0 e^{\frac{-E_A}{RT}}, \tag{4}$$

where

D_0 is the diffusion constant ($m^2.s^{-1}$),

E_A is the activation energy for diffusion ($kJ.mol^{-1}$) and

R is the universal gas constant, (8.3145×10^{-3} $kJ.mol^{-1}.K^{-1}$).

The diffusion equation is solved numerically for coated particles through all the coating layers, failed particles, and transport through the matrix material.

2.1.3 Surface sorption and mass transfer

The most important boundary condition used in solving the diffusion equation is the transport from the fuel surface to the coolant gas through a mass transfer coefficient that is controlled by a sorption isotherm. It is assumed that the diffusant forms a very thin gaseous boundary layer at the surface of the fuel sphere, and the convective mass transfer of the diffusant to the coolant is based on the difference between the boundary layer (C_{bl}) and coolant concentration (C_g) namely:

$$J = -D\left(\nabla c\big|_s\right) = \beta \cdot \left(c_{bl} - c_g\right), \tag{5}$$

where

J is the flux of material transfer at the surface,

$\nabla c\big|_s$ is the concentration gradient of diffusant at the fuel sphere surface, and

β is the mass transfer coefficient,

which is calculated from analogous correlations used for heat transfer, by substitution of the Nusselt and Prandtl numbers with the Sherwood (Sh) and Schmidt (Sc) numbers respectively, so

$$\beta = \frac{Sh \cdot D_g}{d}, \text{ and} \tag{6}$$

$$Sh = 1.27\frac{Sc^{1/3}}{\varepsilon^{1.18}}Re^{0.36} + 0.033\frac{Sc^{1/2}}{\varepsilon^{1.07}}Re^{0.86}. \tag{7}$$

For low diffusant boundary layer pressures and high temperatures, the concentration in the boundary layer is related to the partial pressure (p_{bl}) by the ideal gas relation

$$c_{bl} = \frac{p_{bl}}{RT}N_A, \tag{8}$$

where

N_A is Avogadro's number, (6.022 x 10^{23} mol^{-1}) and

R is the universal gas constant (8.3145 $dm^3.Pa.mol^{-1}.K^{-1}$).

The partial pressure in the boundary layer is determined from the Henry or Freundlich isotherms [2], which give the relationship between partial pressure and matrix surface concentration. The transition from dominant Henry to dominant Freundlich isotherms occurs at very high surface concentrations (>0.1μmol.g^{-1}), which are rarely attained under normal operation conditions.

The partial vapour pressure is a function of the surface concentration and temperature, and is calculated as the sum of the Henry and Freundlich isotherm vapour pressure:

$$p = p_H + p_F\,, \tag{9}$$

where

$$p_H = c_s \exp\left(\left(A + \frac{B}{T}\right) + \left(D - 1 + \frac{E}{T}\right)\ln c_t\right), \tag{10}$$

$$p_F = \exp\left(\left(A + \frac{B}{T}\right) + \left(D + \frac{E}{T}\right)\ln c_s\right) \text{ and} \tag{11}$$

$$\ln c_t = d_1 - d_2 T\,. \tag{12}$$

The constants A, B, D, E, c_1, d_1 and d_2 are empirically derived, where

T is the surface temperature in K,

p_H is the Henry isotherm vapour pressure in Pa,

p_F is the Freundlich isotherm vapour pressure in Pa,

B and E are constants in K,

c_s is the concentration on surface in μmol.gC^{-1} (micromole per gram carbon) and

d_1 and d_2 are constants in K^{-1}.

Simplifications of the above formulae may be made by combining expressions containing constants into new constants. This is especially true for the low concentration Henry region; the correlation can be written as [14]:

$$p_H = c_s \exp\left(E + \frac{1000 \bullet E2}{T}\right) \tag{13}$$

2.2 Molecular Vapour Transport Release Calculation Model

An alternative model, the Molecular Vapour Transport Release Model [8], has been suggested that assumes diffusion transport through all fuel materials except the SiC layer. In this model it is hypothesized that Ag leaks through Nano-Tube Failures (NTF) in the SiC layer from the IPyC to the OPyc layer. Different flow regimes exist depending on the sizes of the NTF and molecule, gas pressure, flow velocities and temperature. Whether molecules travelling through the NTF interact primarily with the walls of the flow channel (molecular flow) or with other molecules in the flow channel (viscous flow), depends primarily on the pressure in the system.

The limits between molecular, transitional, and laminar flow is defined by the Knudsen number, which is the ratio of the mean free path of a molecule to a characteristic dimension of the channel, usually the tube diameter, through which the gas is flowing [6].

$$Kn = \frac{\lambda}{d}, \tag{14}$$

where

λ is the mean free path (m) and

D is the channel diameter (m).

For an ideal gas the mean free path is:

$$\lambda = \frac{RT}{\sqrt{2}\pi d^2 N_A P}, \tag{15}$$

where

R is the universal gas constant (8.3145 J.mol^{-1}.K^{-1}),

T is theTemperature (K),

d is the channel diameter (m),

N_A is Avogadro's number (6.022 x 10^{23} mol^{-1}),

P is the Pressure (Pa).

The gas pressure in the SiC is very low due to the inner PyC layers retaining all fission gases and CO_2 formed in the kernel and buffer layers. The mean free path of gas molecules is much larger than the dimensions of the nano-tubes, therefore molecular flow is the dominating flow regime and viscous or transitional flow are not considered. For molecular flow the following mass transfer equation can be applied [6]:

$$Q_m = \frac{C_m \Delta t}{V_{molar}} M_{molar}, \tag{16}$$

where

Q_m is the mass transfer over time Δt [g],

V_{molar} is the molar volume [$m^3.mol^{-1}$],

M_{molar} is the atomic mass [$g.mol^{-1}$] and C_m is the conductance [$m^3 s^{-1}$].

The conductance is calculated by:

$$C_m = \frac{d^3}{6L}\sqrt{\frac{2\pi RT}{M_{molar}}}, \tag{17}$$

where

d is the nano-tube circular diameter (m) and

L is the nano-tube length (m).

All nano-tubes are assumed to be straight tubes with circular cross sections with the length of each tube equal to the SiC coating thickness. This calculation model calculates transport from UO_2 kernels and through PyC and matrix material similarly to the diffusion calculation model. Since this model has only been used to evaluate experiments and reactor conditions where centre fuel temperatures exceed 900 °C, it ignores recoil effects and sorption from the fuel surface. Should the molecular vapour transport release model be further developed in future, recoil and sorption effects will have to be included, but the effect on total core release from a typical planned HTR operating with reactor outlet temperatures exceeding 900 °C will be small.

3. Evaluation of Material Tests

Material tests are usually separate effect tests that focus on only one or maybe two phenomena at a time. A particular parameter can then be appraised and possibly quantified in order to simplify the assessment of integral effects tests later on. Specific material tests are evaluated first to ensure that all parameters are quantified as well as possible before integral effect evaluations of full sphere irradiation tests are performed.

3.1 Sorption Isotherms

Few attempts have been made to determine silver sorption isotherms during the German fuel programme. Standard procedure such as isopiestic methods [15] did not yield good results due to low sorption of silver on matrix materials. Silver sorption from matrix materials has in general just been ignored in the available literature. The caesium sorption isotherm, on the other hand, has been studied very well and is described in detail in the literature [16]. Sorption isotherms for both Freundlich and Henry regions on a large variety of nuclear graphite have been derived in a Knudsen cell mass spectrometer system for caesium but not for silver [17].

The only silver sorption investigation performed that was published in the literature [18] did not provide sorption isotherms, but did show desorption spectra of caesium and silver using an identical experimental setup and test conditions. The desorption spectra are shown in Figure 3 verbatim. The technique is known as Temperature Programmed Desorption (TPD). It consists of measuring the rate of desorption from a surface as its temperature is increased linearly with time. A monolayer of caesium and silver is evaporated onto the surface of a test sample, and then heated at a constant rate. The desorption rate is presented as a fraction of the highest rate achieved, which is also the point where all the available atoms have been released from the surface. A broadening tail after the caesium peak is observed, which are most likely atoms that have diffused into the porous matrix material, and have a delayed release mechanism.

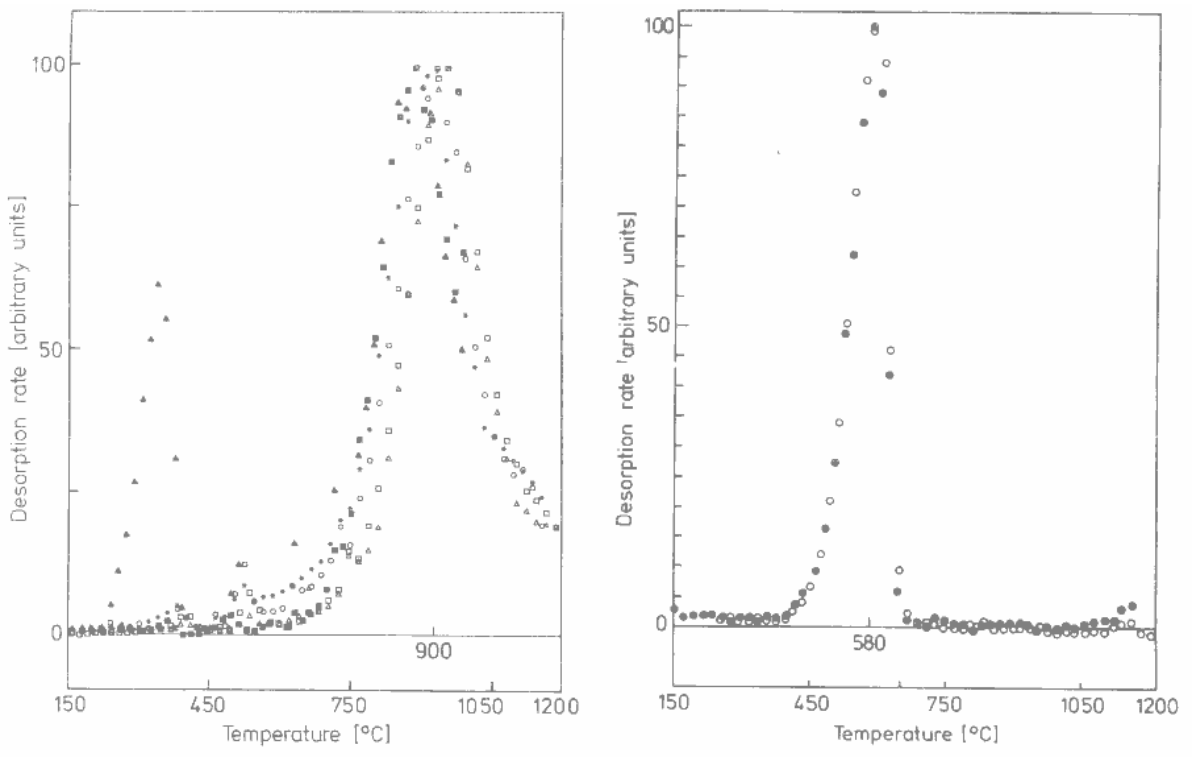

Figure 3: Experimental Desorption Spectra of Caesium (left) and Silver (right)

Several experiments are plotted on each graph. The first graph shows the caesium desorption spectra. The peak at ~320 °C in the first graph corresponds to a test performed under oxidizing conditions and should be ignored. The first graph shows that caesium starts to desorb at approximately 500 °C. The maximum desorption rate occurs at ~890°C, but that is due to the fact that the caesium atoms deposited onto the matrix material surface are depleted and no more atoms are available to be measured. Should there be an 'infinite source' of caesium inside the sample material, a peak would not be observed but a curve where the desorption rate approaches a maximum depending on how fast caesium atoms are supplied to the surface of the sample. This is exactly the case when this data is evaluated with a fuel transport code utilizing sorption models such as found in GETTER.

The second graph shows silver desorption rates under the same conditions as some of the caesium spectra. Silver starts to desorb from the surface at approximately 400 °C and peaks at 580 °C. What is immediately obvious is that silver desorbs at much lower temperatures than caesium, and this also explains why it is relatively difficult to estimate silver sorption isotherms using isopiestic methods. These graphs show that matrix material sorption is a significant retention mechanism for caesium and silver for temperatures up to 1 000 °C and 700 °C respectively, after which desorption from the fuel surface occurs so quickly that it has a negligible effect on overall fuel release.

An attempt was made to evaluate these desorption spectra with the sorption isotherms used in GETTER [13]. The caesium fractional release with a desorption rate using the known sorption isotherms was compared with the fractional release when graphite sorption was set to almost zero. This was achieved by setting the sorption isotherms *E* and *E2* defined in paragraph 2.1.3 to their accepted values of 10.44 and -41.9 K first to simulate real sorption and then setting *E* (dimensionless parameter) so high (1 000x partial pressure) that sorption becomes negligible in the temperature region under consideration. The GETTER desorption rate curve and the experimental curve are shown in Figure 4 with desorption temperature (^{o}C) and rate (arbitrary units) axis. The maximum GETTER desorption rate is achieved at 1 150 °C after which sorption has no effect on caesium release. At the maximum experimental desorption rate temperature, the GETTER desorption rate is 66% of the maximum desorption rate.

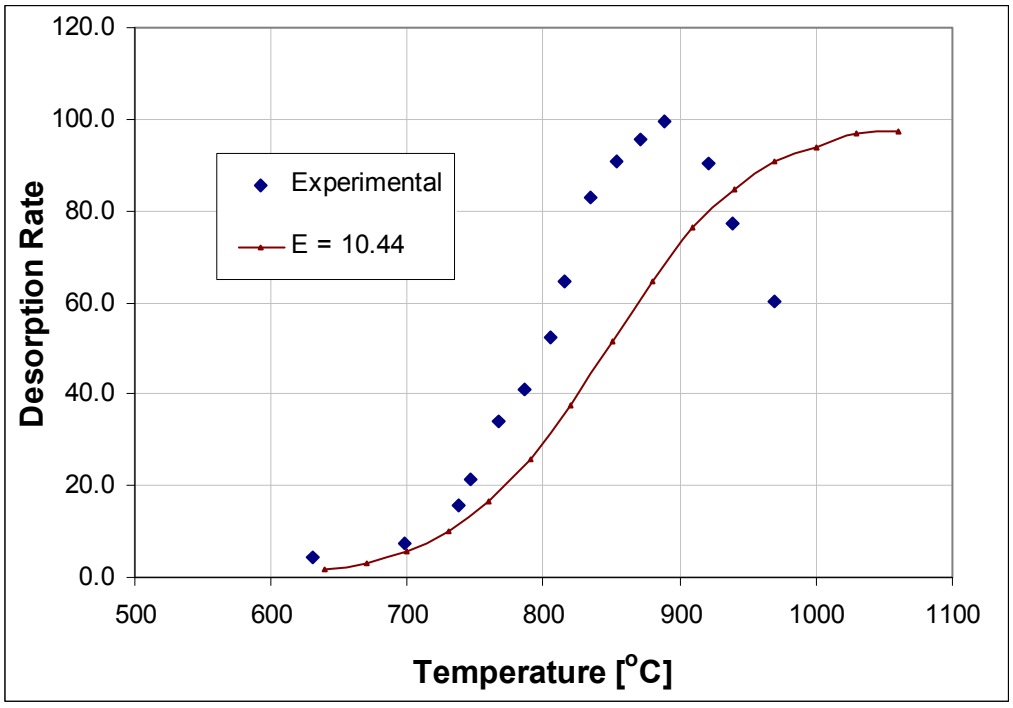

Figure 4: Cs sorption: Experimental vs. GETTER Sorption Isotherm

The GETTER evaluation above was repeated for silver experimental results. Caesium results could then be used as a benchmark to determine a realistic silver sorption isotherm. This is of course assuming that the same desorption model applies to both caesium and silver, and that the caesium sorption isotherm is correct for this experiment. Previously the HRB approach to modelling silver sorption was to assume that the silver partial pressure is a hundred times higher than the caesium partial pressure [13]. The sorption isotherm *E2* was kept constant and the *E* sorption isotherm was increased to 12.74.

Curves that were conservative for lower temperatures could be obtained by keeping the sorption isotherm *E2* constant as per the HRB approach and further increasing the dimensionless *E* sorption isotherm. In Figure 5 silver experimental desorption rates are compared with GETTER calculated desorption rates for the sorption isotherm *E* set to 16, 17 and 18. In all cases the maximum desorption rate was achieved at about 720 °C. When the dimensionless sorption isotherm *E* is set to 17, GETTER calculates a desorption rate (with arbitrary units) of 66% of the maximum desorption rate at the maximum experimental desorption rate temperature. This compares with the caesium sorption evaluation using best available sorption isotherms. It is therefore recommended that values of 17 and -41.9 K be used for *E* and *E2* respectively for best estimate analyses and 18 and -41.9 K for design limit calculations.

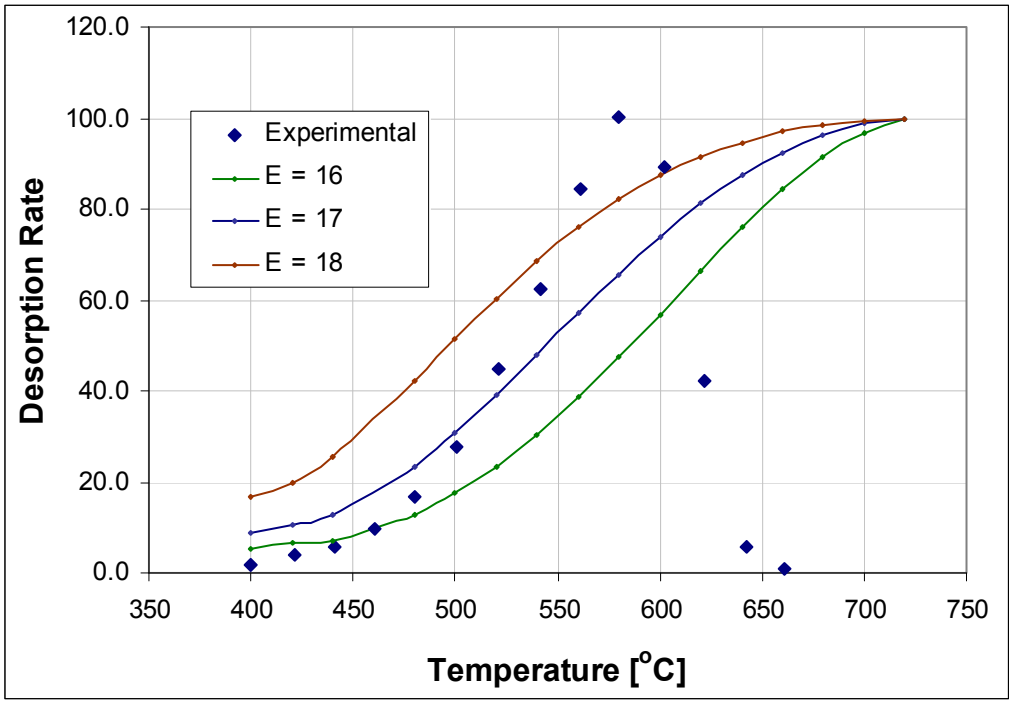

Figure 5: Ag Sorption: Experimental vs. GETTER Sorption Isotherm

The newly derived and HRB sorption isotherms' effect on silver partial pressures at different surface concentrations are shown in Figure 6. The new sorption isotherms increase the silver partial pressures by a factor of 70. Most modern high-temperature gas-cooled reactor designs are planned to operate with reactor outlet temperatures between 750 °C and 950 °C. It can therefore be argued that the silver sorption isotherm is only of academic importance, and will not influence the total ^{110m}Ag source term significantly. It is, however, still important to show that all phenomena have been considered and that similar calculation models are employed for all radiological significant nuclides.

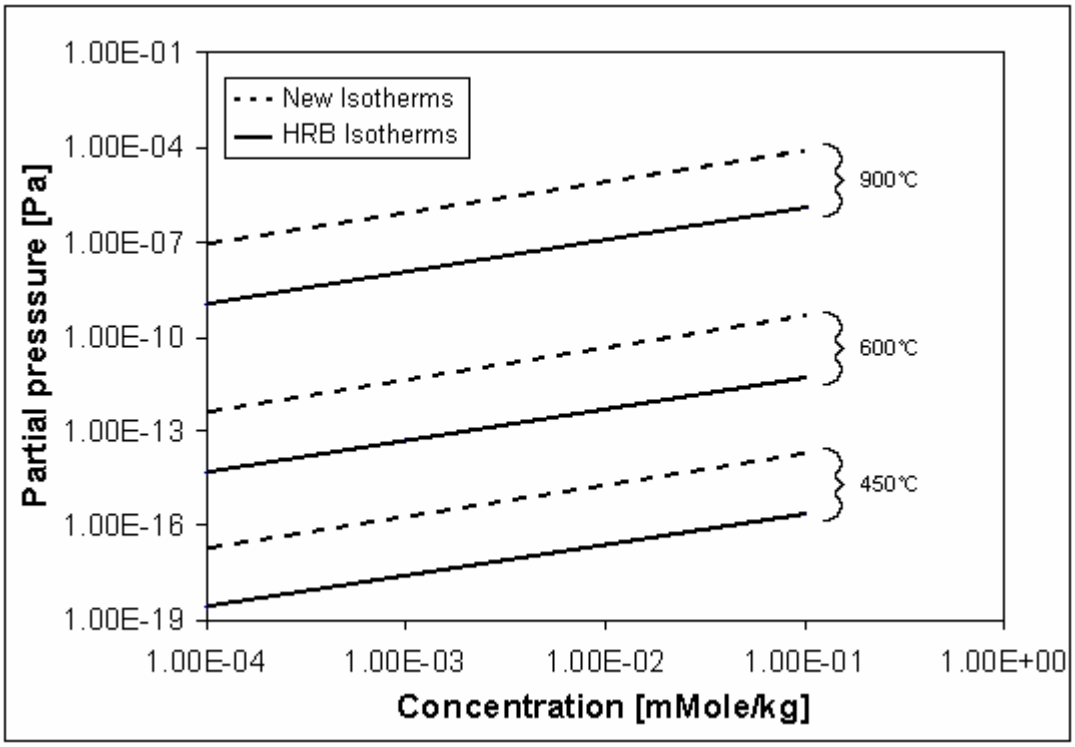

Figure 6: Old and New Ag Sorption Isotherms on A3-3 Matrix Graphite

3.2 Matrix Material Transport

Transport of silver through graphitic matrix material has been investigated in detail in [19] and [20]. The diffusion of silver in original, oxidized and fast neutron irradiated A3-3 and in original A3-27 matrix materials were studied in vacuum by measuring the ^{110m}Ag release kinetics and concentration profiles from cylindrical samples.

The release kinetics and concentration profiles both satisfied Fick's law of diffusion and diffusion coefficients for temperatures between 800 °C and 1 300 °C were derived [20]. Since PBMR is only considering A3-3 equivalent matrix material for its demonstration plant's fuel, only A3-3 diffusion coefficients will be evaluated. Silver retention in A3-3 matrix material increases with irradiation up to ~7 displacements per atom (equivalent to a fast neutron fluence of approximately 5 x 10^{25} m^{-2}). Diffusion coefficients show typical Arrhenius behaviour where R is the universal gas constant (8.3145 x 10^{-3} kJ. $mol^{-1}.K^{-1}$) and T is the absolute temperature.

Original A3-3: $D = 6.80 \times 10^{1} e^{-262/RT}$ $m^2 s^{-1}$

Irradiated A3-3: $D = 1.60 \times 10^{0} e^{-258/RT}$ $m^2 s^{-1}$

Pebble fuelled HTRs employ dynamic core loading schemes so that an equilibrium core contains from fresh fuel to highly irradiated spent fuel. For best estimate analyses, the irradiated diffusion constant and activation energy has been used. This can be justified as the ^{110m}Ag inventory is small in the beginning of a sphere's irradiation life and releases are modest due to the fact that the ^{235}U fission yield for ^{109}Ag is very small. Later in a sphere's life when the matrix material is highly irradiated, the ^{110m}Ag inventory grows very quickly as high silver yield ^{239}Pu and ^{241}Pu fission contribution becomes significant. For best estimate analyses this may be fair, but for safety analyses design calculations, a more conservative approach is required.

In Figure 7 diffusion coefficients for both original and irradiated A3-3 matrix material is plotted against temperature. It may be overly conservative to simply assume the fastest diffusion coefficient for safety analyses. A more fitting approach would be to assume that irradiation effects have a linear effect on the silver retention ability of A3-3 matrix material. It will still be conservative in the sense that the high inventory and highly irradiated end-of-life fuel will have faster silver transport than experimentally measured.

However, the fresh fuel release (although several factors less than end-of-life fuel release) will not be underestimated. The suggested PBMR design diffusion constant is plotted in Figure 7. The recommended best estimate and design silver diffusion coefficient is thus:

PBMR best estimate $: D = 1.60 \times 10^{0} e^{-258/RT}$ $m^2 s^{-1}$

PBMR design : $D = 1.10 \times 10^{1} e^{-260/RT}$ $m^2 s^{-1}$

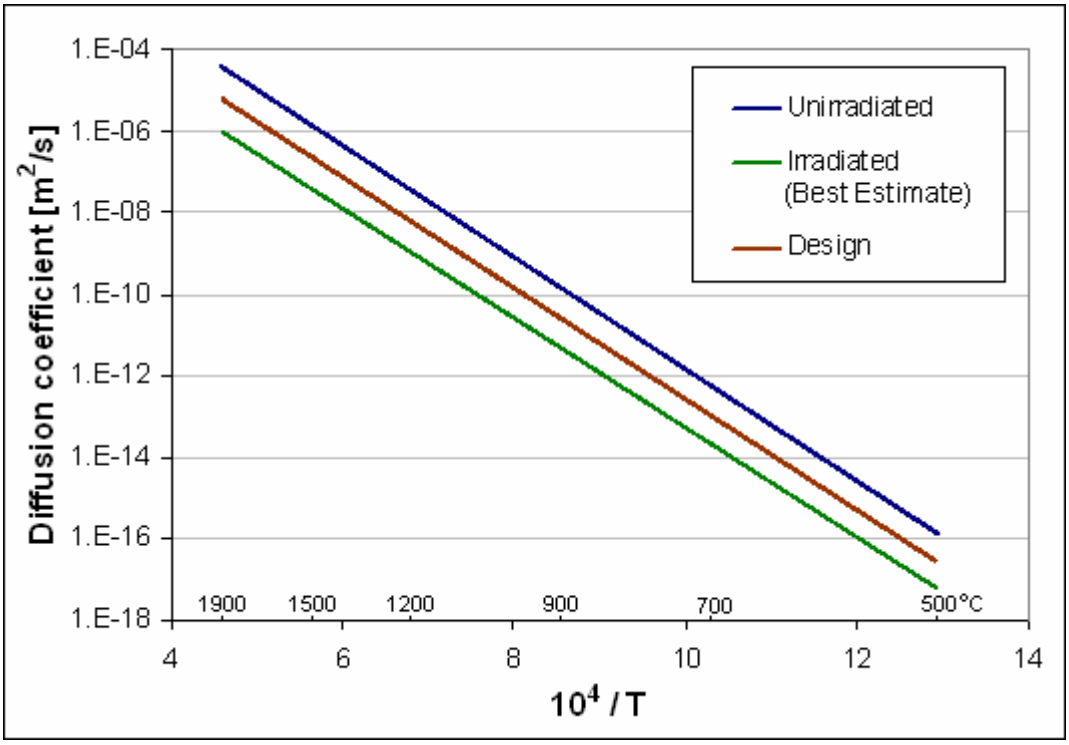

Figure 7: Silver Diffusion Coefficient in the Matrix Material

3.3 Coated Particle Transport

The transport of silver through coating layers of a coated particle has been studied in depth by many researchers [2]. Compared to transport through the SiC layer, transport through the UO_2 kernel and PyC layers are relatively quick. The diffusion coefficients of silver in the UO_2 kernel and PyC layers are 200 and 500 times larger than in SiC at 1 000 °C. Both German and United States fuel development programmes suggested the same diffusion coefficients for best estimate analyses for UO_2 kernel and PyC layers [2].

Best estimate UO_2: $D = 6.70 \times 10^{-9} e^{-165/RT}$ m^2s^{-1}

Best estimate PyC: $D = 5.30 \times 10^{-9} e^{-154/RT}$ m^2s^{-1}

For safety analyses to determine design limits, an uncertainty for the above diffusion constants of a factor of two was suggested before [21]. This uncertainty, or even more conservative safety factors, has only a small effect on the overall silver release rate.

The most efficient barrier to the release of silver in an HTR fuel element remains the SiC layer and it has been studied in detail (e.g. [1], [2], [3] and [6]). Nabielek *et al*. measured silver release by gamma-ray spectrometric measurements of fuel tubes and other graphite components from a variety of fuel particles during irradiation and post-irradiation heating tests between 850 °C and 1 500 °C. An effective diffusion coefficient for silver in silicon carbide was derived:

Nabielek *et al*. [1]: $D = 6.76 \times 10^{-9} e^{-213/RT}$ m^2s^{-1}

Silver and caesium release from loose particles that had been previously irradiated in compacts or test spheres were measured by Amian and Stöver during heat-up tests [3]. Irradiation temperatures varied from 400 °C to 1 050 °C and burn-ups between 2.3% and 12.1% Fissions per Initial Metal Atom (FIMA) with fast fluences between 0.5×10^{25} m^{-2} to 8.2×10^{25} m^{-2} were achieved. Annealing temperatures between 1 000 °C and 1 500 °C were used for up to 2 340 hours. Different particle types had different fuel kernel materials with slight variations in coating dimensions. Diffusion coefficients for silver in silicon carbide was derived for all types of kernels (UO_2, UC_2, ThO_2, mixtures, etc.) and for reference quality fuel (UO_2, $(U,Th)O_2$) and published in [3]:

All fuel types: $D = 4.5 \times 10^{-9} e^{-218/RT}$ m^2s^{-1}

Reference fuel only: $D = 3.6 \times 10^{-9} e^{-215/RT}$ m^2s^{-1}

Both research efforts found scatter up to one order of magnitude of the diffusion coefficient at any temperature. Silver is released from particles that retain caesium, which means from coated particles with intact SiC layers, but ion implantation experiments suggest that silver does not undergo bulk SiC diffusion [1]. This anomaly was resolved by suggesting that implanted silver is stopped primarily in the SiC grains, while fission product silver in a fuel element is transported along crystal grain boundaries which contain traces of free silicon [3]. Free silicon is a function of coating conditions and it goes a long way to describe the scatter in the experimentally measured silver diffusion coefficients. Grain boundary diffusion depends on the exact microstructure of the sample, which varies from sample to sample. Accordingly, activation energies for diffusion in pyrolytically deposited SiC coatings are approximately 200 kJ/mol while the activation energies for diffusion in single crystals are about 450 kJ/mol.

Other studies did not agree, as the scatter in the reported data exceeds the expected variations in SiC structure and the silver path length travelled through the SiC coatings [6]. From ion implantation studies [5] and diffusion couple investigations [22] an alternative transport mechanism that entails transport of silver though cracks in the SiC layer were suggested. From this mechanism a model was derived and used to perform an estimate of silver release from a typical PBMR core based on a first estimate of some German irradiation data [8].

Measurements made on loose particles remain problematic. The silver inventory in a single particle is very small and measurement errors on such small activities continue to be challenging. Furthermore, it must be asked if packing into a sphere and high-temperature heat treatment during final annealing of fuel spheres do not affect coated particle characteristics. Measurements in material samples only also remain problematic. Geometric effects, irradiation fluxes and temperatures cannot be repeated and these effects on silver transport cannot be comprehended.

The exact SiC transport mechanism cannot be derived from the available material test data. Innovative and new material tests must be invented and performed to understand the exact mechanism. Considering tests and experiments already performed, which yielded varying results and contradicting mechanisms, it seems unlikely that clear proof will be available any time soon. The only recourse in the meantime is to evaluate all the available real data, in other words, the actual measured release from complete fuel spheres under conditions that are similar to expected reactor conditions.

3.4 Material Test Evaluation Discussion

Transport phenomena investigated in material tests can be divided into two groups:

- A secondary effects group that only has a limited consequence on the silver release source term. These include recoil, diffusion transport through UO_2, PyC and matrix material, and sorption on the fuel surface. These phenomena have either negligible effects (recoil and sorption) or are very well understood (diffusion through UO_2, PyC and matrix material) and do not have a controlling function on silver release.
- A primary effects group is phenomena that control silver release under most reactor conditions considered. In this case, it is only silver transport through SiC which is also the least understood phenomenon. In order to derive the best calculation model to predict the ^{110m}Ag source term, secondary transport phenomena are assumed to be correct, based on separate effects materials tests evaluated in Chapter 3, and the primary effect, SiC transport, is evaluated by integral effects of irradiation tests in Chapter 4.

4. Evaluation of Irradiation tests

4.1 Selection of Irradiation Tests

A study of all available irradiation tests has been performed [23] and applicable tests that might be used to derive silver transport models and parameters have been described. Table 1 shows all applicable irradiation tests to be considered. All values in Table 1 are as reported in the literature before any evaluation has been performed. Temperatures and fluences are often pre-irradiation targets and burn-ups are first-calculated estimates. All tests are listed from most applicable to least applicable. Applicability in this case is defined according to fuel type, irradiation conditions and availability of irradiation data and silver fractional release results.

4.1.1 Fuel type

Ideally, considered irradiation tests must have tested fuel containing low enriched UO_2 TRISO coated particles, where coating layers are as close as possible to that of the PBMR fuel design [10]. Due to low retention of silver in kernel and graphite materials, and for the purpose of this study, the nature of the kernel and pyrocarbon layers is not considered as an inhibitive factor for evaluation of an irradiation or heat-up test. Therefore, UC_2- and Th-based fuels and matrix materials other than A3-3 may be considered. For the same reason, non-spherical fuel such as compacts may be considered as well, but the geometry must be taken into account. Additionally, coated particle failure and defect fractions must be more than a factor of ten lower than the fractional release of silver in a test. This is to ensure that silver release evaluations are governed by silicon carbide retention.

4.1.2 Irradiation history

Irradiation history refers to the availability of data (such as time-dependent temperatures, release rates of fission gases, neutron fluxes, etc.) describing irradiation conditions which coated particle fuel in the test were exposed to. Ideally the irradiation history must be comparable with expected reactor conditions considered and detailed data sets must be available.

Unfortunately much of the detailed German data have been lost or are very difficult to find. In some cases only ‘single values’ could be found, for example, a single maximum fuel temperature rather than all the temperatures measured during irradiation.

Where complete irradiation histories are unavailable, an evaluation can still be performed by assuming steady state irradiation conditions, but this is of course much less satisfactory. Often the only option is to make a conservative assumption that adds extra uncertainty in the final result.

Sometimes irradiation history data is presented as graphs in documents, typically surface temperature, burn-up (% FIMA), and release rates of gaseous isotopes. The origin of these graphs is from tabulated data, which is often unavailable. The raw data may be estimated from these graphs using opto-digital software.

Thermal fluxes can be back-calculated quite accurately from the burn-up history (% FIMA) of the fuel, and this can be done quite precisely if final inventories of some isotopes in the fuel element are available. The most important irradiation history parameter required is the fuel temperature, as evaluations matching fractional releases do not require accurate estimates of the inventory. Fast neutron dose (irradiation damage) has recently come under consideration as a factor affecting silver retention in silicon carbide and influencing thermal conductivity in fuel materials. In most cases the history of this dose is relatively linear in nature, and easily estimated once final values are known.

4.1.3 Fractional release data

If the fractional release of silver could not be found in the literature, there is little point in carrying out the irradiation evaluation. In some cases, silver released from a sphere is given as an absolute amount, and it is necessary to calculate the total silver inventory from burn-up. Other times, silver profiles are given, either in the complete sphere, or just in the fuel-free zone. Here an evaluation can still be performed for some models, but deriving transport parameters becomes questionable.

The availability of fractional release rates for other radionuclides is very valuable in evaluating silver fractional release data. Release over birth ratio (R/B) for krypton fission gases are valuable indicators of coated particle performance and caesium fractional release rates indicate the quality of SiC layers.

Fractional releases of above irradiation tests for ^{110m}Ag, ^{134}Cs, ^{137}Cs and end-of-life release over birth ratio (R/B) of ^{85m}Kr is graphically presented in Figure 8.

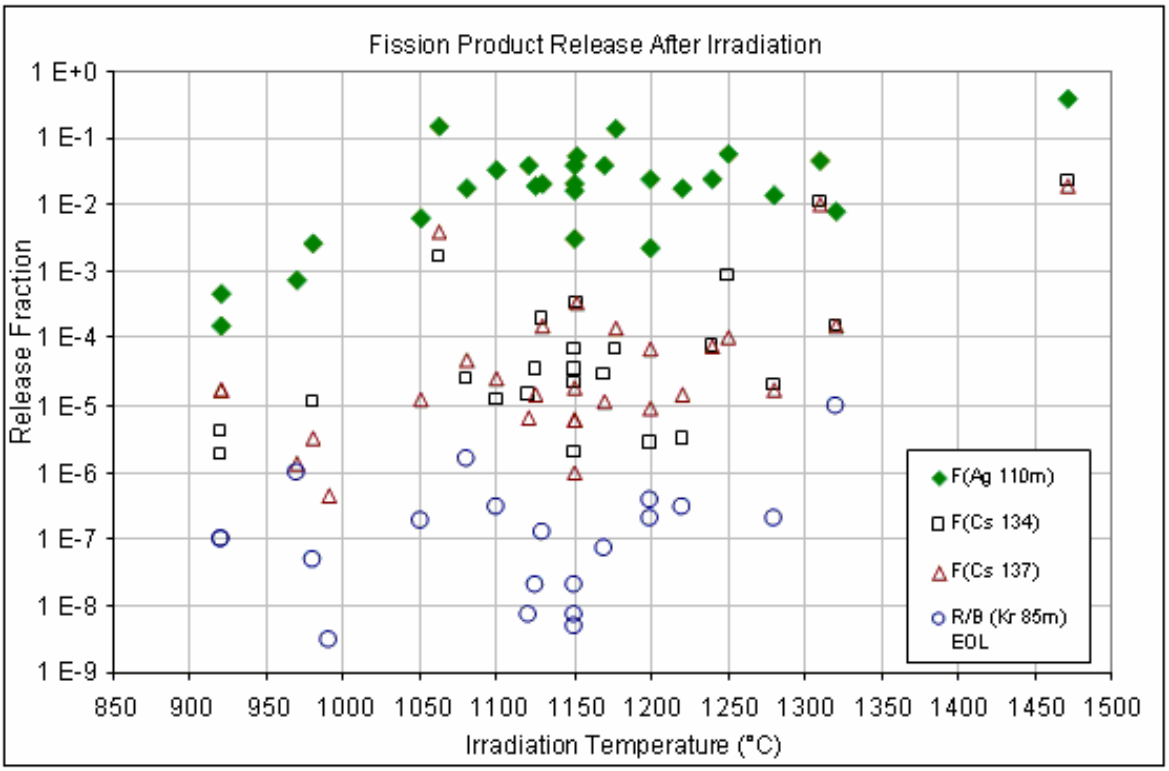

Figure 8: Fractional Release of Fission Products after Irradiation

In Table 1 considered irradiation tests are divided into three groups:

- Highly applicable irradiation tests' evaluations can be carried out relatively quickly on most models currently used for silver transport, as sufficient information is available, and a good degree of certainty is ensured by many literature sources. Transport parameters derived from these evaluations must be considered the most valuable and weigh the most in terms of importance.
- Medium applicable irradiation tests' evaluations should basically be done after the high priority set, as some more data may be needed, or additional work needs to be carried out that would take much longer than a high priority evaluation. Derived transport parameters must be considered less important than the high applicable results.
- Low applicable irradiation tests' evaluations would typically take much longer than other evaluations and need a significant amount of source information. Assumptions have to be made that would reduce the value of derived transport parameters and therefore should have the lowest weight when final transport parameters are considered. Many other irradiation tests have been considered as well but rejected as significant data is missing, could not be sourced, and in some cases was not even measured.

Table 1: Considered Irradiation Tests

Experiment	Irradiation Time (EFPD)	Maximum Fuel Temperature	Burn-up % FIMA	R/B ^{85m}Kr	Fractional ^{110m}Ag Release	Fractional ^{137}Cs Release	Fuel Type
High Applicability							
HFR-K3/1	359	1 200 °C	7.5	2×10^{-7}	2.2×10^{-3}	9.1×10^{-6}	UO_2 fuel reload 19
HFR-K3/2	359	920 °C	10	1×10^{-7}	4.5×10^{-4}	1.7×10^{-5}	UO_2 fuel reload 19
HFR-K3/3	359	920 °C	10.6	1×10^{-7}	3.2×10^{-4}	1.7×10^{-5}	UO_2 fuel reload 19
HFR-K3/4	359	1 220 °C	9	3×10^{-7}	1.8×10^{-2}	1.4×10^{-5}	UO_2 fuel reload 19
FRJ2-K13/1	396	1 125 °C	7.5	2×10^{-8}	1.9×10^{-2}	1.4×10^{-5}	UO_2 fuel reload 19
FRJ2-K13/2	396	1 150 °C	8	2×10^{-8}	2.0×10^{-2}	1.8×10^{-5}	UO_2 fuel reload 19
FRJ2-K13/3	396	1 150 °C	7.9	7×10^{-9}	1.7×10^{-2}	6.1×10^{-6}	UO_2 fuel reload 19
FRJ2-K13/4	396	1 120 °C	7.6	7×10^{-9}	3.9×10^{-2}	6.4×10^{-6}	UO_2 fuel reload 19
FRJ2-K15/1	533	970 °C	14.1	1×10^{-6}	7.5×10^{-4}	1.3×10^{-6}	UO_2 fuel reload 21
FRJ2-K15/2	533	1 150 °C	15.3	5×10^{-9}	3.2×10^{-3}	9.5×10^{-7}	UO_2 fuel reload 21
Medium Applicability							
R2-K13/1	517	1 170 °C	10.2	7×10^{-8}	3.9×10^{-2}	1.1×10^{-5}	UO_2/Th fuel
R2-K13/4	517	980 °C	9.8	5×10^{-8}	2.7×10^{-3}	3.2×10^{-6}	UO_2/Th fuel
R2-K12/1	308	1 100 °C	11.1	3×10^{-7}	3.3×10^{-2}	2.4×10^{-5}	UO_2/Th fuel
R2-K12/2	308	1 280 °C	12.4	2×10^{-7}	1.4×10^{-2}	1.7×10^{-5}	UO_2/Th fuel
FRJ2-K11/3	260	1 150 °C	11.5	-	4.0×10^{-2}	6.0×10^{-6}	UO_2/Th fuel
FRJ2-K11/4	260	1 152 °C	8.5	-	5.4×10^{-2}	3.3×10^{-4}	UO_2/Th fuel

Experiment	Irradiation Time (EFPD)	Maximum Fuel Temperature	Burn-up % FIMA	R/B ^{85m}Kr	Fractional ^{110m}Ag Release	Fractional ^{137}Cs Release	Fuel Type
Low Applicability							
R2-K12/3	308	1 200 °C	10.3	4×10^{-7}	2.4×10^{-2}	6.8×10^{-5}	UC_2/Th fuel
R2-K12/4	308	1 050 °C	11.8	2×10^{-7}	6.3×10^{-3}	1.2×10^{-5}	UC_2/Th fuel
FRJ2-K10/3	291	1 250 °C	73	-	5.6×10^{-2}	1.0×10^{-4}	UC_2 fuel
FRJ2-K10/4	291	1 240 °C	70	-	2.5×10^{-2}	7.5×10^{-5}	UC_2 fuel
FRJ2-P27/1	232	1 080 °C	7.6	2×10^{-6}	1.8×10^{-2}	4.7×10^{-5}	Compact U fuel
FRJ2-P27/2	232	1 320 °C	8	1×10^{-5}	8.2×10^{-3}	1.5×10^{-4}	Compact U fuel
FRJ2-P27/3	232	1 130 °C	7.6	1×10^{-7}	2.0×10^{-2}	1.6×10^{-4}	Compact U fuel
FRJ2-P23/1	177	1 250 °C	12.5	-	1.5×10^{-1}	3.9×10^{-3}	Compact Th fuel
FRJ2-P23/2	177	1 210 °C	12.5	-	1.4×10^{-1}	1.4×10^{-4}	Compact Th fuel
FRJ2-P23/3	177	1 472 °C	11.9	-	4.0×10^{-1}	1.9×10^{-2}	Compact Th fuel
FRJ2-P23/4	177	1 310 °C	12.1	-	4.6×10^{-2}	9.9×10^{-3}	Compact Th fuel
BR2-P21/1	380	1 350 °C	9	-	1.1×10^{-1}	7.6×10^{-2}	Compact U fuel
BR2-P21/2a	380	1 550 °C	10	-	2.2×10^{-1}	7.6×10^{-2}	Compact Th fuel
BR2-P21/2b	380	1 550 °C	9		6.0×10^{-2}	3.0×10^{-2}	Compact Th fuel
BR2-P22/2	257	1 350 °C	6	-	5.0×10^{-3}	2.1×10^{-3}	Compact Th fuel

4.2 Molecular Vapour Transport Release Model

A first analysis was performed to evaluate the ^{110m}Ag source term for a typical PBMR core design [24]. Readily available German irradiation test data was used in a calculation model that could utilize both diffusion and MVR transport through SiC layers [8]. The evaluation performed did not attempt to establish whether the MVR transport mechanism is a valid physical explanation for silver transport through SiC, but only assessed the ability of the model to reproduce real experimental results. Two statistical quantities are required for MVR analyses: nano tube failures (NTF) and the total nano-tube cross-sectional surface. For example, an NTF of 10% would mean that 10% of 14 400 particles in a sphere would release Ag through nano-tubes and the other 90% would fully contain all Ag inside the particle. NTF is a statistical quantity since it could vary from sphere to sphere depending on the reasons for the existence of nano-tubes. NTF can be determined from observed Ag release fractions from available test data if the nano-tube cross-sectional surface is known or fixed.

Since NTF has never been observed in coated fuel particles, it is impossible to know the value of the cross-sectional surface. For each particle, a fixed, accumulated total nano-tube diameter of 2.5 x 10^{-7} m was used in this work. If it is assumed that an average nano-tube has a diameter of 20 nm, then 2.5 x 10^{-7} m would correspond to about 156 nano-tubes per particle or 70 nano-tubes/mm^2. All values listed here are arbitrary; they were selected based on the fact that these values could reproduce the limited available data reasonably well in a first evaluation. It was also assumed that released activities reported in German irradiation test reports were actual measured activities on collection cups used in the experiments at the end of the irradiation period. This would overestimate release fractions since ^{109}Ag activation to ^{110m}Ag on plated-out surfaces would be far more than neutronic removal of ^{110m}Ag from these surfaces. These effects were included in the calculation model.

Test results and corresponding NTF are listed in Table 2. In total 12 irradiation tests have been analysed. From this an average NTF value and a 95% confidence interval have been determined to be used as input into ^{110m}Ag release calculations for a PBMR core. Experiment R2-K12/1 had an exceptional high silver release and could be considered an outlier. Considering all test results, an average NTF value of 7.51% was derived. By excluding the possible outlier R2-K12/1, the NTF value decreases to 4.71% [8].

The NTF value of 7.51% was used in an MVR calculation model to compare with a simplified diffusion model (recoil and sorption ignored) and experimental measured data. The diffusion model used currently accepted diffusion constant and activation energies described in the literature [2]. Fractional releases for both MVR and diffusion calculations are listed in Table 2 and presented in Figure 9.

It can be seen that at temperatures below 1 050 °C, MVR calculates slightly higher releases than diffusion, but for temperatures above 1 150 °C, both models over-predict silver release, with diffusion predicting the highest releases. This is because of the possible outlier R2-K12 being included in the NTF value and the strong temperature-dependence of the silver diffusion coefficient in SiC. Even though diffusion generally predicts higher releases, in the critical region 970 °C to 1 120 °C MVR predicts slightly higher releases. The MVR and diffusion models used in this evaluation concentrated on SiC retention and ignored sorption effects. This causes a difference of up to one order of magnitude in the estimated source term by MVR and PBMR diffusion calculation models. This raised the concern that the ^{110m}Ag source term may be underestimated for PBMR safety analyses which in turn led to the revaluation of the diffusion model described in the next paragraph.

Table 2: MVR (NTF) and Diffusion Evaluation

Experiment	Irradiation Time (EFPD)	Maximum Fuel Temperature	FIMA (%)	NTF (%)	Fractional Silver Release	MVR Fractional Release	Diffusion Fractional Release
R2-K12/1	308	1 100	11.1	38.26	3.30E-02	6.42E-03	7.48E-03
R2-K12/2	308	1 280	12.4	1.37	1.40E-02	8.19E-02	1.77E-01
R2-K13/1	517	1 170	10.2	3.74	3.90E-02	8.17E-02	1.22E-01
R2-K13/4	517	980	9.8	2.46	2.70E-03	8.29E-03	7.08E-03
HFR K3/1	359	1 200	7.5	0.37	2.20E-03	4.61E-02	5.18E-02
HFR K3/4	359	1 220	9	3.52	1.80E-02	3.94E-02	7.32E-02
FRJ2 K13/1	396	1 125	7.5	5.75	1.90E-02	2.49E-02	1.64E-02
FRJ2 K13/2	396	1 150	8	5.47	2.00E-02	2.76E-02	2.83E-02
FRJ2 K13/3	396	1 150	7.9	4.237	1.70E-02	3.04E-02	3.05E-02
FRJ2 K13/4	396	1 120	7.6	13.25	3.90E-02	2.17E-02	1.46E-02
FRJ2 K15/1	533	970	14.1	10.54	7.50E-04	5.34E-04	3.99E-04
FRJ2 K15/2	533	1 150	15.3	1.12	3.20E-03	2.18E-02	1.00E-01

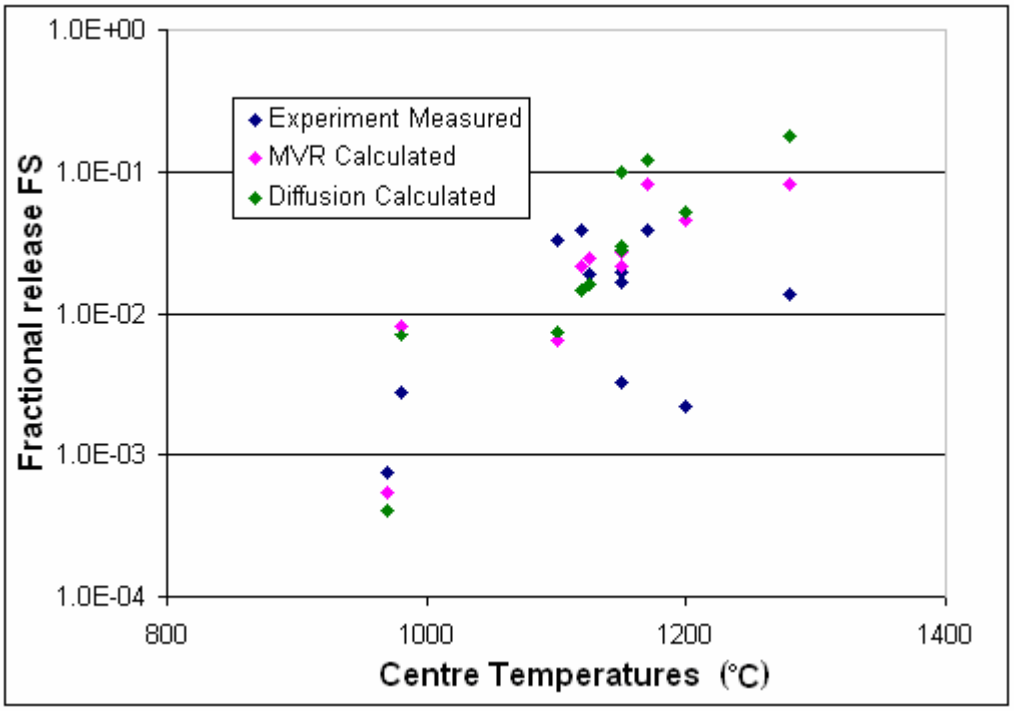

Figure 9: Fractional ^{110m}Ag Release: Experiment vs. MVR vs. Diffusion

4.3 Diffusion Model

After the interesting results of the MVR evaluation, it became clear that the diffusion model used at PBMR must be re-evaluated and proven not to underestimate the ^{110m}Ag source term under all operating conditions or be replaced by a MVR-type calculation model. However, no verification and validation (V&V) had been performed on the MVR calculation model, which would include a proper in-depth evaluation of all applicable German irradiation tests. It was decided to evaluate applicable German irradiation tests first with an updated diffusion calculation model based on a first estimate evaluation of all data. This is to be followed by an in-depth evaluation of all the German irradiation results by either a diffusion model (if the first estimate evaluation showed diffusion to be acceptable) or a MVR calculation model (should diffusion be found unacceptable). The first estimate evaluation is described in the following paragraph.

4.3.1 First estimate evaluation

A first evaluation of all data was performed to get a first estimate of all transport parameters to be used during detailed evaluations of each selected irradiation test [24]. In Figure 10 fractional releases for 31 selected irradiation tests (from Table 1) are plotted against maximum centre temperatures achieved during irradiation.

All data points below 1 100 °C were fitted by one line and all data points 1 100 °C and higher by a second fitting line. These fitting lines represent the average of the data for the two temperature regimes and provide guidelines as to where a diffusion curve should go through the plotted experimental data. All data points are plotted and are considered equally important for this first estimate.

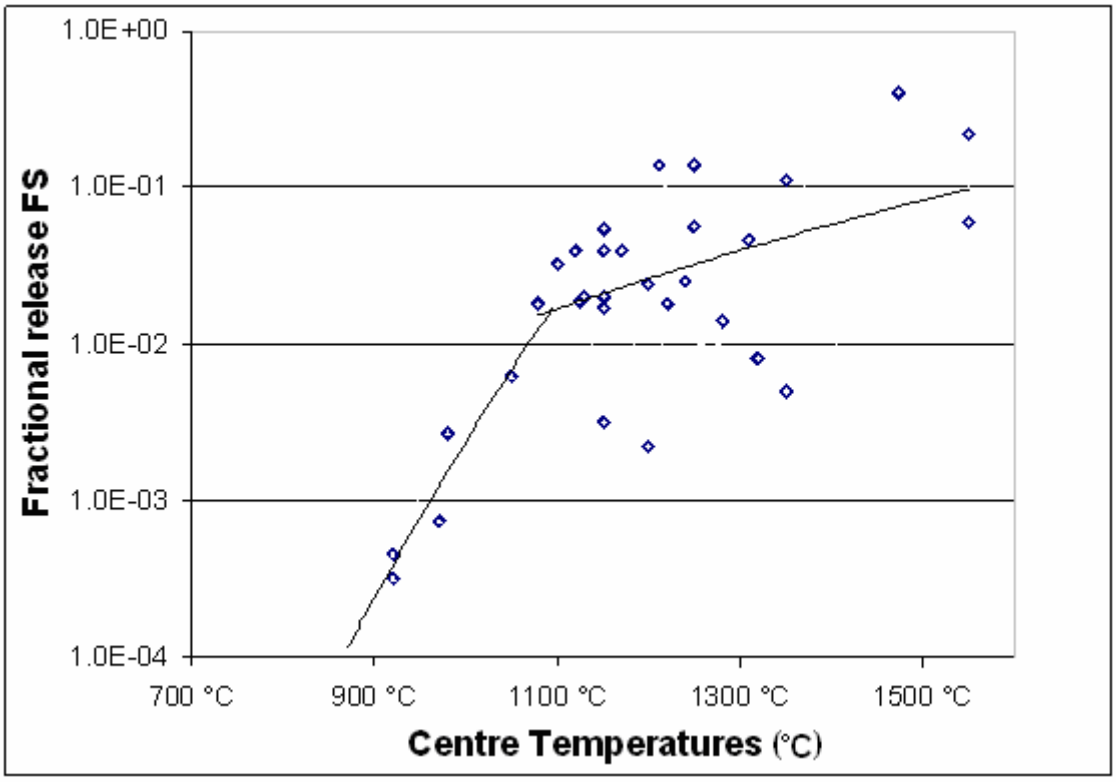

Figure 10: Fractional ^{110m}Ag Release after Irradiation

Based on analyses of natural silver contamination in sphere cups and capsules [25] and the expected natural silver contamination in matrix material, a natural silver contamination of 0.8 ng/g Ag/C was suggested [26]. Approximately 48.7% of natural silver is ^{109}Ag and the graphite cups housing each test sphere are assumed to be of equal volume. It was also decided to use the standard verified GETTER routines and to include all contaminations in the matrix material contamination of the fuel. Considering the above, a slightly conservative 8 x 10^{12} atoms/cm^3 ^{109}Ag/C was used as GETTER input.

The majority of released silver is released as fission product ^{109}Ag before being activated to ^{110m}Ag. Released ^{109}Ag is deposited on cups and capsules that house the test spheres. Contrary to what happens in a reactor, released ^{109}Ag is not removed from the neutron flux field and deposited in the cooler areas of the main power system, but remain in the neutron flux field. ^{109}Ag continues to be activated in the cups and capsules at a similar rate to what ^{109}Ag is activated in the fuel elements.

Fractional release is experimentally determined by comparing the ^{110m}Ag activity on the cups and capsules that house the test spheres and the total ^{110m}Ag produced during irradiation. The ratios of ^{109}Ag released to ^{109}Ag produced (the ^{109}Ag fractional release) and ^{110m}Ag released to ^{110m}Ag produced (the ^{110m}Ag fractional release) is therefore the same as long as the released silver nuclides remain in the same irradiation field as the fuel. The differences between ^{109}Ag and ^{110m}Ag absorption cross sections and neutron flux spectra in the fuel and cups cause differences between production of ^{110m}Ag from ^{109}Ag of less than 10% [27]. This is less than the expected measurement uncertainty of ^{110m}Ag on cups and capsules or the calculated ^{110m}Ag inventory in the test spheres (~10%), cross section uncertainties (~20%) and flux uncertainties (10%) [27]. Therefore this assumption is adequate as a first estimate. It was conservatively assumed that fuel spheres were irradiated at a constant centre temperature and fission power and coolant temperatures were adjusted accordingly.

A diffusion curve is drawn by using the existing accepted diffusion coefficient of Ag in SiC (IAEA data [2]) and the current diffusion calculation model used at PBMR. A new calculation model using parameters and models used to describe fission product recoil from fission sites, diffusion through UO_2, PyC and matrix materials and desorption from the fuel surface as was suggested in Chapter 3, was developed.

The SiC diffusion coefficient was adjusted so that a diffusion curve based on the new diffusion calculation model would follow the two fitted lines in Figure 10 as closely as possible. The two diffusion lines are shown in Figure 11. The new diffusion curve that matches the fitted lines as closely as possible should be considered a best estimate curve as it fits the average of the available data. Similarly, a new design limit diffusion curve was drawn by setting the SiC diffusion coefficient so that 95% of the experimental data lies below the diffusion curve. The design limit also includes the upper limit uranium and thorium fuel contamination, and design diffusion coefficients for PyC and matrix material transport. Both the best estimate and design limit curve show an inflection at approximately 900 °C. This the point where the contribution of the natural silver contamination to the silver source term becomes significant.

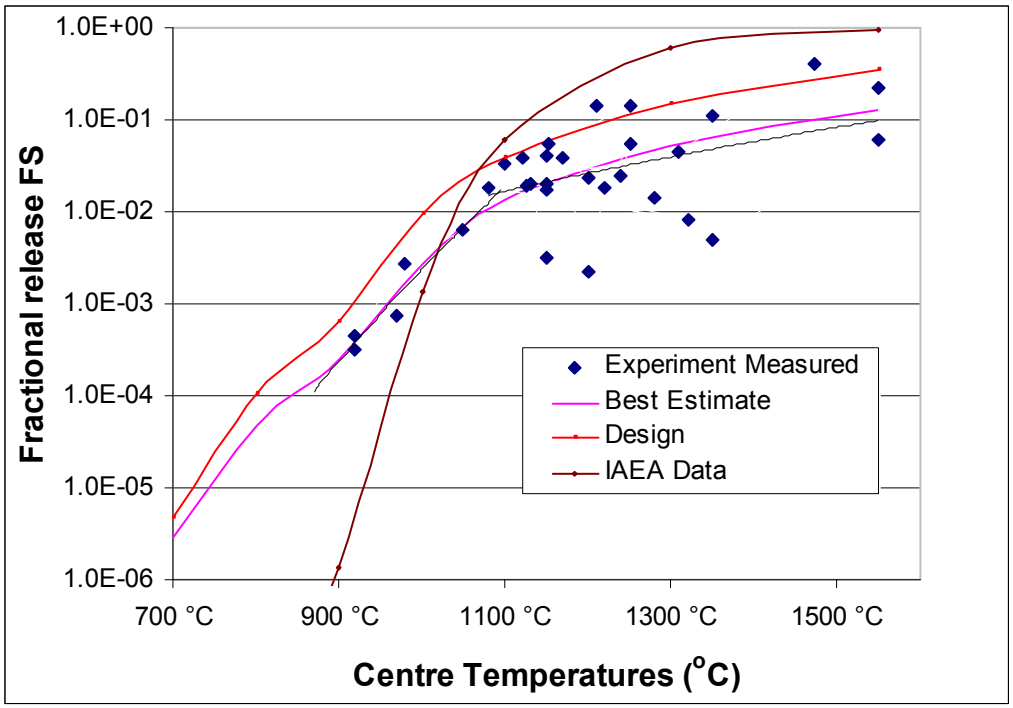

Figure 11: Fitted IAEA, and First Estimate Best Estimate and Design Limit Curves

The biggest difference between the old diffusion curve and the two new curves are the SiC diffusion constant and activation energy and are as follows:

IAEA best estimate [2]: $D = 3.60 \times 10^{-9} e^{-215/RT}$ m^2s^{-1}

First estimate best estimate: $D = 1.70 \times 10^{-15} e^{-63/RT}$ m^2s^{-1}

First estimate design limit: $D = 1.30 \times 10^{-14} e^{-75/RT}$ m^2s^{-1}

The very small activation energy for silver diffusion appears very radical and seems to contradict the findings of previous work [3], but it is much less drastic than the suggested molecular vapour transport release model. The new suggested SiC diffusion coefficient from this first estimate analyses is plotted with the current IAEA best estimate diffusion coefficient as a function of temperature in Figure 12. Figure 11 shows that a carefully selected set of diffusion constants can in principle simulate the irradiation tests results. This analysis showed that diffusion theory remains a viable option to model transport of silver and that further detailed analyses of all applicable irradiation tests are required.

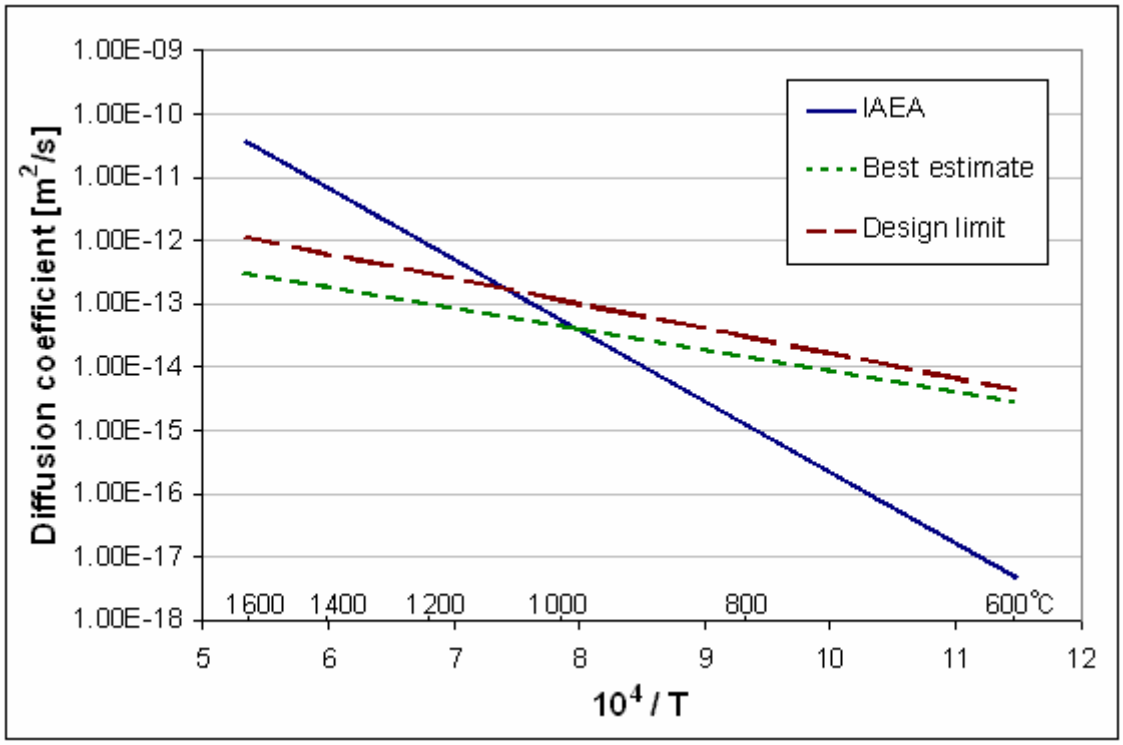

Figure 12: IAEA and First Estimate Best and Design SiC Diffusion Coefficients

5. Detailed Evaluation

After first estimate diffusion analyses showed that an effective diffusion model is still a viable solution to predict silver transport and release from TRISO particle spherical fuel, detailed analyses of all high and medium applicable tests (Table 1) were performed.

Detailed evaluation starts with fuel spheres from the top of the table, performing analyses of the most important tests first.

5.1 HFR-K3

5.1.1 Reactor

The High Flux Reactor (HFR) at Petten, the Netherlands, is a closed-tank in-pool type material testing reactor, being in operation since 1962 with a thermal power of 45 MW [28]. It is a light water moderated, beryllium reflector water-cooled reactor with fast and thermal fluxes in the order of 4.5×10^{18} $m^{-2}s^{-1}$ and 2.4×10^{18} $m^{-2}s^{-1}$ respectively. The reactor was extensively used in the British and German HTR programmes. Special full-scale rigs were developed to test HTR fuel elements under realistic conditions, with appropriate correlation between burn-up, neutron fluence, and temperature.

Four spherical fuel elements were tested simultaneously in a so-called BEST-rig. Each rig contained four individual and independently-monitored capsules arranged in line. A binary mixture of helium and neon achieved temperature control, with helium providing the best cooling.

Fluence, temperature and fission product release were measured for each capsule in real time. Full sphere irradiation tests of interest performed were HFR-K3, -K5 and -K6. Several other irradiation tests were done on fuel and compacts but only these three experiments are of interest for modern fuel evaluation. Unfortunately, the HFR-K5 and -K6 tests were performed at the end of the German HTR programme when interest had waned. Post-irradiation evaluation of tests spheres and fuel rig materials was not done in time and no measurements of silver release from these tests were recorded. The earlier irradiation test HFR-K3 underwent comprehensive post-irradiation testing and heating examinations.

5.1.2 Irradiation test

Four elements from Arbeitsgemeinschaft Versuchsreaktor (AVR) reload 19 with LEU-TRISO fuel were inserted into the core inside a three-capsule BEST rig. The middle capsule contained two spheres with both outer capsules containing one sphere each. Each capsule consisted of a steel container with graphite cups which housed the test spheres. Fuel spheres were numbered 1, 2, 3 and 4 starting from the top with planned irradiation temperatures of 1 020 °C, 700 °C, 700 °C and 1 020 °C surface and 1 200 °C, 920 °C, 920 °C and 1 200 °C centre, respectively [29]. Instrumentation consisted of thermocouples, flux monitors and SPN-monitors, as well as sweep and temperature regulation tubes for each single capsule.

The placement of flux detectors and thermocouples relative to the four fuel spheres in the irradiation rig are shown in Figure 13. Due to flux gradients present in the HFR irradiation positions used, the rig was turned through 180^{o} during the test in order to minimize the effect of gradients inside the fuel elements. HFR-K3 started on 15 April 1982 and ended successfully on 5 September 1983. Burn-up values of 10.6% FIMA were attained, with fast fluences of 6.3 x 10^{25} m^{-2}. Heating tests up to 1 800 °C were conducted during the post-irradiation examination. The objectives for this test were as follows [25]:

a. Accelerated reference test on LEU-TRISO fuel spheres for an HTR steam cycle process heat applications.

b. Providing irradiation data and Post-irradiation Examination (PIE) results for a data set of a licensable fuel element for HTR with LEU cycle.

c. Examination of mechanical performance of particles of 1981 standard quality.

d. Determination of release of relevant fission product nuclides from the fuel elements.

e. Testing of the BEST-rig with sweep and regulation gas circuits and out of pile experimental installations at the HFR.

Post-irradiation examination was completed, with ceramographic examinations on particles from test element HFR-K3/1 after a high-temperature annealing test, and fission product inventories measured on all four test elements. All capsule components and graphite cups were leached and fission products in the solutions determined with gamma spectrometry. Further gamma spectrometric measurements were made of drilling samples in the fuel-free zone of the fuel elements to determine ^{137}Cs and ^{110m}Ag profiles in the fuel-free zone. This was a two times accelerated test that ran for 359 Effective Full Power Days (EFPD).

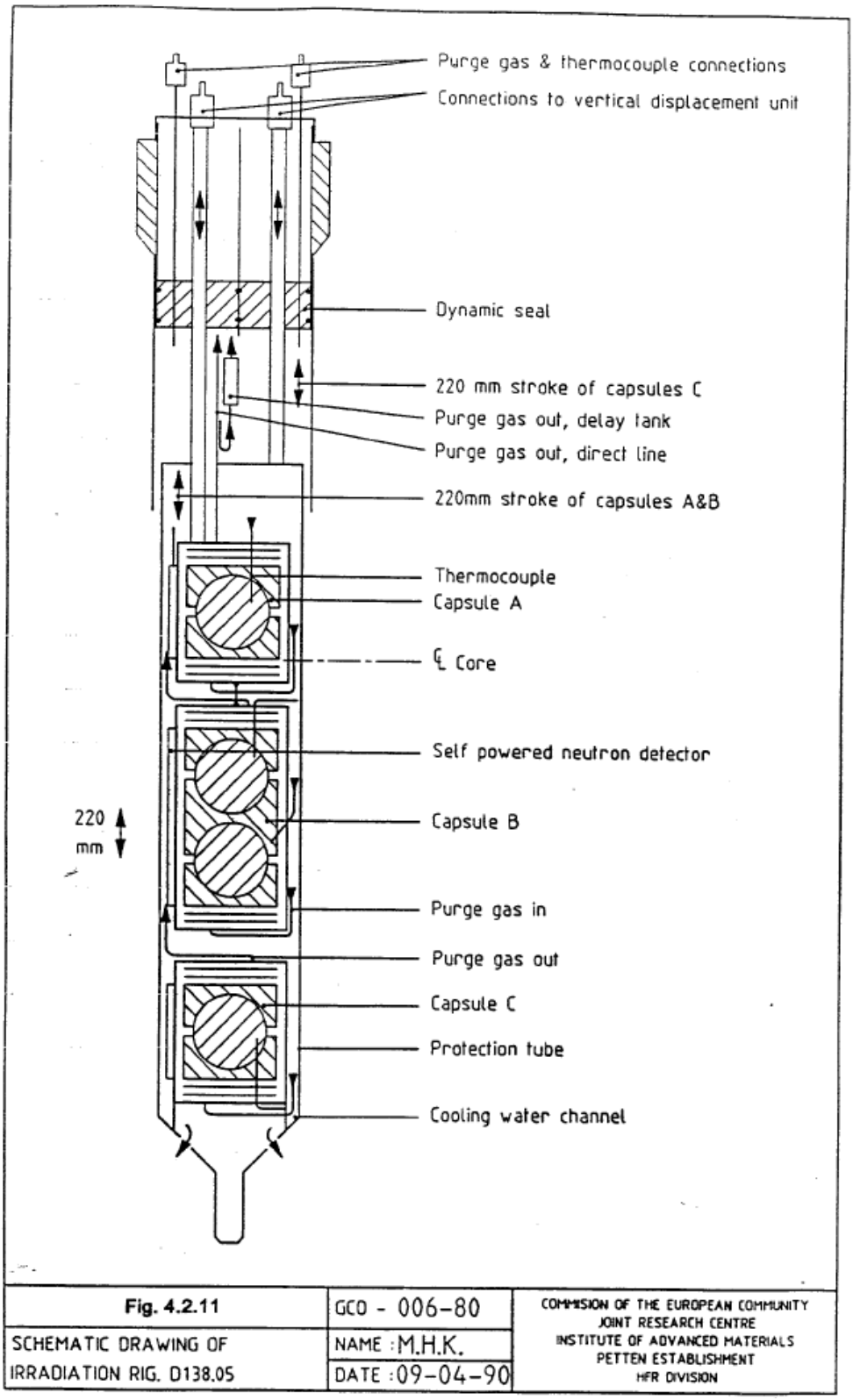

Figure 13: HFR-K3: Flux Detector and Thermocouple Placement

Due to the neutron flux gradient present in the HFR, the rig was turned 180° several times during irradiation to minimize the effect of uneven azimuthal burn-up. Burn-ups of 7.5, 10.0, 10.6, and 9.0% FIMA and fast fluences of 4.1, 5.8, 5.9 and 4.3 x 10^{25} m^{-2} for the four tests spheres respectively were achieved [30]. The ^{85m}Kr fractional release remained very low (< 10^{-6}) so it can be assumed that no particles failed during irradiation nor were there any particles defective from manufacture.

AVR reload 19 is comparable with PBMR design fuel, and the irradiation conditions of HFR-K3 are acceptable and comparable to expected PBMR operational conditions. The data received from HFR-K3 progress reports and post-irradiation examination reports is sufficient to evaluate silver transport. Important test element data of HFR-K3 is listed in Table 3 with expected PBMR fuel specification and irradiation data.

Table 3: HFR-K3 Test Element Specification and Irradiation Data

Parameter	Unit	1	2	3	4	PBMR
Specification						
Uranium content	g	10.22	10.22	10.22	10.22	9.00
^{235}U enrichment	%	9.82	9.82	9.82	9.82	9.6
CP content		16 350	16 350	16 350	16 350	~ 14 500
Failed CP content	per FE	0	0	0	0	~ 0.2[(b)]
Irradiation data						
Burn-up (FIMA)	%	7.53	10.02	10.57	8.97	9.8
Neutron fluence (> 0.1 MeV)	10^{25} m^{-2}	4.1	6.1	6.3	4.3	2.7
Average centre temperature[(a)]	°C	1 247	1 121	1 115	1 278	1 040
Max power output	kW/FE	2.72	3.41	3.61	3.42	2.1

a. Calculated from the measured surface temperature and FE power output.

b. 1.44 x 10^{-5} failure fraction[1] x 14 500 particles per FE.

[1] The failure fraction from manufacture used for PBMR design analysis of 1.44 x 10^{-5} was derived statistically from German fuel manufacturing experience.

5.1.3 Evaluation

A first evaluation of HFR-K3 fission product release was performed by Christ in 1985, shortly after completion of the first post-irradiation examination [26]. After this evaluation more information about the irradiation test was released and further examinations of the fuel and rig materials changed original fluxes, estimated burn-ups, and temperatures achieved. Further evaluations were performed on this test (e.g. [31] and, most notably, unpublished work by Venter [32]).

5.1.3.1 Input data

A thorough evaluation of thermocouple performance was performed by Venter [32]. As is the case with most irradiation tests [33], a number of thermocouples failed during irradiation with a resulting loss of important temperature data. Thermocouples placed on the surfaces of fuel spheres indicated temperatures several degrees lower than those embedded in fuel-free regions of fuel spheres. This is especially clear for capsules 1, 2, and 4. It is to be expected that there would be a difference between temperatures measured on fuel sphere surfaces and temperatures measured 3 mm from the surface but, as graphite is a good conductor of heat, one would expect a difference of a few degrees at most and not 100 to 200 degrees Celsius.

Thus all temperatures measured by surface thermocouples are suspect and should be discarded. Unfortunately capsule 3 had six surface thermocouples and only one embedded thermocouple. Temperature values for the embedded thermocouple form the upper bound for capsule 3 temperatures and it is safe to conclude that all surface temperatures for this capsule are too low and should be discarded. There are also some temperature values that are obviously wrong and these were also discarded. Cycle-averaged temperatures calculated using only data from embedded thermocouples are shown in Table 4. Also included in the table for comparison is cycle-averaged temperature data obtained from the RUBICON data handling computer code used at HFR. The evaluation of HFR-K3 test spheres was performed with both sets of temperature data.

Table 4: HFR-K3: Cycle Averaged Temperature Data

Cycle Number	Capsule 1		Capsule 2		Capsule 3		Capsule 4	
	Venter	RUBICON	Venter	RUBICON	Venter	RUBICON	Venter	RUBICON
82.04	967	950	703	790	705	735	969	987
82.05	941	960	729	732	705	735	986	975
82.06	944	958	786	739	753	712	996	968
82.07	982	999	727	704	725	718	993	1 010
82.08	981	989	754	725	722	713	1 003	999
82.09	983	987	741	705	725	716	989	985
82.10	990	1 032	767	745	729	721	1 023	1 021
82.11	997	1 034	749	720	733	726	1 017	1 016
83.01	1 027	1 040	763	737	740	728	1 015	1 013
83.02	1 032	1 044	777	761	747	740	1 029	1 037
83.03	1 022	1 044	777	761	744	740	1 028	1 037
83.04	1 037	1 044	772	755	750	741	1 045	1 050
83.05	1 021	-	772	745	750	737	1 037	1 024
83.06	1 028	-	765	745	742	735	1 036	1 038
83.07.1	1 025	-	793	780	747	733	1 040	-
83.07.2	1 025	-	798	780	742	740	1 040	1 020

Table 5: HFR-K3: Thermal and Fast Neutron Fluxes (x 10^{18} $m^{-2}s^{-1}$)

Cycle Number	Capsule 1		Capsule 2		Capsule 3		Capsule 4	
	Thermal	Fast	Thermal	Fast	Thermal	Fast	Thermal	Fast
82.04	0.862	1.24	1.10	1.93	1.11	1.95	0.900	1.29
82.05	0.834	1.23	1.06	1.87	1.07	1.89	0.870	1.28
82.06	0.908	1.30	1.14	1.97	1.15	1.99	0.940	1.36
82.07	0.909	1.38	1.15	1.94	1.16	1.95	0.940	1.45
82.08	0.887	1.43	1.13	2.33	1.14	2.35	0.920	1.45
82.09	0.874	1.34	1.12	1.95	1.13	2.07	0.920	1.40
82.10	0.849	1.31	1.08	2.03	1.09	2.05	0.890	1.38
82.11	0.882	1.38	1.13	2.06	1.14	2.08	0.920	1.39
83.01	0.890	1.35	1.14	2.12	1.15	2.13	0.930	1.42
83.02	0.859	1.32	1.11	1.99	1.12	2.01	0.910	1.37
83.03	0.847	1.31	1.08	2.01	1.09	2.03	0.890	1.36
83.04	0.862	1.38	1.17	2.10	1.18	2.12	0.960	1.43
83.05	0.900	1.23	1.16	1.08	1.17	1.90	0.950	1.31
83.06	0.802	1.32	1.03	2.03	1.04	2.08	0.850	1.37
83.07.1	0.810	1.32	1.03	1.88	1.04	1.90	0.840	1.32
83.07.2	0.838	1.36	1.07	1.99	1.08	2.01	0.880	1.32

Neutron fluxes were taken from the metrology report [30], the first HFR-K3 evaluation [26], and updated with corrections made by Venter [32]. Thermal and fast neutron fluxes are tabled in Table 5. The cross sections used in the burn-up calculation were based on cross sections used in previous HFR evaluations [34] and updated to yield correct fission power and burn-up values.

Table 6: HFR-K3: Gamma Heating (W)

Cycle Number	Capsule 1		Capsule 2		Capsule 3		Capsule 4	
	Venter	Christ	Venter	Christ	Venter	Christ	Venter	Christ
82.04	619	810	964	900	964	900	644	855
82.05	614	770	934	860	954	860	639	815
82.06	649	830	984	930	1 019	930	679	880
82.07	689	880	1173	980	1 083	980	724	930
82.08	714	830	974	920	1 098	920	724	875
82.09	669	810	1 024	900	1 049	900	699	855
82.10	654	740	1 014	830	1 014	830	689	785
82.11	689	800	1 029	890	1 058	890	694	845
83.01	674	820	1 059	910	1 058	910	709	865
83.02	659	800	1 004	880	1 039	880	684	840
83.03	654	690	999	760	1 019	760	679	725
83.04	689	810	1 054	900	1 068	900	714	855
83.05	614	820	939	910	949	910	654	865
83.06	659	700	1 014	780	1 039	780	684	740
83.07.1	659	690	1 034	770	1 034	770	659	730
83.07.2	679	710	994	790	1 039	790	679	750

Gamma heating has been calculated by both Christ [26] and Venter [32]. The method used by Christ is not available in the literature but Venter's method is well described in the reference. Gamma power values were deduced from data from the HFR-K6 irradiation test from two different locations in the HFR core. A linear relationship between gamma power and fast neutron (E > 0.1 MeV) flux was observed and a linear least squares fit was performed. It was found that the gamma power could be expressed by a fitted line:

$$P = 2.3861 \ \phi_{E>0.1MeV} \tag{17}$$

Both Christ and Venter gamma heating results are tabled in Table 6.

5.1.3.2 Evaluation results

Fission powers produced during irradiation and total burn-up achieved were calculated first to ensure that calculated temperatures are as close as possible to actual values. The fission powers were calculated using the best available thermal neutron fluxes (Table 5) and cross sections from later HFR irradiation tests [34] that have been corrected to yield the correct burn-up. These newly calculated fission powers where then used with estimated gamma heating (Table 6) to determine fuel temperatures. He/Ne coolant gas temperatures were adjusted to ensure that calculated and measured surface temperatures (Table 4) agree. Centre fuel temperatures were then calculated from surface temperatures and total power produced (fission and gamma) in each test sphere. Fission powers (in watt), and surface and centre temperatures (all in ^{o}C) for all four test spheres have been determined using both Christ and Venter data and are listed in Table 7 to Table 10.

Table 7: HFR-K3/1: Fission Power (W), Surface and Centre Temperatures (^{o}C)

Cycle Number	Venter Data			Christ Data		
	Fission Power	Surface Temperature	Centre Temperature	Fission Power	Surface Temperature	Centre Temperature
82.04	2 294	967	1 217	2 724	950	1 210
82.05	2 236	941	1 188	2 498	960	1 215
82.06	2 384	944	1 217	2 580	958	1 240
82.07	2 358	982	1 254	2 456	999	1 279
82.08	2 261	981	1 247	2 281	989	1 260
82.09	2 171	983	1 238	2 140	987	1 250
82.10	2 025	990	1 232	1 983	1 032	1 275
82.11	2 050	997	1 241	1 972	1 034	1 278
83.01	1 996	1 027	1 260	1 905	1 040	1 280
83.02	1 875	1 037	1 250	1 759	1 044	1 264
83.03	1 776	1 022	1 235	1 680	1 044	1 255
83.04	1 870	1 037	1 247	1 658	1 044	1 260
83.05	1 788	1 021	1 229	1 662	1 021	1 241
83.06	1 543	1 028	1 216	1 430	1 028	1 219
83.07.1	1 510	1 025	1 212	1 410	1 025	1 214
83.07.2	1 544	1 025	1 216	1 436	1 025	1 218

Table 8: HFR-K3/2: Fission Power (W), Surface and Centre Temperatures (^{o}C)

Cycle Number	Venter Data			Christ Data		
	Fission Power	Surface Temperature	Centre Temperature	Fission Power	Surface Temperature	Centre Temperature
82.04	3 352	703	1 037	3 410	790	1 121
82.05	3 244	729	1 097	3 355	732	1 106
82.06	3 398	786	1 195	3 393	739	1 153
82.07	3 294	727	1 161	3 233	704	1 124
82.08	3 091	754	1 159	3 006	725	1 123
82.09	2 911	741	1 140	2 823	705	1 126
82.10	2 669	767	1 141	2 589	745	1 104
82.11	2 662	749	1 129	2 588	720	1 089
83.01	2 559	763	1 135	2 498	737	1 099
83.02	2 374	777	1 127	2 328	761	1 102
83.03	2 231	777	1 114	2 198	761	1 081
83.04	2 333	772	1 126	2 311	755	1 099
83.05	2 212	772	1 108	2 208	745	1 082
83.06	1 893	765	1 073	1 903	745	1 041
83.07.1	1 844	793	1 092	1 867	780	1 065
83.07.2	1 881	798	1 098	1 916	780	1 073

Table 9: HFR-K3/3: Fission Power (W), Surface and Centre Temperatures (^{o}C)

Cycle Number	Venter Data			Christ Data		
	Fission Power	Surface Temperature	Centre Temperature	Fission Power	Surface Temperature	Centre Temperature
82.04	3 612	705	1 056	3 794	735	1 101
82.05	3 489	705	1 099	3 591	735	1 132
82.06	3 633	753	1 194	3 610	712	1 153
82.07	3 502	725	1 178	3 424	718	1 156
82.08	3 272	722	1 154	3 171	713	1 123
82.09	3 069	725	1 147	2 969	716	1 116
82.10	2 806	729	1 127	2 716	721	1 096
82.11	2 788	733	1 135	2 709	726	1 107
83.01	2 674	740	1 132	2 612	728	1 104
83.02	2 476	747	1 118	2 432	740	1 095
83.03	2 325	744	1 099	2 297	740	1 074
83.04	2 424	750	1 120	2 413	741	1 099
83.05	2 297	750	1 094	2 506	737	1 108
83.06	1 968	742	1 064	1 991	735	1 042
83.07.1	1 917	747	1 062	1 955	733	1 036
83.07.2	1 953	742	1 062	2 006	740	1 049

Table 10: HFR-K3/4: Fission Power (W), Surface and Centre Temperatures (^{o}C)

Cycle Number	Venter Data			Christ Data		
	Fission Power	Surface Temperature	Centre Temperature	Fission Power	Surface Temperature	Centre Temperature
82.04	2 878	969	1 276	3 426	987	1 306
82.05	2 803	986	1 285	3 092	975	1 284
82.06	2 976	996	1 313	3 126	968	1 300
82.07	2 886	993	1 307	2 937	1 010	1 334
82.08	2 721	1 003	1 304	2 707	999	1 310
82.09	2 608	989	1 282	2 550	985	1 288
82.10	2 416	1 023	1 293	2 332	1 021	1 297
82.11	2 394	1 017	1 287	2 290	1 016	1 295
83.01	2 319	1 015	1 279	2 202	1 013	1 286
83.02	2 172	1 029	1 276	2 048	1 037	1 291
83.03	2 058	1 028	1 265	1 934	1 037	1 275
83.04	2 149	1 045	1 286	2 014	1 050	1 298
83.05	2 040	1 037	1 266	1 907	1 024	1 269
83.06	1 764	1 036	1 245	1 646	1 038	1 250
83.07.1	1 700	1 040	1 240	1 518	1 040	1 241
83.07.2	1 751	1 040	1 247	1 638	1 030	1 243

The fractional releases of silver from the test spheres during irradiation are listed in Table 11. Fractional releases are simply the total measured released ^{110m}Ag activity divided by the total ^{110m}Ag inventory in the fuel sphere. For test sphere 3, no measured value is reported for the graphite cup. It is not possible that there is no silver in the graphite cup. Some silver must be measurable just from contamination sources alone. The absence of a value means that the measurement failed and not that no silver was measurable.

Comparing fractional releases from sphere 2 and other test spheres, it can be conservatively estimated that the fractional release on the graphite cup should be between 1.6 and 2.2 x 10^{-4}. For the sake of conservatism in nuclear analyses, the higher value is included in the total fractional release.

Table 11: Fractional ^{110m}Ag Release from Fuel Elements of HFR-K3 [25]

Fuel Sphere	Steel Capsule	Graphite Cup	Total Fractional Release
1	1.0 x 10^{-3}	1.2 x 10^{-3}	2.2 x 10^{-3}
2	2.3 x 10^{-4}	2.2 x 10^{-4}	4.5 x 10^{-4}
3	1.6 x 10^{-4}	(2.2 x 10^{-4})	3.8 x 10^{-4}
4	2.1 x 10^{-3}	1.6 x 10^{-2}	1.8 x 10^{-2}

Measured values were obtained by dissolving the graphite cups that surrounded fuel spheres during irradiation and by leaching the surfaces of the stainless steel containers and measuring the ^{110m}Ag concentration in the liquids. Thus there are some additional sources of ^{110m}Ag in fuel spheres and graphite cups that should be considered; firstly the natural uranium and thorium contamination of the graphite cups that housed the test spheres.

The total mass of the graphite cups that house each sphere (~190 g) is approximately the same as the mass of graphite in a test sphere (~200 g). It can be conservatively assumed that uranium and thorium contamination in the graphite cups is at least as much as the contamination in the fuel sphere. This graphite contamination was reduced to an effective uranium contamination only and added to the fuel-free zone contamination.

In addition to natural uranium and thorium contamination in the cups, the graphite of which the cups and fuel spheres are manufactured also contains silver as an impurity. Christ [26] gives a value of 0.8 ± 0.5 ng/g for the concentration of silver in the graphite used for fuel spheres and graphite cups. Thus a fuel sphere of mass 209 g of which 200 g is graphite, will contain 1.6 x 10^{-7} grams of silver. The number of silver atoms in the fuel sphere will be 8.8 x 10^{14} atoms. Only 48% of these will be ^{109}Ag so that the number of ^{109}Ag atoms is 4.2 x 10^{14} atoms. For a 60 mm diameter sphere, the volume concentration of ^{109}Ag in a fuel sphere will be between 3.7 and 6.0 x 10^{12} ^{109}Ag atoms per cm^3. In the Gontard report [25] the natural silver contamination in A3-27 is estimated at 2.7 ng/g, which translates to about 1.3 x 10^{13} ^{109}Ag atoms per cm^3.

The graphite cups and steel capsules also contain silver as a contaminant. At Studsvik during the R2-K12 irradiation tests, the reserve graphite cups used in that irradiation rig were measured prior to irradiation. Silver contamination was found to be as high as 180 ng/g [25], and for low-temperature irradiation tests, these contaminations dominate the measured silver outside the test sphere. Therefore, total silver contaminations between 8 x 10^{12} and 2.6 x 10^{13} ^{109}Ag atoms per cm^3 for each test capsule must be considered.

Using all input data from both Christ and Venter discussed in paragraph 5.1.3.1, and contamination sources discussed above, diffusion coefficients were derived for all four test spheres in Table 12. The temperatures and diffusion coefficients listed are the average centre fuel temperatures for each test sphere and diffusion coefficients at those specific temperatures. For the hotter test spheres there is very little difference between diffusion coefficients derived from the two data sets. For the two cooler test spheres, contamination of irradiation rig materials dominate measured release fractions and derived diffusion coefficients are much more dependent on the data set used. A range of contamination values was considered in order to derive realistic diffusion coefficients. For the purpose of final evaluation of all derived diffusion coefficients, the Venter data coefficients may be seen as the lower limit and the Christ data coefficients as the upper limit of the range of coefficients for this test.

Table 12: Derived Diffusion Coefficients: HFR-K3

Fuel Sphere	Venter Data		Christ Data	
	Temperature	Coefficient (m^2s^{-1})	Temperature	Coefficient (m^2s^{-1})
1	1 231 °C	7.75 x 10^{-18}	1 247 °C	7.63 x 10^{-18}
2	1 121 °C	6.58 x 10^{-18}	1 099 °C	1.37 x 10^{-17}
3	1 115 °C	5.96 x 10^{-18}	1 099 °C	1.50 x 10^{-17}
4	1 278 °C	2.54 x 10^{-17}	1 285 °C	2.55 x 10^{-17}

HFR-K3 is the most important irradiation test to evaluate not only silver but also caesium release from fuel from the German irradiation programme. It is the best-documented test that also underwent full post-irradiation examination and irradiation conditions achieved during the test is the most applicable to future HTRs. Diffusion coefficients derived here can therefore be considered the most valuable in deriving final transport data.

5.2 FRJ2-K13

5.2.1 Reactor

The FRJ2-DIDO reactor in Jülich, Germany, is a heavy-water-moderated and -cooled material test reactor with a nominal power of 32 MW_{th}. The facilities for irradiating samples in core are limited to a diameter of 52 mm. Full sphere tests are therefore not possible inside the core and fuel sphere tests are performed in reflector positions. The neutron spectra are therefore very well moderated and high fast fluences are precluded from fuel sphere test requirements. On the other hand, very high thermal neutron fluxes could be achieved as the irradiation rig could be moved into the radial maximum of the thermal neutron flux profile.

Similar to the HFR BEST-rig, four spherical fuel elements are tested simultaneously in a two individually swept capsule irradiation rig shown in Figure 14. Temperatures in the rig are measured by nine thermocouples, and temperature is controlled by a binary mixture of helium and neon. During reactor operation neutron fluxes are measured at various positions in the core in order to evaluate neutron fluxes at the irradiation positions. In addition the integrated fluence is measured with neutron activation wires inserted into ceramic and steel tubes. Full sphere irradiation tests of interest performed were FRJ2-K11, -K13 and -K15. Several other irradiation tests were done on compacts and fuel elements but only these three fuel experiments are considered for silver transport evaluation.

5.2.2 Irradiation test

Four elements with AVR reload 19 fuel spheres with LEU-TRISO fuel were inserted into the reflector outside the core in a two-capsule irradiation rig. Each capsule contained two spheres and consisted of a steel container with graphite cups which houses the test spheres. Fuel spheres were numbered as K13/1, K13/2, K13/3 and K13/4 with planned irradiation temperatures of 985 °C, 990 °C, 990 °C and 980 °C surface and 1 131 °C, 1 149 °C, 1 148 °C, 1 127 °C centre, respectively [29]. FRJ2-K13 started on 24 June 1982 and ended successfully on 12 February 1984. Burn-up values of 7.5, 8.0, 7.9, and 7.6% FIMA were attained, with fast fluences of ~0.2 x 10^{25} m^{-2}.

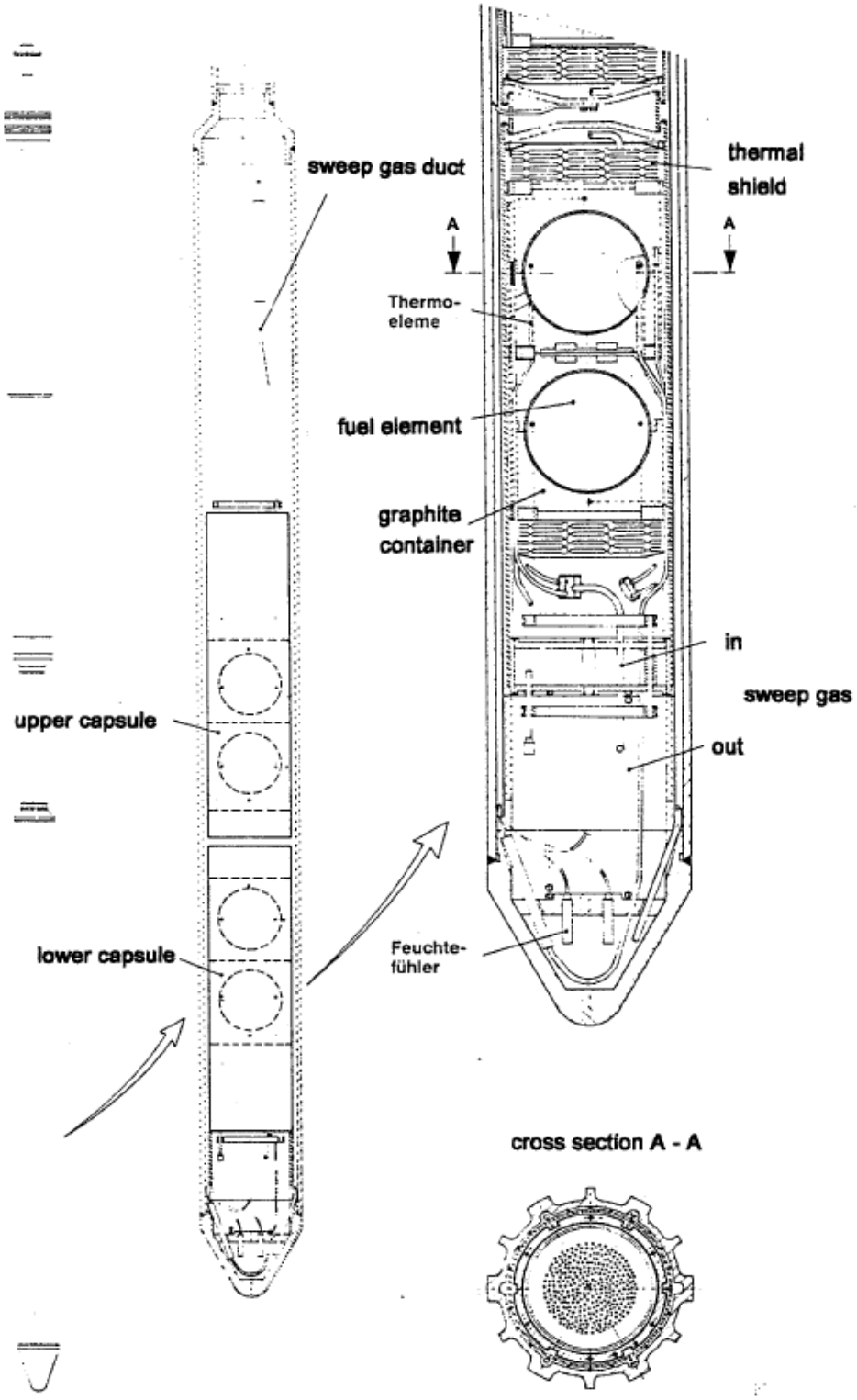

Figure 14: FRJ2-K13: Irradiation Rig

The objectives for this test were as follows [25]:

a. Irradiation test of AVR reload 19 fuel.

b. Providing irradiation data under highly controlled irradiation conditions.

c. Examination of coated particle performance without the influence of fast fluence.

d. Investigation of transport coefficients of metallic fission products.

e. Supplying irradiated fuel for accident simulation tests in the KÜFA.

Post-irradiation examination was completed, with full gamma spectrometric analyses and deconsolidation of the rig. All capsule components and graphite cups were leached and fission products in the solutions determined with gamma spectrometry. Further gamma spectrometric measurements were made by drilling samples in the fuel-free zone of the fuel elements to determine the ^{137}Cs and ^{110m}Ag profile in the fuel-free zones of test spheres 1, 2 and 3.

Test sphere FRJ2-K13/2 was heated after irradiation at 1 600 °C followed by deconsolidation of the element to get loose particles. Ceramographic investigations of these particles showed punctuated deposits of metallic fission products in the kernel and coagulated pores. Test sphere FRJ2-K13/4 underwent accident testing up to 1 800 °C. The test spheres were of the same manufacturing batch and all fuel sphere data used in evaluating silver transport are the same as for the HFR-K3 evaluation. The ^{85m}Kr fractional release remained very low ($< 10^{-6}$) so it can be assumed that no particles failed during irradiation nor were there any particles defective from manufacture.

5.2.3 Evaluation

Much less information about the irradiation conditions is available compared to HFR-K3, but measured irradiation temperatures are available from published graphs and good estimates of the neutron fluxes can be made from reported values [35]. Cross sections were selected to achieve correct burn-ups and plutonium contributions supplied in the literature [25]. Fission power values determined from a neutronic calculation and estimated gamma-powers were then used to determine fuel temperatures. Coolant gas temperatures were adjusted to ensure that calculated and measured surface temperatures agreed. Centre fuel temperatures were calculated from surface temperatures and total power produced (fission and gamma) in each test sphere. The fission powers (in watt) and the surface and centre fuel temperatures (in ^{o}C) are presented in Table 13 and Table 14.

Table 13: FRJ2-K13/1 and /2: Fission Power, Surface and Centre Temperatures

Cycle Number	K13/1			K13/2		
	Fission Power	Surface Temperature	Centre Temperature	Fission Power	Surface Temperature	Centre Temperature
1	1 640	985	1 106	1 829	985	1 123
2	1 630	995	1 116	1 801	1 000	1 140
3	2 086	980	1 135	2 385	990	1 173
4	1 971	1 005	1 154	2 231	1 010	1 185
5	1 872	1 000	1 143	2 100	995	1 160
6	1 781	980	1 116	1 982	980	1 136
7	2 400	985	1 172	2 548	995	1 199
8	2 288	990	1 169	2 416	980	1 174
9	2 176	995	1 166	2 283	1 000	1 188
10	2 017	985	1 145	2 098	995	1 165
11	2 072	980	1 145	2 120	990	1 164
12	1 809	995	1 140	1 858	1 005	1 166
13	1 710	985	1 124	1 746	985	1 131
14	1 591	980	1 110	1 613	995	1 133
15	1 674	980	1 116	1 675	970	1 112
16	1 747	975	1 120	1 727	975	1 124
17	1 641	980	1 118	1 617	990	1 133
18	1 533	970	1 100	1 503	985	1 119
19	1 432	975	1 097	1 398	990	1 117

Table 14: FRJ2-K13/3 and /4: Fission Power, Surface and Centre Temperatures

Cycle Number	K13/3			K13/4		
	Fission Power	Surface Temperature	Centre Temperature	Fission Power	Surface Temperature	Centre Temperature
1	1 812	1 000	1 139	1 663	970	1 092
2	1 785	1 005	1 144	1 652	975	1 097
3	2 364	985	1 167	2 113	965	1 121
4	2 214	1 010	1 183	1 995	975	1 124
5	2 085	1 000	1 165	1 894	980	1 123
6	1 968	995	1 151	1 801	975	1 112
7	2 532	990	1 193	2 424	980	1 168
8	2 401	995	1 189	2 311	985	1 166
9	2 270	1 000	1 185	2 196	975	1 147
10	2 088	980	1 150	2 035	980	1 141
11	2 111	975	1 148	2 088	970	1 135
12	1 851	995	1 150	1 822	1 000	1 147
13	1 740	990	1 137	1 722	985	1 124
14	1 607	975	1 112	1 601	975	1 106
15	1 670	980	1 122	1 684	985	1 122
16	1 724	975	1 124	1 756	980	1 126
17	1 613	985	1 127	1 650	1 000	1 139
18	1 500	990	1 124	1 541	990	1 122
19	1 395	980	1 106	1 439	980	1 104

Fractional releases of silver from test spheres during irradiation are listed in Table 15. The fraction of silver on the steel capsules for test spheres 1 to 3 has a constant value of 1.3×10^{-2} although fractions on the graphite cups vary between 3.7×10^{-3} to 7.5×10^{-3}, which suggests that the silver fraction from the steel capsules is dominated by some other source than the fuel sphere. This is out of line with measurements made after the HFR-K3, R2-K12 and R2-K13 irradiation tests where capsule steel fractions were always less than graphite cup fractions. The fraction of silver on the steel cups for test sphere 4 is 3.1×10^{-2} which is much higher than for the other spheres although the factions on the graphite cups remain comparable. The sphere 4 measurement must be questioned and most probably is a transcription error where the 1 and the 3 have been swapped. If this is the case, the silver fraction for all capsules is exactly the same and may be from silver contamination of the steel. Considering a reasonable silver contamination of 10 ppm of the capsule steel could explain the measured silver fraction on the steel capsule.

Table 15: Fractional ^{110m}Ag Release from Fuel Elements of FRJ2-K13 [25]

Fuel Sphere	Steel Capsule	Graphite Cup	Total Fractional Release
1	1.3×10^{-2}	5.7×10^{-3}	1.9×10^{-2}
2	1.3×10^{-2}	7.5×10^{-3}	2.0×10^{-2}
3	1.3×10^{-2}	3.7×10^{-3}	1.7×10^{-2}
4	$3.1\ (1.3) \times 10^{-2}$	8.0×10^{-3}	$3.9\ (2.1) \times 10^{-2}$

Natural uranium and thorium contamination of the graphite cups that housed the test spheres were treated in the same way as for the HFR-K3 evaluation. Similarly, it was assumed that comparable silver contamination of the graphite cups existed. Much uncertainty remains about silver contamination of the steel capsules. For best estimate analyses it was assumed that the silver fraction measured from the steel capsules was predominantly from natural silver contamination of rig materials and a fraction of 1×10^{-2} was deducted from the measured fraction of this source. This leaves a fraction of 3×10^{-3} from test sphere release which is significantly more than what was measured in HFR-K3 and R2-K12, and very similar to what was measured during R2-K13. By ignoring any silver contamination in the steel capsules and assuming that all measured silver originated from the test spheres, an upper limit diffusion coefficient can be derived.

The resulting diffusion coefficients are shown in Table 16. The lower diffusion coefficient set will be used in deriving the final best estimate coefficients, and the upper limit results to derive final coefficients that may be used for safety and design analyses.

Table 16: Derived Diffusion Coefficients: FRJ2-K13

Fuel Sphere	Best Estimate		Upper Limit	
	Temperature	Coefficient (m^2s^{-1})	Temperature	Coefficient (m^2s^{-1})
1	1 131 °C	1.67×10^{-17}	1 131 °C	2.56×10^{-17}
2	1 149 °C	1.71×10^{-17}	1 149 °C	2.57×10^{-17}
3	1 148 °C	1.43×10^{-17}	1 148 °C	2.37×10^{-17}
4	1 127 °C	1.79×10^{-17}	1 127 °C	2.64×10^{-17}

5.3 FRJ2-K15

5.3.1 Irradiation test

Three elements from AVR reload 21-1 with LEU-TRISO fuel were inserted into the reflector outside the core in a three-capsule irradiation rig as is shown in Figure 15. Each capsule contained one sphere and was individually swept and temperature-controlled. Fuel spheres were numbered as K15/1, K15/2 and K15/3 with planned irradiation temperatures of 808 °C, 980 °C and 803 °C surface and 970 °C, 1 150 °C and 990 °C centre, respectively [36]. FRJ2-K13 started on 4 September 1986 and ended successfully on 21 October 1990. Burn-up values of 14.1, 15.3, and 14.8% FIMA were attained, with fast fluences of ~0.2×10^{25} m^{-2} [37]. The objectives for this test were as follows [25]:

a. Irradiation test of AVR reload 21-2 fuel (type GLE-4).

b. Experimental demonstration of high burn-up potential of LEU TRISO particle.

c. Determination of coated particle performance under high burn-up.

d. R/B measurements during transients tests at different burn-ups.

e. Examination of fission product transport.

Post-irradiation examination was completed, with gamma spectrometric analyses and deconsolidation of the rig. Only the graphite cups were analysed for fission products with gamma spectrometry. The ^{85m}Kr fractional release remained very low ($< 10^{-6}$) so it can be assumed that no particles failed during irradiation nor were there any particles defective from manufacture. All three test elements underwent KORA corrosion and KÜFA heat-up testing after irradiation.

5.3.2 Evaluation

Fuel characteristics and final irradiation data of the test spheres are provided in Table 17 [38]. The silver fractional release for test sphere 3 was not successfully measured and is not discussed further.

Table 17: FRJ2-K15 Test Element Specification and Irradiation Data

Parameter	Unit	1	2	3
Specification				
Sphere weight	g	201.7	201.8	201.7
Uranium content	g	6.0	6.0	6.0
^{235}U enrichment	%	16.76	16.76	16.76
CP content		9 500	9 500	9 500
Failed CP content	per FE	0	0	0
Irradiation Data				
Burn-up (FIMA)	%	14.1	15.3	14.8
Neutron fluence (> 0.1 MeV)	10^{25} m^{-2}	0.181	0.227	0.155
Average centre temperature	°C	920	1 095	960
Max power output	kW/FE	1.94	2.24	2.15

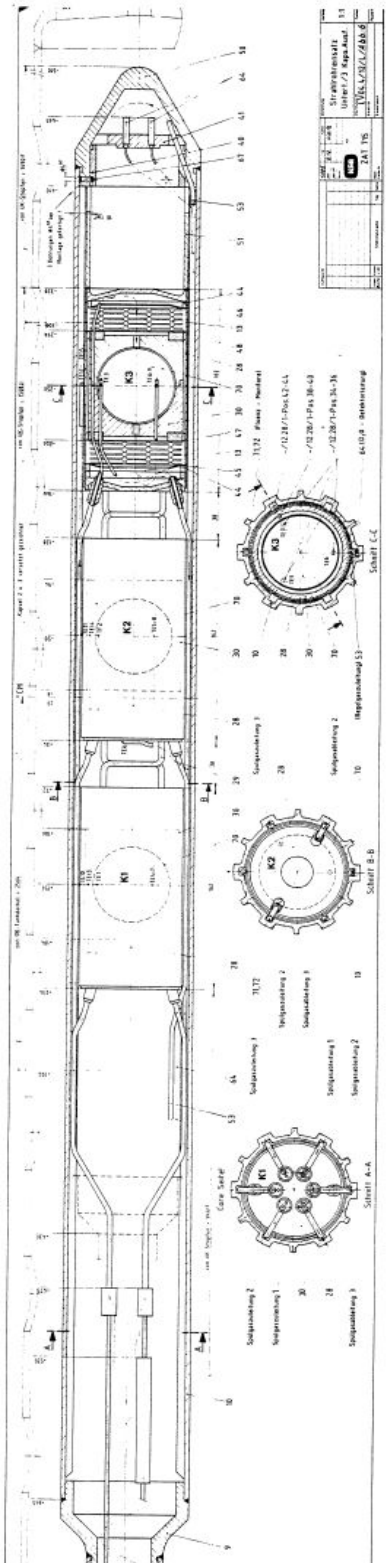

Figure 15: FRJ2-K15: Irradiation Rig

Fast and thermal neutron fluxes are available from irradiation progress reports. Cross sections were selected to achieve correct burn-ups and plutonium contributions. Fission power values determined from a neutronic calculation and estimated gamma-power values were used to determine fuel temperatures. Coolant gas temperatures were adjusted to ensure that calculated and measured surface temperatures agreed. Centre fuel temperatures were calculated from surface temperatures and total power produced (fission and gamma) in each test sphere. Calculated fission powers, surface temperatures (from irradiation progress reports) and calculated centre temperatures are listed in Table 18. Also included are initial Hochtemperatur Anlage (HTA) calculated fission power values extracted from original irradiation progress reports. Not all the progress reports could be found and in some cases HTA calculations were not performed.

Table 18: FRJ2-K15/1 and /2: Fission Power, Surface, and Centre Temperature

Cycle Number	K15/1				K15/2			
	Fission Power		Temperature		Fission Power		Temperature	
	GETTER	HTA	Surface	Centre	GETTER	HTA	Surface	Centre
1	1 935	1 910	795	954	2 244	2 220	998	1 204
2	1 868	-	800	955	2 157	-	996	1 195
3	1 850	1 800	792	947	2 105	2 070	988	1 184
4	1 755	-	800	949	1 987	-	993	1 180
5	1 702	-	805	952	1 897	-	995	1 177
6	1 595	-	800	939	1 769	-	997	1 149
7	1 646	-	795	942	1 770	-	996	1 165
8	1 671	-	800	951	1 840	-	995	1 171
9	1 515	-	805	942	1 728	-	998	1 165
10	1 388	1 350	793	923	1 475	1 520	993	1 145
11	1 221	1 240	792	910	1 325	1 410	991	1 134
12	1 153	1 220	801	907	1 248	1 330	996	1 128
13	1 178	1 180	787	902	1 245	1 250	995	1 131
14	1 115	1 120	795	906	1 178	1 270	996	1 127

Cycle Number	K15/1				K15/2			
	Fission Power		Temperature		Fission Power		Temperature	
	GETTER	HTA	Surface	Centre	GETTER	HTA	Surface	Centre
15	1 553	1 560	812	965	1 640	1 700	986	1 138
16	1 386	-	801	940	1 447	-	1008	1 169
17	1 247	1 250	803	933	1 288	1 260	998	1 141
18	1 125	1 160	800	923	1 110	1 190	995	1 130
19	1 027	1 080	809	924	950	1 090	975	1 096
20	953	997	814	924	876	999	984	1 099
21	900	940	794	901	857	936	948	1 084
22	821	886	802	903	823	875	943	1 042
23	764	825	804	905	807	808	917	998
24	725	791	797	891	782	771	888	1 000
25	701	778	805	901	785	757	892	997
26	682	711	786	875	767	689	909	1 014
27	651	677	792	880	738	654	896	1 000
28	618	645	798	891	707	625	850	958
29	592	620	800	896	684	600	852	960
30	571	600	806	892	665	590	829	930
31	582	580	803	890	648	580	841	944

Fractional releases of silver from the test spheres during irradiation are listed in Table 19. AVR reload 21 fuel represents the best-quality German fuel manufactured and considerably lower heavy metal contaminations in the matrix materials were achieved than for previous batches. Natural uranium and thorium contamination of graphite cups that housed the test spheres were treated in the same way as for HFR-K3 and FRJ2-K13 evaluations. Similarly, it was assumed that comparable silver contamination of the graphite cups existed.

No measurement data for fractional silver release on steel capsules are available in the literature but only fractional release activities of the graphite cups on spheres 1 and 2. Considering the activity ratios of FRJ2-K13, it was conservatively assumed to use a capsule activity equal to the cup activity for best estimate analyses, and two to three times the cup activity for design limit values. Correspondingly, the natural silver contaminations in the steel capsules were also adjusted.

Table 19: Fractional ^{110m}Ag Release from Fuel Elements of FRJ2-K15 [38]

Fuel Sphere	Steel Capsule	Graphite Cup	Total Fractional Release
1	7.5×10^{-4}	7.5×10^{-4}	1.5×10^{-3}
2	3.2×10^{-3}	3.2×10^{-3}	6.4×10^{-3}

Resulting diffusion coefficients are shown in Table 20. The lower diffusion coefficient set will be used in deriving the final best estimate coefficients, and the upper limit results to derive final coefficients that may be used for safety and design analyses. The diffusion coefficient derived for the lower temperature sphere 1 is highly dependent on the level of natural silver contamination assumed in the evaluation. The natural silver contamination has therefore been selected inside the acceptable range to give a diffusion coefficient as conservative as possible but still in line with other diffusion coefficients derived in the detailed evaluation. The diffusion coefficient for sphere 1 is rather too high than too low and is also the only coefficient derived during this evaluation that exceeds the current IAEA-recommended diffusion coefficient (refer to Figure 17).

Table 20: Derived Diffusion Coefficients: FRJ2-K15

Fuel Sphere	Best Estimate		Upper Limit	
	Temperature	Coefficient (m^2s^{-1})	Temperature	Coefficient (m^2s^{-1})
1	920 °C	1.50×10^{-18}	920 °C	3.21×10^{-18}
2	1 095 °C	7.82×10^{-18}	1 095 °C	1.15×10^{-17}

5.4 R2-K12

5.4.1 Reactor

The R2 reactor in Studsvik, Sweden, is a light-water-moderated and -cooled reactor similar to the HFR in Petten. It generates 50 MW thermal power and utilizes 90% enriched fuel. Suitable irradiation conditions for sphere irradiation are available in both the core and reflector regions, with high thermal and fast neutron fluxes in the core.

5.4.2 Irradiation test

In this experiment, four fuel elements were irradiated in a four-capsule rig in the R2 reactor core. Two elements contained mixed oxide $(Th,U)O_2$ TRISO particles and the other two elements contained a two-particle system. The two-particle fuel was an investigation into the viability of combining fissile UC_2 and fertile ThO_2 TRISO particles. The two-particle system was abandoned and only the one-particle test spheres are considered here. The two test spheres of interest were inserted into the top two capsules of the irradiation rig shown in Figure 16 [25].

Basic fuel and irradiation parameters are listed in Table 21. The test spheres contained 10 960 TRISO particles imbedded in A3-27 matrix material. The total heavy metal load of 6.08 g per sphere consisted of 1.12 g uranium enriched to 89.6% and 4.96 g thorium. Effective uranium contaminations used in evaluations were 2.2×10^{-5} and 1.0×10^{-6} in fuel and fuel-free zones respectively [39]. This was a two times accelerated test that ran for 308 effective full power days. The ^{85m}Kr fractional release remained very low ($< 10^{-6}$) so it can be assumed that no particles failed during irradiation nor were there any particles defective from manufacture.

Each capsule consisted of a steel container with graphite cups which housed the test spheres. Fuel spheres were numbered as R2-K12/1 and R2-K12/2 with planned irradiation temperatures of 950 °C and 1 120 °C surface and 1 100 °C and 1 280 °C centre, respectively [37]. Instrumentation consisted of five thermocouples per sphere and wire flux monitors as well as sweep and temperature regulation tubes for each single capsule. R2-K12 started on 28 November 1978 and ended successfully on 12 February 1980. Burn-up values up to 12.4% FIMA were attained, with fast fluences of 6.9×10^{25} m^{-2}.

Table 21: R2-K12 Test Element Specification and Irradiation Data

Parameter	Unit	Sphere 1	Sphere 2
Specification			
Sphere weight	g	203.2	203.2
Uranium content	g	1.12	1.12
Thorium content	g	4.96	4.96
Heavy metal content	g	6.08	6.08
^{235}U enrichment	%	89.6	89.6
CP content		10 960	10 960
Failed CP content	per FE	0	0
Irradiation Data			
Burn-up (FIMA)	%	11.1	12.4
Neutron fluence (> 0.1 MeV)	10^{25} m^{-2}	5.6	6.9
Average centre temperature	^{o}C	1 120	1 290
Max power output	kW/FE	3.29	3.95

The objectives for this test were as follows [25]:

a. Accelerated reference test on HEU-TRISO fuel spheres with different particle types.

b. Evaluating irradiation conditions corresponding to a 3 000 MWth process heat plant.

c. Examination of mechanical performance of particles of 1977 standard quality.

d. Evaluating the differences between one- and two-particle fuel systems.

The capsules underwent gamma-scanning and deconsolidation at Studsvik before being sent to the KFA at Jülich for final analyses. Fission product inventories were measured in test spheres and capsule components in order to determine fractional releases

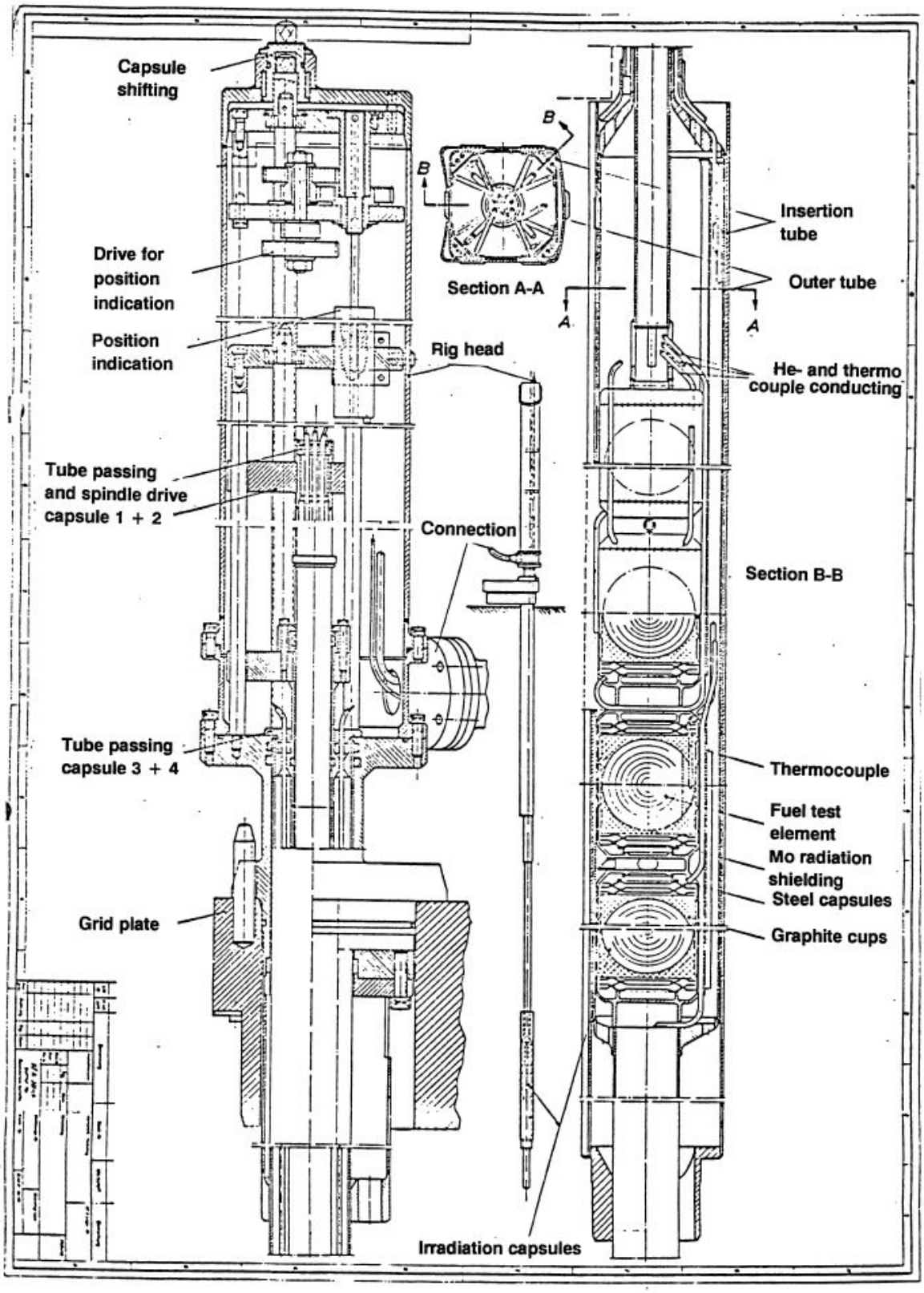

Figure 16: R2-K12: Irradiation Rig for Spherical Fuel Elements

5.4.3 Evaluation

A first evaluation of R2-K12 fission product release was performed by Acharya in 1983, shortly after completion of the first post-irradiation examinations [39]. In the Acharya report mention is made of other analyses performed by Muncke, but these reports could not be found. These studies did not try to derive transport parameters for silver in the different fuel materials, but attempted to explain the observed results using transport parameters and models accepted at that time. Results from both studies are compared without explanation of all observed results. A more serious attempt to explain observed release fractions are discussed later by Röllig and Muncke (HRB) as reported by Gontard [25], and their recommendations are used in this evaluation.

5.4.3.1 Input data

Measured surface temperatures [40] and thermal neutron fluxes [39] are available directly from the literature and fast neutron fluxes can be derived from fast neutron fluence values. Surface temperatures and neutron fluxes used in the evaluation is presented in Table 22.

5.4.3.2 Evaluation results

Fission powers produced during irradiation and total burn-up achieved were calculated to ensure that calculated temperatures are as close as possible to actual values. Fission power values were calculated using best available thermal neutron fluxes (Table 22) and cross sections that have been corrected to yield the correct burn-up. These newly calculated fission power values were then used with literature-supplied gamma heating to determine fuel temperatures. He/Ne coolant gas temperatures were adjusted to ensure that calculated and measured surface temperatures agree. Centre fuel temperatures were then calculated from surface temperatures and total power produced (fission and gamma) in each test sphere. Fission power values as calculated by HBK and this evaluation are presented with the gamma heating for each cycle in Table 23.

Centre fuel temperatures were calculated for both GA and HBK studies and are presented with this evaluation results in Table 24. There is not a very big variation in calculated centre temperatures between the three calculations, even though all three sets use different thermal conductivity relations for A3-27 matrix material.

Table 22: R2-K12: Surface Temperature (°C) and Neutron Flux (10^{18} $m^{-2}s^{-1}$)

Cycle Number	Capsule 1			Capsule 2		
	Surface Temperature	Thermal Flux	Fast Flux	Surface Temperature	Thermal Flux	Fast Flux
1	824	0.78	2.09	898	0.93	2.59
2	779	0.79	1.90	874	0.95	2.34
3	786	0.75	1.81	886	0.91	2.33
4	821	0.81	2.19	927	1.01	3.09
5	827	0.81	2.17	935	0.98	2.73
6	819	0.78	2.13	940	0.96	2.82
7	857	0.81	2.33	966	1.05	2.72
8	853	0.82	2.13	994	0.99	2.73
9	864	0.83	2.16	1 006	0.98	2.71
10	838	0.84	2.30	1 003	1.01	2.79
11	847	0.79	2.04	987	0.99	2.72
12	827	0.86	2.00	977	0.98	2.69
13	818	0.79	2.26	982	0.93	2.46
14	806	0.81	1.97	979	0.98	2.66
15	796	0.85	2.10	975	0.94	2.33
16	862	0.86	1.99	980	0.99	2.68
17	892	0.91	2.12	947	1.03	2.44
18	901	0.86	1.94	988	0.89	2.31
19	829	0.88	2.11	999	0.96	2.45
20	822	0.86	2.20	1 000	0.96	2.59
21	795	0.62	2.01	965	0.85	2.16
22	595	0.62	1.93	780	0.85	2.14

Table 23: R2-K12: Fission and Gamma Power (W)

Cycle Number	Capsule 1			Capsule 2		
	Gamma Power	Fission Power		Gamma Power	Fission Power	
		HBK	GETTER		HBK	GETTER
1	1 200	3 132	3 290	1 403	3 658	3 953
2	1 035	2 846	3 116	1 114	3 437	3 725
3	1 077	2 658	2 796	1 443	3 104	3 335
4	1 301	2 653	2 852	1 647	2 799	3 453
5	1 301	2 496	2 689	1 565	2 544	3 121
6	1 240	2 243	2 450	1 554	2 569	2 863
7	1 484	2 442	2 407	1 667	2 225	2 924
8	1 423	2 868	2 292	1 748	2 059	2 562
9	1 463	1 948	2 184	1 738	1 987	2 368
10	1 484	1 861	2 094	1 748	1 862	2 296
11	1 321	1 704	1 882	1 728	1 807	2 137
12	1 484	1 486	1 968	1 667	1 580	2 023
13	1 260	1 527	1 924	1 484	1 566	1 814
14	1 382	1 484	1 652	1 667	1 411	1 801
15	1 218	1 304	1 646	1 604	1 400	1 635
16	1 360	1 408	1 575	1 580	1 350	1 626
17	1 382	1 385	1 565	1 647	1 125	1 586
18	1 338	1 115	1 398	1 464	1 161	1 298
19	1 379	1 164	1 365	1 464	1 120	1 341
20	1 379	1 186	1 276	1 443	1 009	1 285
21	1 274	847	895	1 240	1 009	1 106
22	1 274	822	882	1 240	970	1 088

Table 24: R2-K12: Calculated Centre Temperatures

Cycle Number	Capsule 1			Capsule 2		
	GA	HBK	GETTER	GA	HBK	GETTER
1	1 124	1 166	1 150	1 282	1 345	1 300
2	1 096	1 115	1 113	1 269	1 304	1 291
3	1 093	1 106	1 100	1 269	1 291	1 286
4	1 161	1 171	1 171	1 342	1 363	1 359
5	1 159	1 163	1 165	1 326	1 340	1 338
6	1 128	1 126	1 163	1 312	1 323	1 320
7	1 200	1 211	1 211	1 341	1 352	1 359
8	1 177	1 175	1 178	1 334	1 341	1 355
9	1 185	1 182	1 190	1 332	1 337	1 345
10	1 162	1 157	1 163	1 327	1 330	1 338
11	1 149	1 145	1 150	1 310	1 311	1 312
12	1 161	1 154	1 153	1 300	1 299	1 300
13	1 109	1 101	1 110	1 276	1 274	1 267
14	1 111	1 101	1 101	1 291	1 288	1 291
15	1 074	1 055	1 072	1 274	1 270	1 287
16	1 150	1 141	1 140	1 289	1 285	1 275
17	1 183	1 174	1 175	1 277	1 268	1 260
18	1 147	1 137	1 154	1 273	1 268	1 263
19	1 107	1 093	1 095	1 292	1 290	1 275
20	1 109	1 092	1 101	1 290	1 286	1 277
21	1 023	1 037	1 008	1 250	1 242	1 227
22	845	825	847	1 125	1 093	1 039

Fractional releases of silver from test spheres during irradiation are listed in Table 25. Röllig and Muncke estimated natural silver contamination in A3-27 to be in the order of 2.7 ng/g which translates to about 1.3×10^{13} ^{109}Ag atoms per cm^3. At Studsvik during the R2-K12 irradiation tests, reserve graphite cups used in that irradiation rig were measured prior to irradiation. Silver contamination was found to be as high as 180 ng/g or around 8.3×10^{14} ^{109}Ag atoms per cm^3 [25]. It is not known if the reserve graphite cups are really representative of the irradiated graphite cups. For example, the irradiated graphite cups may have undergone high-temperature annealing prior to insertion in the irradiation rig that may have reduced the natural silver contamination. By reducing this contamination by a factor of 10 and taking into account the relative weight of the graphite cups, a maximum ^{109}Ag contamination in graphite materials of 7.8×10^{13} atoms/cm^3 was used. The case where natural silver contamination might have been reduced to levels estimated for other irradiation rig graphite cups (1.3×10^{13} ^{109}Ag atoms/cm^3) have been investigated as well.

Table 25: Fractional ^{110m}Ag Release from the Fuel Elements of R2-K12 [39]

Fuel Sphere	Steel Capsule	Graphite Cup	Total Fractional Release
1	3.7×10^{-3}	2.9×10^{-2}	3.3×10^{-2}
2	9.1×10^{-3}	4.9×10^{-3}	1.4×10^{-2}

After considering recommendations from previous evaluations and all calculated results, diffusion coefficients were derived for both test spheres in Table 26. The temperatures and coefficients listed are the average centre fuel temperatures for each test sphere and coefficients at those specific temperatures. For evaluation where the spread of data is limited due to a lack of detailed information, an upper limit of a factor of two higher than the best estimate value was suggested by Röllig [21].

Table 26: Derived Diffusion Coefficients: R2-K12

Fuel Sphere	Best Estimate		Upper Limit	
	Temperature	Coefficient (m^2s^{-1})	Temperature	Coefficient (m^2s^{-1})
1	1 123 °C	7.39×10^{-18}	1 123 °C	1.48×10^{-17}
2	1 289 °C	1.68×10^{-17}	1 289 °C	3.36×10^{-17}

5.5 R2-K13

5.5.1 Irradiation test

This experiment was a combined test with high-enriched $(Th,U)O_2$ spherical fuel and low-enriched UCO/ThO_2 block fuel segments from a block fuel assembly. Initially it was planned to test LEU fuel but due to production delays HEU fuel was tested, and this test was therefore the last test performed on HEU spherical fuel. The two fuel spheres were inserted into capsules 1 and 4 of a four-capsule fuel rig.

Basic fuel and irradiation parameters are listed in Table 27**.** The test spheres contained 19 780 EUO 1674 TRISO particles imbedded in A3-27 matrix material. The total heavy metal loading of 11.3 g per sphere consisted of 1.14 g uranium enriched to 89.0% and 10.1 g thorium. Effective uranium contamination and natural silver content used in evaluations were the same as for the R2-K12 evaluation. This test ran for 517 effective full power days after which burn-up values up to 10.2% FIMA and fast fluences of 8.5×10^{25} m^{-2} was attained. The ^{85m}Kr fractional release remained very low ($< 10^{-6}$) so that it can be assumed that no particles failed during irradiation nor were there any particles defective from manufacture.

Each capsule consisted of a steel container with graphite cups which housed the test spheres. Fuel spheres were numbered as R2-K13/1 and R2-K13/4 with planned irradiation temperatures of 960 °C and 750 °C surface and 1 170 °C and 980 °C centre, respectively [37]. R2-K13 started on 22 April 1980 and ended successfully on 19 September 1982. Burn-up values up to 12.4% FIMA was attained, with fast fluences of 6.9×10^{25} m^{-2}.

The objectives for this test were as follows [25]:

a. Demonstration test of HEU-TRISO fuel spheres irradiation performance.

b. Evaluating fission product transport behaviour.

c. Examination of particles performance under long-term irradiation.

d. Evaluating A3-27 matrix material irradiation behaviour.

e. Supplying spherical fuel elements for PIE annealing tests.

The capsules underwent gamma-scanning and deconsolidation at Studsvik before being sent to KFA at Jülich for final analyses. With results from gamma spectrometry on graphite cups, leach tests on steel capsules together with inventory measurements and calculations, relative fission product release from the fuel was investigated. Both fuel spheres were deconsolidated and particles were analysed. It was found that coated particle retention of fission products were exceptional and only ^{110m}Ag had been released in detectable quantities.

Table 27: R2-K13 Test Element Specification and Irradiation Data

Parameter	Unit	1	4
Specification			
Sphere weight	g	207.9	207.9
Uranium content	g	1.14	1.14
Thorium content	g	10.1	10.1
Heavy metal content	g	11.3	11.3
235U enrichment	%	89.0	89.0
CP content		19 780	19 780
Failed CP content	per FE	0	0
Irradiation Data			
Burn-up (FIMA)	%	10.2	9.8
Neutron fluence (> 0.1 MeV)	10^{25} m^{-2}	8.5	6.8
Average centre temperature	°C	1 211	1 020
Max power output	kW/FE	2.97	2.55

5.5.2 Evaluation

A first evaluation of R2-K13 fission product release was performed by Muncke, but these reports could not be found. A short discussion of this work is provided in the Gontard report [25].

5.5.2.1 Input data

Measured surface temperatures and neutron fluence values are available directly from the literature [41]. Calculated fission powers are also available with measured R/B values for ^{85m}Kr. The surface temperatures and neutron fluxes used in this evaluation are listed in Table 28.

Table 28: R2-K13: Surface Temperature (°C) and Neutron Flux (10^{18} $m^{-2}s^{-1}$)

Cycle Number	Capsule 1			Capsule 4		
	Surface Temperature	Thermal Flux	Fast Flux	Surface Temperature	Thermal Flux	Fast Flux
1	900	0.88	1.27	755	0.68	0.83
2	860	0.86	1.49	730	0.78	0.96
3	855	0.84	1.34	720	0.70	0.85
4	840	0.86	1.31	700	0.68	0.87
5	840	0.85	1.45	700	0.64	0.93
6	880	0.75	1.25	700	0.62	0.96
7	840	0.80	1.24	700	0.75	0.96
8	860	0.86	1.47	720	0.73	0.95
9	900	0.87	1.42	750	0.96	0.96
10	900	0.92	1.38	760	0.88	1.38
11	900	0.84	1.31	760	0.78	1.23
12	940	0.92	1.58	760	0.61	1.29
13	940	0.99	1.55	760	0.95	0.83
14	960	1.05	1.63	755	0.94	1.43
15	960	1.30	1.99	760	1.03	1.37
16	970	1.20	1.91	760	1.01	1.31
17	970	1.10	1.84	760	1.05	1.62
18	970	1.05	1.74	755	1.10	1.54
19	980	1.20	2.02	760	1.10	1.65
20	980	0.84	1.60	770	0.74	1.29
21	975	0.87	1.71	780	1.15	1.45
22	980	1.20	2.30	780	1.05	2.38
23	960	1.20	2.31	760	1.00	1.93

Cycle Number	Capsule 1			Capsule 4		
	Surface Temperature	Thermal Flux	Fast Flux	Surface Temperature	Thermal Flux	Fast Flux
24	970	1.10	2.22	760	1.10	1.81
25	980	1.35	2.50	770	0.90	2.04
26	970	1.20	2.37	770	1.00	2.20
27	960	1.20	2.31	770	0.90	1.91
28	970	0.11	2.24	780	1.15	1.98
29	960	1.10	2.26	780	1.03	1.85
30	980	0.99	2.28	800	0.90	2.28
31	990	1.05	2.28	800	0.91	1.95
32	980	0.87	2.31	790	0.85	1.74
33	990	0.82	2.31	800	0.85	1.81
34	990	0.80	2.53	780	0.78	1.81
35	980	0.75	2.70	780	0.77	2.31
36	980	0.80	2.70	770	0.75	1.93
37	990	0.78	2.31	780	0.75	1.93

5.5.2.2 Evaluation results

Fission power values produced during irradiation and total burn-up achieved were calculated to ensure that calculated temperatures were as close as possible to actual values. Fission power values were calculated using best available thermal neutron fluxes (Table 28) and cross sections that have been corrected to yield the correct burn-up. These newly calculated fission power values where then used with literature-supplied gamma heating to determine fuel temperatures. He/Ne coolant gas temperatures were adjusted to ensure that calculated and measured surface temperatures agree. Centre fuel temperatures were calculated from surface temperatures and total power produced (fission and gamma) in each test sphere. Fission power values as calculated by HBK and this evaluation are presented with gamma heating for each cycle in Table 29. Centre fuel temperatures were calculated and are also included in Table 29.

Table 29: R2-K13: Fission and Gamma Power (W) and Centre Temperatures (°C)

Cycle Number	Capsule 1				Capsule 2			
	Centre Temp	Gamma Power	Fission Power		Centre Temp	Gamma Power	Fission Power	
			HBK	GETTER			HBK	GETTER
1	1 166	800	2 980	2 968	948	580	2 310	2 309
2	1 125	780	2 760	2 765	956	600	2 540	2 547
3	1 123	760	2 610	2 604	932	600	2 220	2 215
4	1 117	750	2 680	2 588	910	580	2 090	2 101
5	1 125	820	2 520	2 503	906	600	1 940	1 947
6	1 134	740	2 150	2 159	906	600	1 860	1 854
7	1 117	760	2 260	2 251	948	600	2 190	2 195
8	1 153	800	2 350	2 340	965	600	2 070	2 073
9	1 183	720	2 280	2 298	1 049	580	2 620	2 639
10	1 195	800	2 350	2 356	1 044	560	2 340	2 338
11	1 169	740	2 100	2 100	1 022	600	2 040	2 028
12	1 225	840	2 251	2 247	977	620	1 550	1 562
13	1 236	780	2 400	2 396	1 066	620	2 420	2 420
14	1 259	740	2 470	2 477	1 055	620	2 330	2 338
15	1 307	780	2 970	2 985	1 076	600	2 500	2 506
16	1 288	760	2 680	2 687	1 068	600	2 420	2 411
17	1 272	840	2 460	2 447	1 078	580	2 470	2 487
18	1 256	800	2 280	2 288	1 080	580	2 530	2 545
19	1 286	780	2 540	2 555	1 079	560	2 450	2 486
20	1 218	840	1 760	1 764	1 004	600	1 650	1 655
21	1 220	860	1 810	1 804	1 106	600	2 510	2 513
22	1 277	780	2 440	2 442	1 081	620	2 190	2 243
23	1 258	820	2 360	2 365	1 045	560	2 080	2 088

Cycle Number	Capsule 1				Capsule 2			
	Centre Temp	Gamma Power	Fission Power		Centre Temp	Gamma Power	Fission Power	
			HBK	GETTER			HBK	GETTER
24	1 247	860	2 120	2 127	1 010	620	2 250	2 259
25	1 286	740	2 490	2 553	1 031	600	1 810	1 818
26	1 256	840	2 230	2 239	1 010	620	2 040	2 080
27	1 241	740	2 170	2 210	1 029	560	1 790	1 794
28	1 234	820	1 990	1 984	1 087	580	2 220	2 240
29	1 223	840	1 960	1 949	1 061	600	1 950	1 961
30	1 219	840	1 750	1 741	1 049	580	1 690	1 700
31	1 232	740	1 900	1 861	1 056	620	1 740	1 734
32	1 207	820	1 620	1 625	1 042	600	1 690	1 695
33	1 205	860	1 490	1 491	1 047	600	1 640	1 648
34	1 198	840	1 420	1 431	1 013	620	1 480	1 487
35	1 180	840	1 330	1 328	1 010	620	1 450	1 453
36	1 182	760	1 390	1 405	996	640	1 420	1 404
37	1 186	760	1 350	1 359	1 002	620	1 400	1 395

Fractional releases of silver from test spheres during irradiation are listed in Table 30. Diffusion coefficients were derived for both test spheres in Table 31 using the same reasoning as for the R2-K12 evaluation. Natural silver contaminations between 1.3 and 7.8 x 10^{13} ^{109}Ag atoms/cm^3 were investigated. For best estimate analyses, the higher value was used and for upper limit evaluations the lower number was used. Temperatures and coefficients listed are average centre fuel temperatures for each test sphere and coefficients at those specific temperatures. For evaluation where the spread of data is limited due to a lack of detailed information, an upper limit of a factor of two higher than the best estimate value was suggested by Röllig [21].

Table 30: Fractional ^{110m}Ag Release from Fuel Elements of R2-K13 [25]

Fuel Sphere	Steel Capsule	Graphite Cup	Total Fractional Release
1	8.8×10^{-5}	3.9×10^{-2}	3.9×10^{-2}
4	1.3×10^{-3}	1.4×10^{-3}	2.7×10^{-3}

Table 31: Derived Diffusion Coefficients: R2-K13

Fuel Sphere	Best Estimate		Upper Limit	
	Temperature	Coefficient (m^2s^{-1})	Temperature	Coefficient (m^2s^{-1})
1	1 211 °C	1.64×10^{-17}	1 211 °C	4.30×10^{-17}
4	1 020 °C	3.33×10^{-18}	1 020 °C	6.66×10^{-18}

5.6 FRJ2-K11

Irradiation data, temperature graphs and fuel parameters were summarized in a number of HBK quarterly reports [42], [43] and [44]. The irradiation report [45] contains early handwritten tables of first estimations of thermal neutron fluxes, burn-up and power production. Irradiation test conditions were extracted from all these sources.

5.6.1 Irradiation test

Two spheres from AVR reload 13 and two spheres from AVR reload 15 with HEU-TRISO fuel were inserted into the reflector outside the core in a two-capsule irradiation rig. FRJ2-K11 started on 27 April 1979 and ended successfully on 30 October 1980. Burn-up values of 10.0 and 9.7% FIMA were attained, with fast fluences of $\sim 0.2 \times 10^{25}$ m^{-2} [43]. ^{85m}Kr fractional release remained very low ($< 10^{-6}$) so that it can be assumed that no particles failed during irradiation nor were there any particles defective from manufacture. Post-irradiation examinations were performed on all test spheres but fractional fission product releases were successfully measured for spheres 3 and 4 only.

5.6.2 Evaluation

A first evaluation of fission product release from FRJ2-K11 was performed by Muncke, but the report could not be retrieved. Fuel characteristics [44] and final irradiation data [43] for test spheres are provided in Table 32.

Table 32: FRJ2-K11 Test Element Specification and Irradiation Data

Parameter	Unit	3	4
Specification			
Sphere weight	g	200	200
Uranium content	g	1.12	1.12
^{235}U enrichment	%	89	89
Thorium content	g	4.9	4.9
CP content		10 700	10 700
Failed CP content	per FE	0	0
Irradiation Data			
Irradiation time	EFPD	260	260
Burn-up (FIMA)	%	10.0	9.72
Neutron fluence (> 0.1 MeV)	10^{25} m^{-2}	0.2	0.2
Average centre temperature	^{o}C	1 183	1 176
Max power output	kW/FE	2.55	2.44

Fast neutron fluxes in the reflector of the DIDO reactor are very low and values similar to FRJ2-K13 evaluation were used. Cross sections were selected to achieve correct burn-ups. Fission power values determined from a neutronic calculation and estimated gamma-power values were used to determine fuel temperatures. In this test it was attempted to keep surface fuel temperatures constant in the region of 1 000 °C. Therefore coolant gas temperatures were adjusted to ensure that calculated and experiment-estimated surface temperatures agreed. Calculated fission power values, surface temperatures and calculated centre temperatures are listed in Table 33.

Table 33: FRJ2-K11/3 and /4: Fission Power, Surface and Centre Temperatures

Cycle Number	K11/3			K11/4		
	Fission Power	Temperature		Fission Power	Temperature	
		Surface	Centre		Surface	Centre
1	2 237	1 040	1 210	2 143	1 050	1 213
2	2 545	1 040	1 233	2 441	1 030	1 215
3	2 399	1 030	1 213	2 307	1 030	1 199
4	2 234	1 020	1 190	2 154	1 040	1 206
5	2 110	1 000	1 158	2 041	1 010	1 166
6	1 992	1 030	1 186	1 933	1 050	1 201
7	1 870	1 040	1 186	1 819	1 030	1 172
8	2 053	1 040	1 203	1 993	1 020	1 175
9	1 861	950	1 092	1 815	960	1 098
10	1 991	1 010	1 167	1 952	980	1 131
11	2 494	1 020	1 218	2 434	990	1 181
12	2 193	1 010	1 184	2 152	1 020	1 190
13	1 951	990	1 144	1 943	990	1 143

Post-irradiation-examinations were performed at Harwell in the UK [46]. Fractional releases of silver from test spheres during irradiation were 4 x 10^{-2} for both spheres according to the project report [43] although a fraction of 5.4 x 10^{-2} for test sphere 4 has also been reported in other literature [23]. Natural uranium and thorium contamination in the matrix material of the test spheres were in the order of 1 x 10^{-4} [47]. Heavy metal contamination in the graphite cups that housed the test spheres were treated in the same way as for the FRJ2-K13 evaluation. Similarly, it was assumed that comparable silver contamination of the graphite cups existed. Resulting diffusion coefficients are shown in Table 34. The lower diffusion coefficient set was calculated using best estimate input data and will be used in deriving final best estimate coefficients. Upper limit results are simply a factor of two higher than expected results and may be used for safety and design analyses.

Table 34: Derived Diffusion Coefficients: FRJ2-K11

Fuel Sphere	Best Estimate		Upper Limit	
	Temperature	Coefficient (m^2s^{-1})	Temperature	Coefficient (m^2s^{-1})
3	1 183 °C	4.19×10^{-17}	1 183 °C	8.38×10^{-17}
4	1 176 °C	4.26×10^{-17}	1 176 °C	8.52×10^{-17}

5.7 Discussion of results

All six applicable irradiation tests have been evaluated with the best available information and assumptions based on the best available engineering judgement. The level of information available for each irradiation test varies greatly from almost complete neutronic and thermohydraulic histories available for HFR-K3 to only brief summaries for FRJ2-K11. Furthermore it is unknown whether the quality of the SiC layers changed significantly from the early tests to the latest. Comparing derived diffusion coefficients for each test sphere of each test in Table 35, there are significant differences between diffusion coefficients derived for the earliest (FRJ2-K11) test and the latest (FRJ2-K15) tests. Similarly, there appears to be an influence from the irradiation facility used. The FRJ2 tests appear to have higher diffusion coefficients compared to the HFR and R2 tests.

What is important for all irradiation tests, irrespective of facility or fuel tested is the effect of natural uranium, thorium and silver contamination occurring in the fuel and irradiation rig materials. Especially for lower irradiation temperatures (< 1 100 °C), naturally occurring silver in graphite cups dominate measured fractional release. Natural silver contamination was only measured on R2 graphite cups and estimated for A2-27 matrix material used in fuel sphere manufacture. Silver contamination in irradiation capsule steels is unknown; however, measurements made during FRJ2-K13 appear significant. Another complicating effect that contributes to uncertainty in results is the efficiency of wet chemistry techniques used to leach and remove released silver from irradiation rig materials and the accuracy of gamma spectrometry used to measure ^{110m}Ag activities in leach solutions.

Considering the above, it must be asked whether all irradiation tests should be weighed equally in determining a final diffusion coefficient for silver in SiC. Confidence in diffusion coefficients derived from the HFR-K3 irradiation test is higher than in any of the other evaluations and is significantly higher than for FRJ2-K11. If weighing of results is to be considered, the first question to be answered is, what weight to apply to which evaluation?

This is highly subjective and since the 'better' evaluations generally produced lower diffusion coefficients, it can be viewed as an attempt to lower diffusion coefficients in order to simplify reactor analyses. It was therefore decided to rather consider all irradiation tests evaluated as equal and err on the conservative side. The only exception is where both evaluations performed for HFR-K3 using Christ and Venter data respectively will be used. In effect HFR-K3 irradiation test evaluation for spheres 1 and 4 will therefore be weighted by a factor of two. For the two colder spheres, 1 and 2, the Venter and Christ data represent the lower and upper limits and are used to evaluate best estimate and design limits.

All derived diffusion coefficients were plotted against average centre fuel temperatures in Figure 17. The following best estimate and design limit diffusion coefficients were derived by fitting all results to a straight line:

Best estimate: $D = 1.14 \times 10^{-13} e^{-109/RT}$ m^2s^{-1}

Design limit: $D = 2.28 \times 10^{-13} e^{-109/RT}$ m^2s^{-1}

The recommended IAEA diffusion coefficient is also plotted against temperature in Figure 17. All derived diffusion coefficients for all test spheres evaluated are below the recommended IAEA diffusion coefficient line except for the lowest temperature sphere (FRJ2-K15/1). Almost all design limit diffusion coefficients are also below the IAEA line with FRJ2-K11 and FRJ2-K15/1 being the exceptions. It appears that the currently recommended diffusion coefficient is overly conservative. Considering that the current silver diffusion coefficient in SiC was derived from particle heat-up tests after being irradiated in compacts, it might also be possible that the silver retention ability of a TRISO particle somehow improves during the sphere-making process. Also under consideration is the much higher diffusion coefficients derived for FRJ2-K11 and by Amian [48]. Amian performed his investigations on coated particles manufactured before 1978. This evaluation focused on fuel manufactured after 1978 (with the exceptions being FRJ2-K11 and R2-K12). The best-performing fuels have been the ones irradiated in the later fuel tests: FRJ2-K15 and -K13 as well as HFR-K3. These are fuel spheres from AVR reloads 19 and 21, which were manufactured well after 1980. It could well be that Chemical Vapour Deposition (CVD) coater performance has increased, resulting in higher quality SiC that have superior silver-retention abilities.

Table 35: Summary of Derived Diffusion Coefficients

Fuel Sphere	Best Estimate		Upper Limit	
	Temperature	Coefficient (m^2s^{-1})	Temperature	Coefficient (m^2s^{-1})
HFR-K3 - Christ Data				
1	1 247 °C	7.63×10^{-18}	1 247 °C	1.53×10^{-17}
2	-	-	1 099 °C	1.37×10^{-17}
3	-	-	1 099 °C	1.50×10^{-17}
4	1 278 °C	2.55×10^{-17}	1 285 °C	5.10×10^{-17}
HFR-K3 - Venter Data				
1	1 231 °C	7.75×10^{-18}	1 231 °C	1.55×10^{-17}
2	1 121 °C	6.58×10^{-18}	-	-
3	1 115 °C	5.96×10^{-18}	-	-
4	1 285 °C	2.63×10^{-17}	1 285 °C	5.26×10^{-17}
FRJ2-K13				
1	1 131 °C	1.67×10^{-17}	1 131 °C	2.56×10^{-17}
2	1 149 °C	1.71×10^{-17}	1 149 °C	2.57×10^{-17}
3	1 148 °C	1.43×10^{-17}	1 148 °C	2.37×10^{-17}
4	1 127 °C	1.79×10^{-17}	1 127 °C	2.64×10^{-17}
FRJ2-K15				
1	920 °C	1.50×10^{-18}	920 °C	3.21×10^{-18}
2	1095 °C	7.82×10^{-18}	1 095 °C	1.15×10^{-17}
R2-K12				
1	1123 °C	7.39×10^{-18}	1 123 °C	1.48×10^{-17}
2	1289 °C	1.68×10^{-17}	1 289 °C	3.36×10^{-17}
R2-K13				
1	1 211 °C	1.64×10^{-17}	1 211 °C	4.30×10^{-17}
4	1 020 °C	3.33×10^{-18}	1 020 °C	6.66×10^{-18}
FRJ2-K11				
1	1 168 °C	4.93×10^{-17}	1 168 °C	9.82×10^{-17}
2	1 164 °C	4.99×10^{-17}	1 164 °C	9.98×10^{-17}

Both FRJ2-K11 diffusion coefficients' best estimate and upper limit values are approaching the Amian diffusion coefficient line (the official IAEA line in Figure 17). It could possibly be that the Amian line presents the SiC diffusion coefficient for TRISO particles manufactured before 1978 and the new diffusion coefficient derived in this detailed evaluation present the SiC diffusion coefficient for TRISO particles manufactured after 1980. Therefore it might be that there is no discrepancy between the Amian evaluation and this current study. It can then also be argued that diffusion coefficients derived for FRJ2-K11 should be removed as they belong to an 'older' fuel set that have inferior silver-retention abilities compared to the latest state-of-the art German reference fuel. However, justifying such an argument based on only a perceived lower silver-retention ability is difficult, and for the sake of conservatism, it is suggested that the FRJ2-K11 results remain in Table 35 and Figure 17.

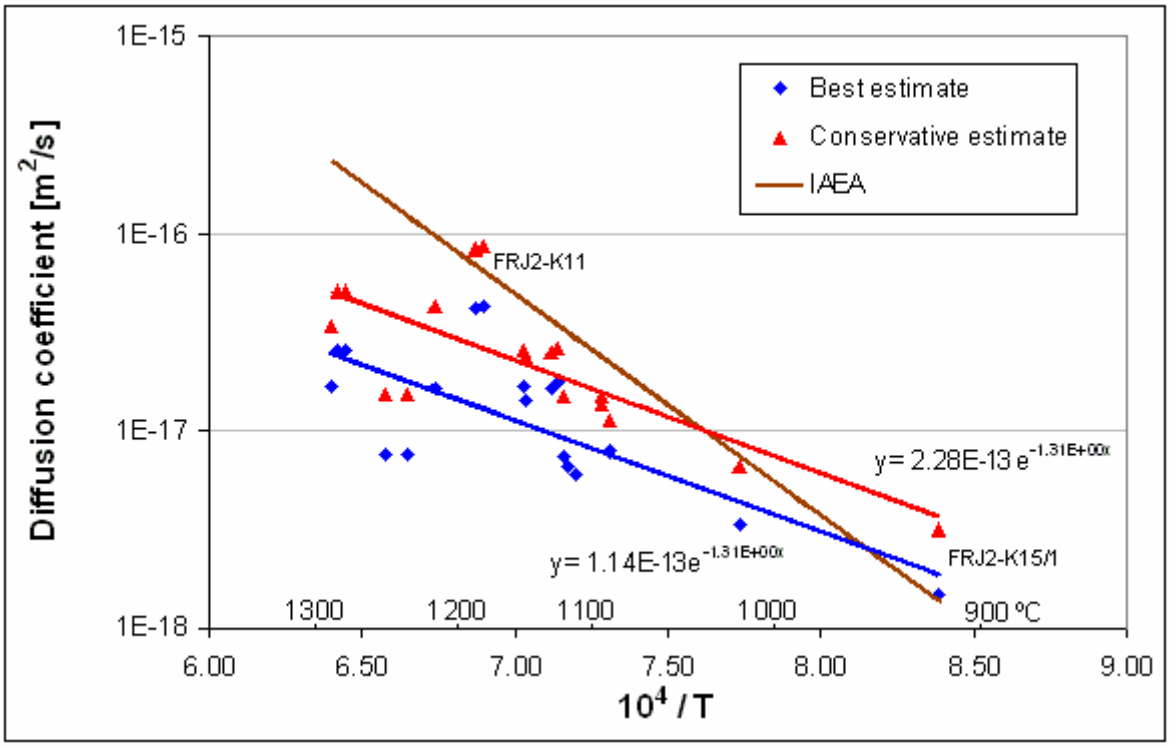

Figure 17: Diffusion Coefficients from the Detailed Evaluation

6. Evaluation of Post irradiation Heat-up Tests

The highest average central fuel temperature evaluated during the detailed irradiation test evaluation in paragraph 5 was 1 289 °C. During postulated accident events, fuel temperatures are expected to rise to 1 600 °C for design base accidents and up to 1 800 °C for beyond design base accidents. The ^{110m}Ag source term during accident events is only of secondary importance due to the relative small inventory in the core, but the release of ^{111}Ag may be significant. It is therefore important to understand the range of applicability of diffusion coefficients derived in paragraph 5.7 and to ensure that release behaviour during temperature transients do not differ to such an extent as to warrant different diffusion coefficients.

Behaviour of fuel spheres under high-temperature transients, as expected during loss of forced coolant events, are best studied through heat-up tests of irradiated fuel spheres in the famous KÜFA-instrument [49].

6.1 The KÜFA Instrument

The KÜFA-instrument is an ingenious device developed to analyse fission product release from a fuel sphere during post-irradiation heat-up testing. KÜFA is a German acronym for 'Cold finger apparatus' which refers to the water-cooled plates inserted into a furnace as illustrated in Figure 18.

A test sphere is inserted into the KÜFA furnace placed in a hot cell and heated to the desired temperature. Noble gas fission products are removed by a sweeping gas (helium at 111 kPa at 30 litres/hour), captured in liquid nitrogen traps outside the hot cell, and measured by a NaI detector. Metallic fission products released from the fuel sphere plate out on the water-cooled condensation plate and can be removed from the furnace while heating continues. Condensation plates are removed from the KÜFA instrument at the desired rate and analysed by gamma spectrometry, and then leached for liquid scintillation analyses to determine beta-emitters quantitatively.

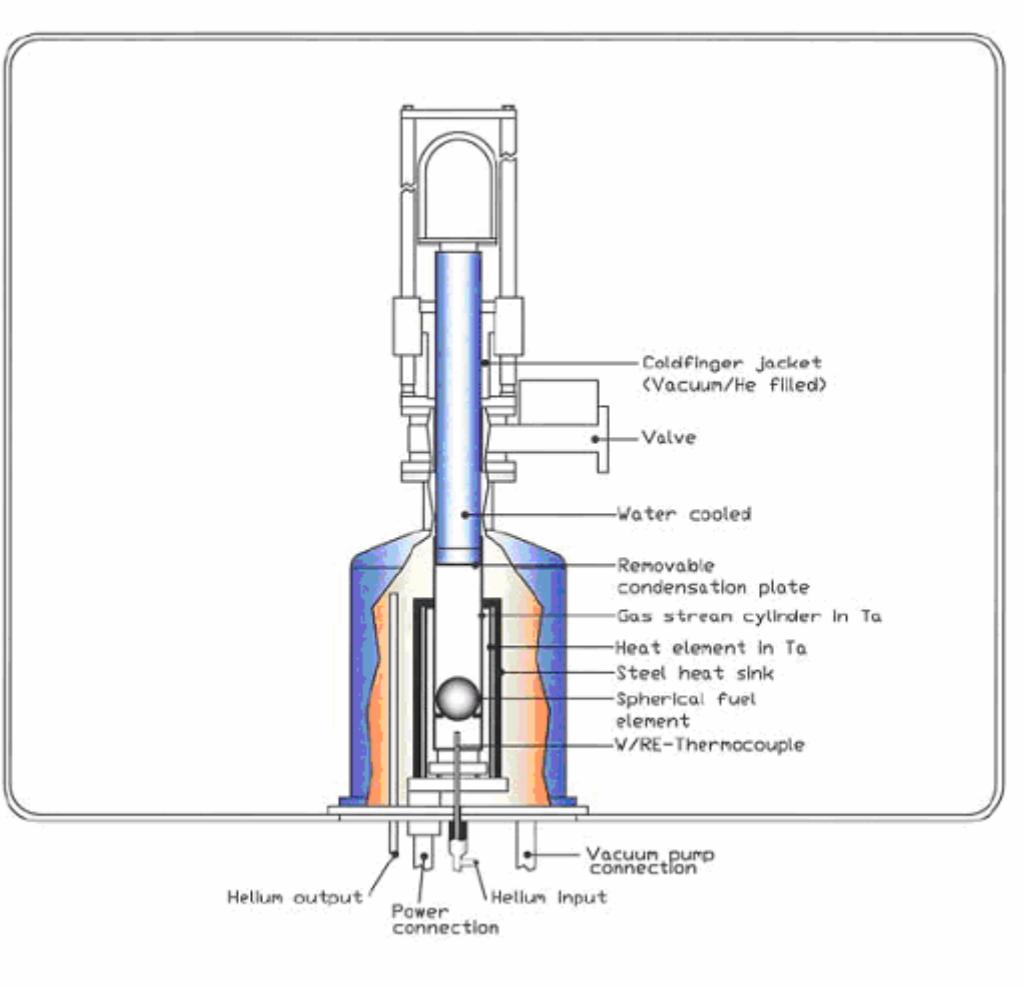

Figure 18: KÜFA-instrument used for Heat-up Testing [49]

6.2 Heat-up Tests

The first investigations into the behaviour of fuel spheres and coated particle compacts during post-irradiation heating have been performed by Schenk [50]. Only heat-up tests of complete spheres of sufficient quality and applicable fuel design are considered for this evaluation. During the German fuel development programme, a total of twenty-nine high-quality fuel spheres underwent post-irradiation heat-up investigations. They were two spheres from each of HFR-K3 (1 and 3) and FRJ2-K13 (2 and 4) respectively, and twenty-five spheres taken from the AVR. Not all heating tests have detailed data available, and only a selection of these tests is evaluated below.

Previously, fuel performance and ^{137}Cs release behaviour of HFR-K3/1 and /3, FRJ2-K13/2 and /4, as well as AVR 76/18 were evaluated [51]. Fuel failure and caesium release were modelled according to the Martin-Goodin-Nabielek model. It was recommended at the time that the study be expanded to include ^{110m}Ag and ^{85} Kr but this was never done.

Further work was done by Nabielek *et al*. on coated particles at temperatures up to 2 500 °C [52]. Their main conclusion was that at temperatures above 1 900 °C, thermal decomposition occurs very rapidly and all fission products including gases are released. For lower temperatures up to 1 700 °C, the SiC decomposition rates were negligible and coated particles preserve their ability to retain fission products. At temperatures above 1 700 °C, SiC becomes highly permeable to caesium, strontium and silver although gaseous fission products are still retained by the outer PyC layer. Further IMGA studies performed on coated particles from deconsolidated fuel spheres showed that at temperatures of 1 800 °C, very large fractions of caesium and other metallic fission products are released without necessarily observing fission gases release [53].

6.2.1 HFR-K3

The HFR-K3 irradiation test has been described in detail in paragraph 5.1. Two of the test spheres, 1 and 3 were selected for post-irradiation heat-up testing. The first sphere in the HFR-K3 experiment underwent post-irradiation heat-up testing at 1 600 °C for 500 hours. The ^{110m}Ag fractional release during the experiment is shown in Figure 19. The measured release curve appears very flat, as if a non-diffusion process has occurred. It was exactly this type of behaviour that gave rise to the MVR theory [8]. The IAEA current diffusion coefficient overestimates the release significantly, while the newly-derived diffusion coefficient is much closer. The strange non-diffusion curve is not replicated by either calculated curve, but at least the new diffusion coefficient describes measured release behaviour much better than currently accepted diffusion parameters.

The third test sphere of the HFR-K3 test underwent post-irradiation heat-up testing at 1 800 °C for 100 hours. After heat-up testing the test sphere was deconsolidated and caesium inventories of coated particles were measured with IMGA [53]. It was found that about 50% of coated particles analysed showed release of about 80% of ^{137}Cs inventory while the rest showed release of about 40% of ^{137}Cs inventory. Even though fission gas release suggests a modest fuel failure fraction, the majority of ‘unfailed’ particles released their metallic fission products. By using a ‘silver retention failure rate’ of 50% at the end of irradiation, the release curves of Figure 20 can be drawn.

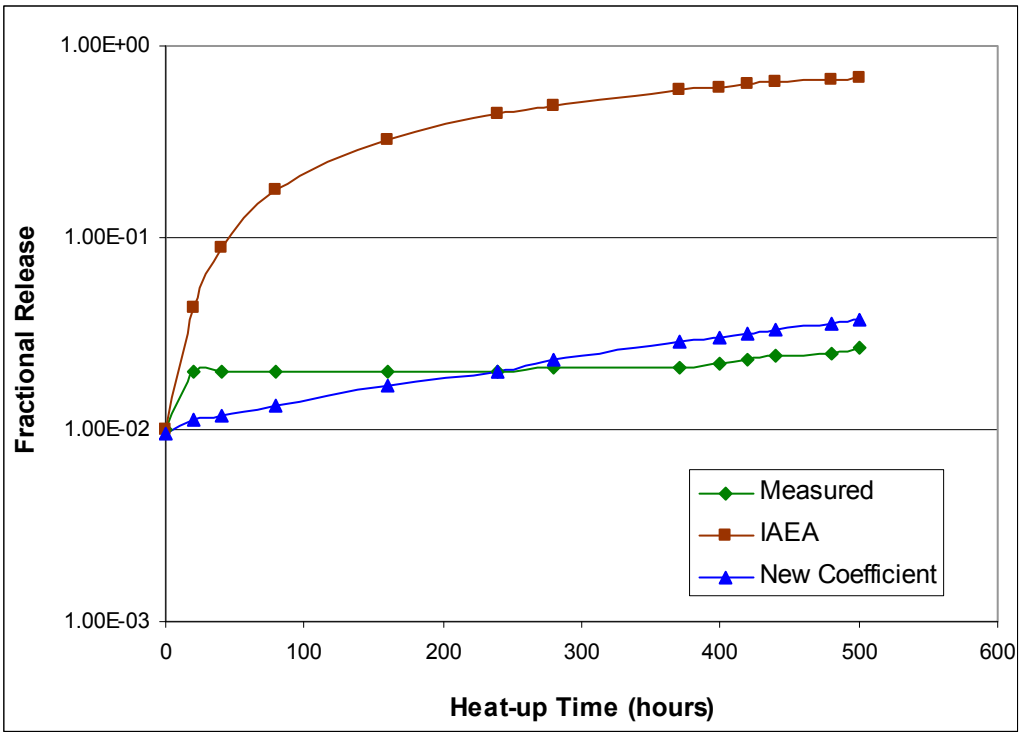

Figure 19: Silver Release during Heat-up of HFR-K3/1

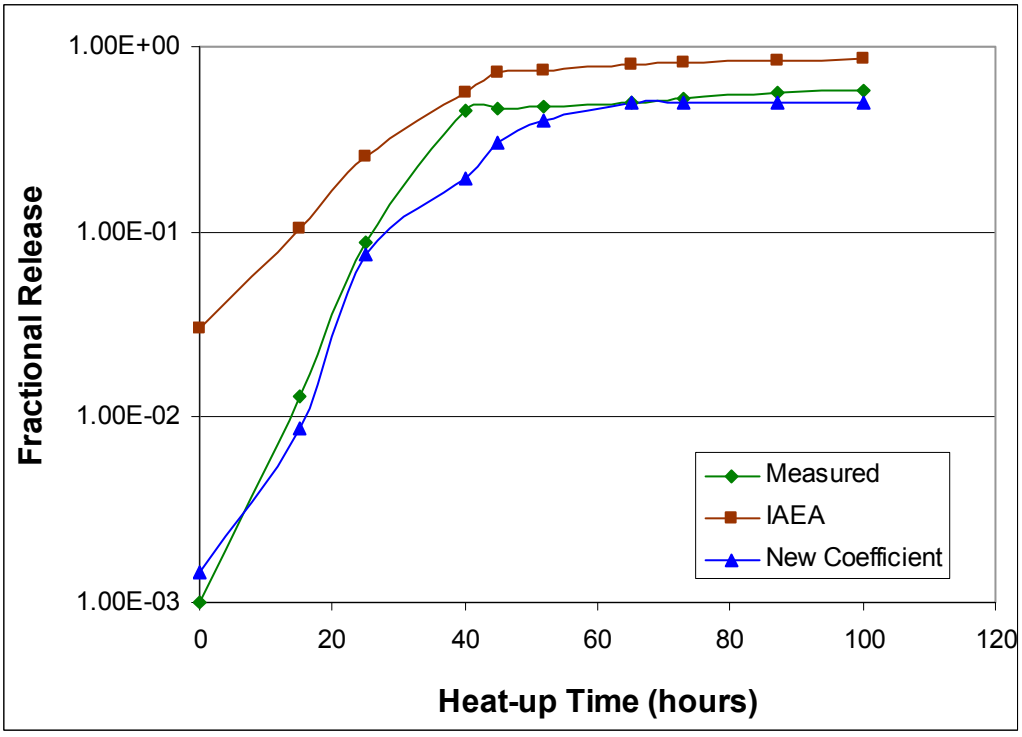

Figure 20: Silver Release during Heat-up of HFR-K3/3

6.2.2 FRJ2-K13

The FRJ2-K13 irradiation test was described in detail in paragraph 5.2. Two of the test spheres, 2 and 4, were selected for post-irradiation heat-up testing. The second sphere in the FRJ2-K13 irradiation test was heated for 138 hours at 1 600 °C. According to ^{85}Kr release during the heat-up test, no coated particles appeared to have failed. In Figure 21, the measured and calculated ^{110m}Ag fractional releases are plotted. Fractional release was calculated with both the existing IAEA diffusion coefficient and the newly-derived diffusion coefficient. Similar to the HFR-K3/1 1 600 °C heat-up test, the IAEA diffusion coefficient produces a very high fractional release. The new diffusion coefficient also over-predicts fractional release, but at the end of heating produces a final fractional release very close to the measured value.

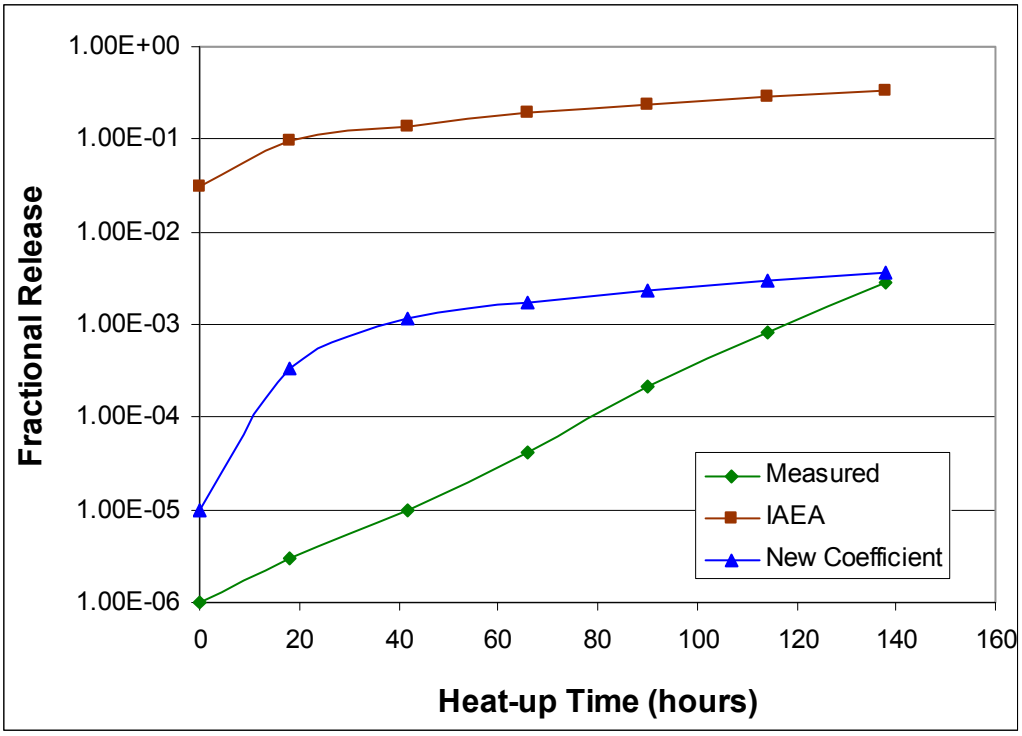

Figure 21: Silver Release during Heat-up of FRJ2-K13/2

The fourth sphere of the FRJ2-K13 test was subjected to 1 600 °C heating for 138 hours and then a further 100 hours at 1 800 °C. The 1 600 °C heating period produces results very similar to the 1 600 °C heating tests performed on the HFR-K3/1 and FRJ2-K13/2 test spheres.

The existing IAEA diffusion coefficient significantly over-predicts release for heating times less than about 140 hours, while the newly-derived diffusion coefficient also over-predicts release, but to a lesser extent. During the 1 800 °C heating period, the ^{85}Kr release increased a hundred-fold and caesium release by three orders of magnitude. Complete silver release was measured after 71 hours of heating at 1 800 °C. This curve could only be reproduced with the new diffusion curve if 100% failure (in terms of silver retention ability) is assumed. Fractional release curves are shown as before in Figure 22.

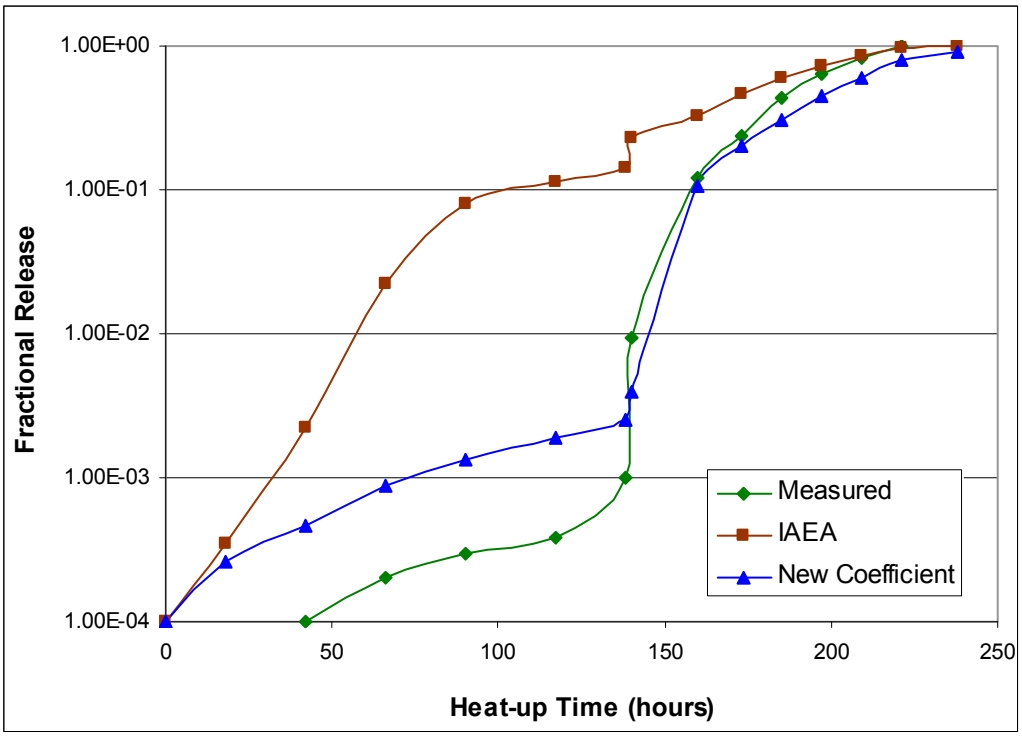

Figure 22: Silver Release during Heat-up of FRJ2-K13/4

6.2.3 AVR 74/11

Fuel sphere AVR 74/11 was irradiated in the AVR for approximately 850 full power days where it achieved a burn-up of 6.2% FIMA and a fast fluence of 1.6 x 10^{25} m^{-2} [25]. It contained 16 400 LEU-TRISO particles. After irradiation in the AVR, the fuel sphere was subjected to heat-up testing at 1 700 °C for 180 hours. ^{85}Kr fractional release measurements show no failure during irradiation or subsequent heating for the first 83 hours. After 89 hours of heating the ^{85}Kr fractional release measurement suggests a coated particle failure fraction of up to 9 x 10^{-4}.

The heat-up test's evaluation is presented in Figure 23. Even for the 1 700 °C case the current IAEA diffusion coefficient over-predicts the silver fractional release by an order of magnitude. The best estimate of the newly-derived diffusion coefficient is about a factor of three too low at the end of the heat-up test that still falls within the previously accepted uncertainty limits for ^{111}Ag release during loss of forced cooling accidents. To test this, the calculation was also performed with the upper limit of the newly-derived diffusion coefficient. The upper limit calculation matches the end of irradiation fractional release, which means that for this specific heat-up test, the newly-derived diffusion coefficient is still feasible.

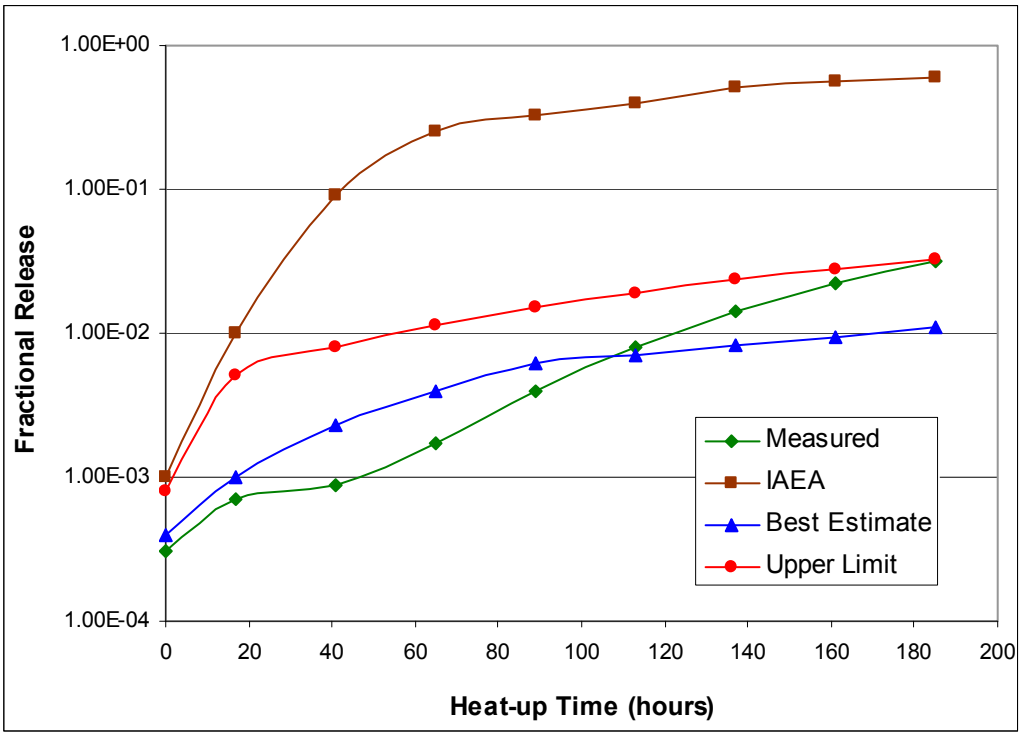

Figure 23: Silver Release during Heat-up of AVR 74/11

6.2.4 AVR 71/22

Fuel sphere AVR 71/22 was irradiated in the AVR for approximately 480 full power days where it achieved a burn-up of 3.5% FIMA and a fast fluence of 0.9 x 10^{25} m^{-2} [25]. It contained 16 400 LEU-TRISO particles. After irradiation in the AVR, the fuel sphere was subjected to heat-up testing at 1 600 °C for 500 hours. ^{85}Kr fractional release measurements show no failure during irradiation or subsequent heating.

The heat-up test's evaluation is presented in Figure 24. This is a relatively low burn-up fuel sphere and both diffusion models over-predicted fractional release significantly. This could be due to the fact that the irradiation history of the fuel sphere is not modelled correctly or that silver transport through the coating layers of a coated particle is more dependent on irradiation time and total burn-up than currently accepted. An irradiation history as recommended in the latest literature was used [55], but it could be that this fuel sphere spent most of its time in cooler regions in the core, and this sphere is then more representative of the average AVR core.

The newly-derived diffusion coefficient over-estimates measured fractional release consistently by an order of a magnitude and the IAEA diffusion coefficient by three orders of magnitude. In order to investigate whether this could be a burn-up induced phenomena, higher burn-up spheres heated up to similar temperature regimes have to be evaluated.

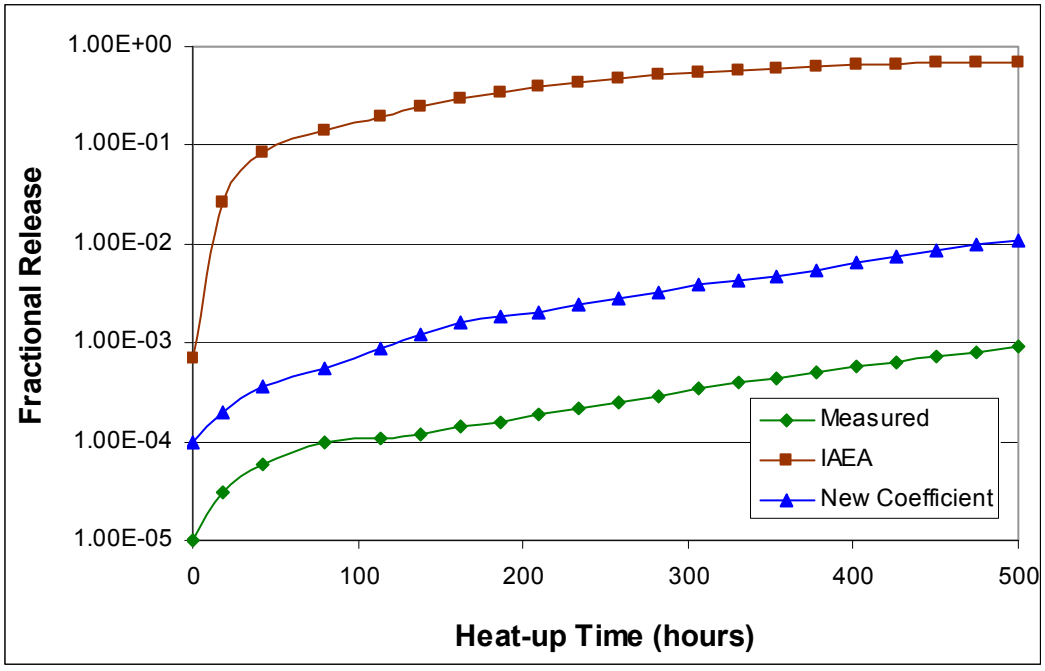

Figure 24: Silver Release during Heat-up of AVR 71/22

6.2.5 AVR 82/9

Fuel sphere AVR 82/9 was irradiated in the AVR for approximately 1 300 full power days where it achieved a burn-up of 8.9% FIMA and a fast fluence of 2.3 x 10^{25} m^{-2} [25]. It contained 16 400 LEU-TRISO particles. After irradiation in AVR, the fuel sphere was subjected to heat-up testing at 1 600 °C for 500 hours. ^{85}Kr fractional release measurements show no failure during post-irradiation heating.

The heat-up test's evaluation is presented in Figure 25. This is a relatively high burn-up fuel sphere and the IAEA diffusion coefficient over-predicts the fractional release significantly. The newly-derived diffusion coefficient calculation matches the measured fractional release very well. When comparing this evaluation with AVR 71/22, it appears as if the diffusion coefficient is irradiation-dependent. Since the newly-derived diffusion coefficient is based on high burn-up irradiation test results, it may be that silver release during the early part of a fuel sphere's irradiation life is over-estimated.

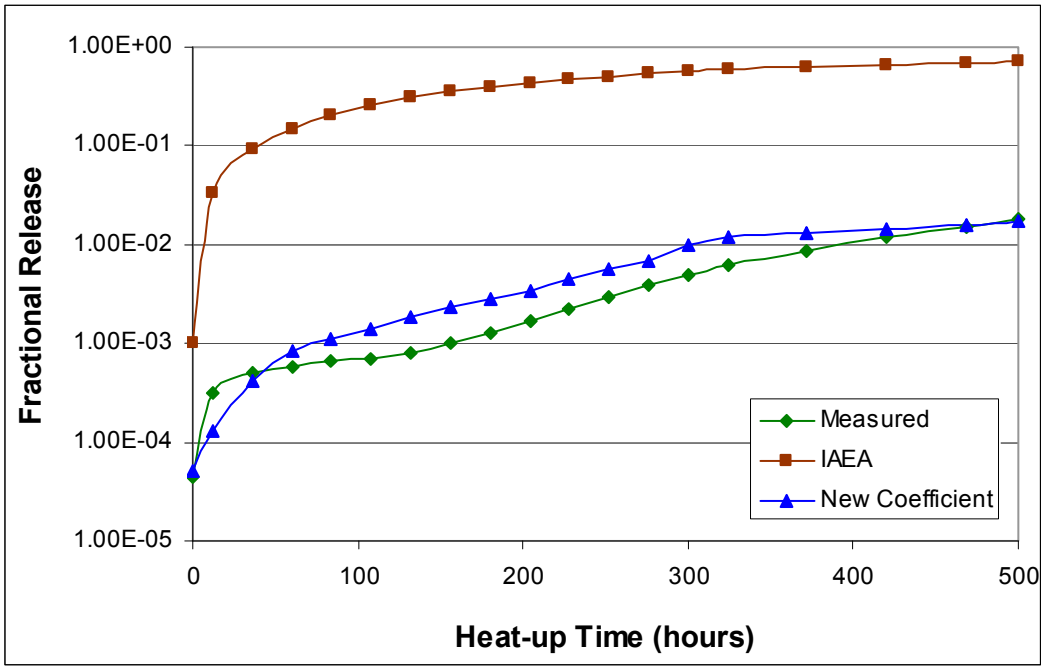

Figure 25: Silver Release during Isothermal Heating of AVR 82/9

6.2.6 AVR 90/5

After evaluating two 1 800 °C heat-up tests (HFR-K3/3, FRJ2-K13/4), which showed that for temperatures above 1 700 °C, metallic fission product release is dominated by SiC layer degradation and not by transport mechanisms through materials, and the only 1 700 °C (AVR-74/11) and several 1 600 °C heat-up tests at various burn-ups (HFR-K3/1, FRJ2-K13/2, AVR-71/22 and AVR-82/9), that showed that the new diffusion coefficient is applicable for temperatures up to 1 600 °C and possibly 1 700 °C, it is time to evaluate a complete loss of forced coolant (LOFC) accident test with the new diffusion coefficient.

Fuel sphere AVR 90/5 was irradiated in the AVR for approximately 1 400 full power days where it achieved a burn-up of 9.2% FIMA and a fast fluence of 2.5 x 10^{25} m^{-2} [28]. It contained 16 400 LEU-TRISO particles. After irradiation in the AVR, the fuel sphere was subjected to heat-up testing to simulate a 1 620 °C loss of forced coolant accident. The temperature was raised to 1 620 °C for 30 hours and then gradually cooled to 1 145 °C over a period of 270 hours. ^{85}Kr fractional release measurements show no failure during irradiation or subsequent heating. The heat-up test's evaluation is presented in Figure 26. The newly-derived diffusion coefficient calculation matches measured fractional release very well. This demonstrates that the new diffusion model will be quite sufficient to model possible ^{111}Ag releases during a loss of forced coolant accident.

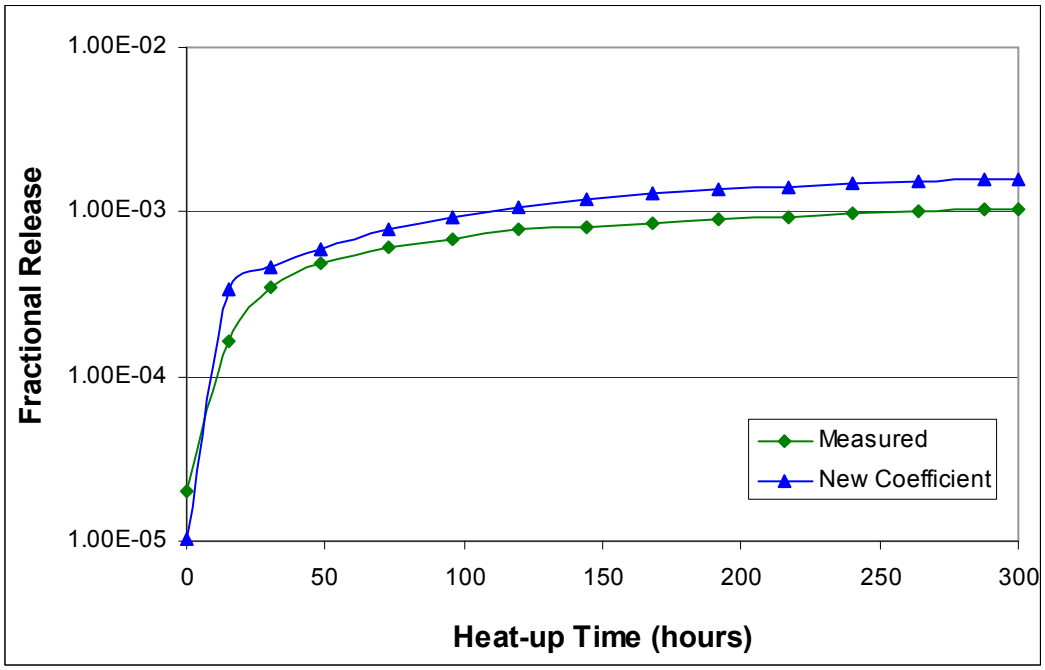

Figure 26: Silver Release LOFC Simulation of AVR 90/5

6.3 Discussion of Heat-up Tests

From the post-irradiation heat-up tests evaluated it is clear that the newly-derived diffusion coefficient may be used up to temperatures of 1 600 °C with confidence. Results for 1 600 °C heating tests tend to be slightly conservative which is acceptable for core analyses. Three high burn-up test spheres as well as spheres from AVR operation of burn-ups between 3.5% and 8.9% FIMA were evaluated. There appear to be some burn-up dependence on the transport of silver through SiC at 1 600 °C.

Silver release during the only 1 700 °C heating test evaluated appears to obey the new diffusion coefficient, however, it is difficult to judge based on only one test. All tests performed above 1 700 °C (1 800 °C) show massive silver release and can only be modelled by assuming that the vast majority of coated particles fail in terms of metallic fission product retention.

This is supported by an evaluation performed on IMGA results from HFR-K3/3 [54]. In this study it was attempted to explain the observed caesium inventories in each coated particle after irradiation and heat-up testing. Very high diffusion coefficients were suggested, which in practice for silver transport means completely permeable coated particle layers. This failure fraction (in terms of metallic fission product retention) cannot be measured by ^{85}Kr release and therefore existing fuel failure curves are not applicable for temperatures above 1 700 °C for metallic fission product release calculations. Unless future tests can prove the contrary, the retention of metallic fission products cannot be modelled by any other means than to accept complete release due to SiC degradation for temperatures above 1 700 °C.

7. Application in PBMR Core Analyses

It is important to understand how the new calculation model affects PBMR core analyses. The new model and parameters derived during this study are compared with current diffusion and alternative MVR models for a sample PBMR core design.

7.1 PBMR Core Model and Analyses

The core design is modelled by reactor analyses to present flow channels consisting of axial layers to form a number of core regions. A typical PBMR core is modelled with several (4 - 10) fuel sphere flow channels, each channel divided into axial layers (10 - 20), to yield 80 to 150 core regions. These core regions are used by core neutronics, thermohydraulic and fission product release codes to model core parameters. Each region is calculated separately to supply thermohydraulic (gas and fuel surface temperatures) and neutronic data (fast and thermal neutron fluxes as well as neutron capture cross sections) to the fission product release analyst.

These data sets are calculated by Very Superior Old Program (VSOP) and Monte Carlo N-particle Transport Code (MCNP) analyses and supplied through an interface document (e.g. [56]) to the fission product release analyst. Fuel passes through the core several times (4 – 16 times) to flatten the axial power profile. Core regions sizes are selected so that a fuel sphere takes an equal amount of time to travel through any core region. A typical PBMR core geometry is presented in Figure 27.

The model used to describe the fuel is explained in paragraph 1.1 and the models used to describe the transport process are explained in paragraphs 2.1 and 2.2 for diffusion and MVR respectively. Diffusion calculations were performed with the software product FIPREX [57] to determine the long-lived fission product release from fuel elements. The software product performs all pre-calculation data manipulation, creates GETTER input files and executes GETTER software. FIPREX then performs post-GETTER calculation data manipulation, delivering fission product release values (inventories, release rates and accumulated releases). The complete FIPREX model is available in the FIPREX theory description [58].

MVR calculations were performed with the VBIST software [8]. All input data (fuel parameters, temperatures, neutronics such as cross section and neutron fluxes, reactor parameters etc., from sources, e.g. [2], [10], [11], [27] and [56]) were entered into the input files. Best estimate calculations are performed with best available values.

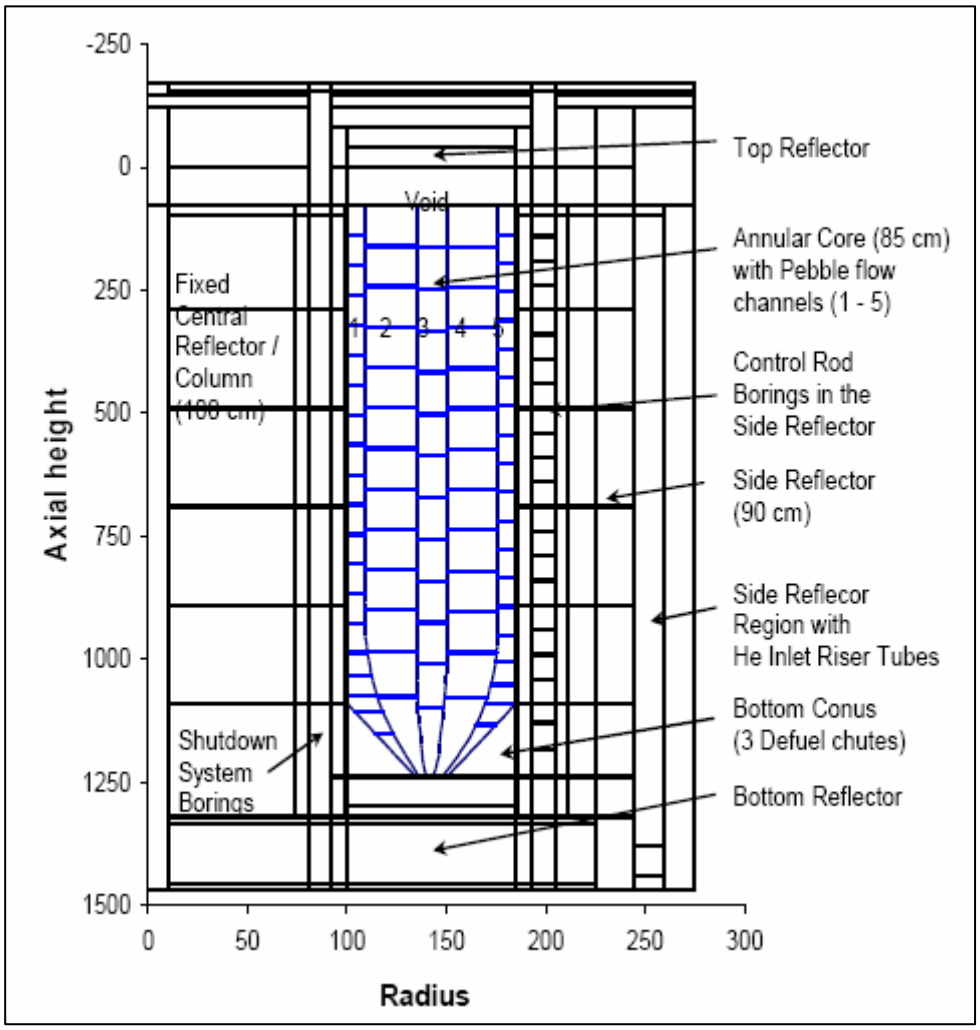

Figure 27: Sample PBMR VSOP Calculation Model Layout

Design values are determined through sensitivity analyses performed on all uncertain parameters. Design calculations presented in paragraph 7.2 are based on a stacked uncertainty analysis where all uncertain parameters are simply set to their design parameters and the calculation is performed. The same thermohydraulic and neutronic data set is used for all cases of each core analysed. GETTER calculates fission product release from one sphere for each time step throughout its residence time in the core. A fuel element spends one time step in each core region. Each fuel element's release history contributes to the total core release, so that the total core release is the average of all the core region releases over all time steps of the irradiation histories of all fuel elements. Furthermore, since the fission products in question are all long-lived, the fission product inventory, and therefore the release from a core region, is dependent on the irradiation history of the fuel elements in that core region.

This implies that GETTER must calculate release histories of all fuel elements in the core for all possible irradiation histories, since irradiation and temperature conditions in each core channel is different from all others. GETTER runs for all 400 000 fuel elements in the PBMR core will take an exorbitant amount of time. Furthermore, calculation of Depressurized Loss of Forced Cooling (DLOFC)-type accidents would be close to impossible since accidents can occur at any time step in a specific fuel element's irradiation history. Calculating such an accident would then require in the order of 35 million GETTER calculations to be performed. It is impossible to perform Monte Carlo-type parametric studies on this large number for all applicable nuclides.

To overcome these problems, the PBMR core's fission product release is calculated by selecting a representative set of fuel elements. This representative set is generated by randomly selecting a large number (~10 000) of individual fuel elements from the core. The average of releases from this selection is assumed to be a good representation of the calculated release from all the fuel elements. Analysing a selection twice the size of the original selection and comparing the average release rates easily verifies this assumption. The size of the selection depends on the accuracy required and the computation time available. The random fuel element set is selected by assigning a random core pass history based on the probability of a fuel element passing through the core in a specific core channel. The probability of a fuel element passing through the core in a specific core channel is dependent on the size of the core channel and the speed at which fuel elements pass through the core channel. Therefore, a specified number of fuel elements are selected with core pass histories randomly selected from the weighted core channel probability.

7.2 Silver Release from a PBMR Core

A sample PBMR core was analysed at 400 MW power and an outlet temperature of 900 °C. The same core design was also analysed at 300 MW and 500 MW power and outlet temperatures of 750 °C and 950 °C respectively. Steady state core release rates (atoms per second) and average fractional releases (for best estimate calculations) for the three cases are presented in Table 36, Table 37 and Table 38 for the different calculation models under consideration. These results are for illustration of the effect of different model assumptions only and should not be used for any other purpose or compared to any other analysis performed elsewhere. The 'Original German' model refers to the legacy model [13] inherited with the original GETTER software and utilizes IAEA Tecdoc 978 [2] parameters and values. This analysis of a 400 MW PBMR core has been reported in [59].

The 'MVR' results are taken from the original Olivier calculation described in [8]. The 'First Estimate' model is based on the material data evaluation of Chapter 3 and the irradiation test evaluation of paragraph 4.3.1. The 'Detailed Evaluation' analysis is based on the final detailed evaluation of all applicable German fuel sphere irradiation tests described in paragraph 5. MVR analyses have not been performed for the 500 MW case, but are expected to predict considerably lower release rates than any of the diffusion models. Since the 500 MW study was only a conceptual study [60], only best estimate analyses were performed.

Table 36: Comparison of Calculated ^{110m}Ag Releases from a 400 MW PBMR Core

	Fractional Release	Best Estimate	Design Limit
Original German	8.90×10^{-4}	8.12×10^{11}	1.22×10^{13}
MVR	2.60×10^{-3}	3.24×10^{12}	1.50×10^{13}
First Estimate	9.73×10^{-4}	9.18×10^{11}	8.95×10^{12}
Detailed Evaluation	6.03×10^{-4}	4.30×10^{11}	3.90×10^{12}

Table 37: Comparison of Calculated ^{110m}Ag Releases from a 300 MW PBMR Core

	Fractional Release	Best Estimate	Design Limit
Original German	6.86×10^{-5}	1.30×10^{10}	2.84×10^{10}
MVR	3.02×10^{-4}	8.10×10^{10}	4.80×10^{11}
First Estimate	1.67×10^{-4}	3.45×10^{10}	2.67×10^{11}
Detailed Evaluation	7.24×10^{-5}	1.35×10^{10}	7.23×10^{10}

Table 38: Comparison of Calculated ^{110m}Ag Releases from a 500 MW PBMR Core

Atoms/s	Fractional Release	Best Estimate
Original German	6.46×10^{-3}	1.90×10^{13}
First Estimate	2.07×10^{-3}	2.59×10^{12}
Detailed Evaluation	2.29×10^{-3}	3.17×10^{12}

7.3 Effect on PBMR Core Analyses Discussion

As can be seen from the tables in paragraph 7.2, differences between the considered calculation models are relatively small. For the 400 MW design, the biggest difference between core release rates is only a factor of seven for best estimate and a factor of four for design limit analyses (between MVR and Detailed evaluation in both cases). There is almost no difference between the diffusion models. Considering that uncertainty factors of up to 20 have been suggested and used in the past [21], the differences are acceptable. The main reason for this is that the fuel temperatures for this specific core design and an outlet gas temperature of 900 °C lie primarily between 900 °C and 1 100 °C. As can be seen in Figure 28 the three considered diffusion coefficients converge in this temperature regime and the differences in silver transport rated through SiC is small.

For the 300 MW case the differences are similarly very small, but in this case it is because the fuel temperatures are simply too low. Fuel temperatures of a 300 MW power and 750 °C coolant outlet design lie between 700 °C and 900 °C and silver transport through the SiC layers is too slow. Releases at these temperatures are generally from matrix material contamination and failed particles. The controlling transport mechanism in this case is diffusion through the matrix material.

The 500 MW core, on the other hand, has significant differences between the different calculation models. The original German parameters predict a higher release rate compared to the two diffusion coefficients derived in this study. Fuel temperatures are high enough that silver transport through SiC dominates the source term.

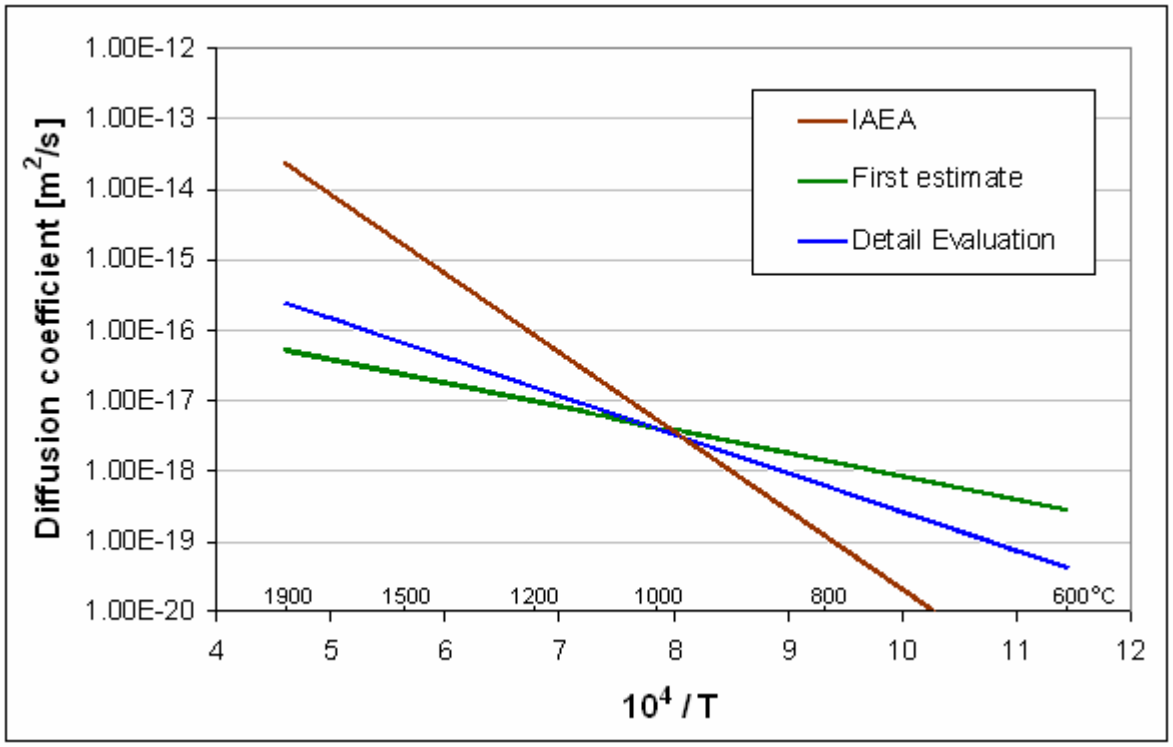

Figure 28: Comparison of the Three Considered Diffusion Coefficients

8. Conclusions

Release of silver fission and activation products from fuel contamination and failed particles are only of importance at low temperatures when the radiological impact of ^{110m}Ag on maintenance is small (< 700 °C). At higher temperatures, intact coated particles release dominates, with the SiC layer being the main retarding layer. Modelling of silver transport through SiC is therefore most important in the analyses of silver release from a planned high-temperature reactor. Material tests and irradiation experiments on coated particles have not been able to clearly identify the exact transport mechanism. Historically the approach was to use 'effective diffusion coefficients' in a diffusion model, but this appears to lead to overestimates at very high temperatures (> 1 100 °C) and possible underestimates in the critical 800 °C – 1 100 °C region.

Other mechanisms have been proposed, the most promising being Molecular Vapour Transport Release (MVR). From a modelling perspective, the best way forward appeared to ignore the exact mechanism and focused on deriving an 'effective transport model' based on all irradiation test (integral effects) and material experiment (separate effect) data. Even though transport through the SiC layer has been identified as the dominating phenomenon, any other transport process has to be quantified as best as possible to ensure that analyses of irradiation tests would provide the best possible SiC transport model and parameters.

Available material tests that would investigate each phenomenon separately were evaluated and current models and parameters used were confirmed or updated. Simplified sorption isotherms for silver from graphitic matrix material was derived for the first time from the limited material tests by using a caesium benchmark for the same test conditions. Matrix material diffusion coefficients were confirmed for best estimate analyses and design limit coefficients have been suggested based on diffusion coefficients for original and irradiated matrix material. Diffusion coefficients for fuel kernel and PyC layers were confirmed. Due to rapid transport through these materials, the recoil effects from UO_2 fuel and contaminations in PyC layers and matrix materials are negligible and are only modelled for the sake of completeness.

Material test data for silver transport in SiC show erratic results which lead to both high and extremely low diffusion coefficients or new contradicting mechanisms. An accurate PBMR model to analyse silver release from a high-temperature core that could be defended using all available test results was required. Two calculation models were identified and first estimate evaluations of the applicable German irradiation tests were performed for both MVR (12

tests) and diffusion (31 tests) models. It was shown that a carefully selected set of diffusion constants can in principle simulate irradiation tests results. Diffusion theory was shown to remain a viable option to model transport of silver.

Based on first estimate results and all material test evaluations, detailed analyses of all applicable irradiation tests were performed. Diffusion coefficients for silver in SiC were derived for both best estimate predictions and design limit analyses. It was found that the newly derived diffusion coefficients for each test were below the current IAEA recommended diffusion coefficient line, which in turn is based on experimental work performed on fuel manufactured before 1978. Detailed evaluations performed during this study are primarily based on fuel manufactured after 1980. The differences between the existing IAEA diffusion coefficient and the newly derived diffusion coefficients could be due to improvements in SiC manufacture that enhanced silver retention.

Heat-up tests of fuel elements irradiated during fuel tests and fuel elements from AVR operation were evaluated in order to justify the range of temperatures where the newly derived diffusion coefficients are applicable. It was found that the new diffusion coefficients are valid for temperatures from 800 °C up to 1 600 °C and may be used for accident analyses up to 1 700 °C. Above 1 700 °C it appears that major particle failure (with respect to silver retention) occurs and the new models should not be used at temperatures above 1 700 °C.

Existing and newly derived diffusion coefficients as well as the MVR model were applied to a sample PBMR core model at 300 MW, 400 MW and 500 MW power with reactor outlet coolant gas temperatures of 750 °C, 900 °C and 950 °C respectively. It was found that only under the high temperature and power conditions are there significant differences between the release rates of ^{110m}Ag calculated by the different models.

9. Recommendations

It is recommended that the transport parameters suggested in Chapter 3 and the diffusion model and diffusion coefficients derived in Chapter 5 be used for future core analyses until new data from fuel qualification programs become available. The applicable temperature range for these new diffusion coefficients lie between 800 °C and 1 700 °C. For temperatures above 1 700 °C coated particle failure due to SiC degradation become the dominant source term contributor and diffusion coefficients cannot be effectively evaluated. For temperatures below 800 °C, transport through PyC layers is slow enough that it does not matter which diffusion coefficient is used for SiC.

Differences between MVR and the new diffusion-based calculation model are relatively small and will be reduced even further if sorption is included in the MVR model. The MVR model must not be discarded though. In future it may be shown through fuel characterization efforts, that silver is transported by a physical process that could be modelled by MVR. The MVR model can then be further developed and used in reactor analyses. The main problem with the MVR model is absence of any reported nanotubes in polycrystalline SiC making the relatively good correlation with the experimental data fortuitous. In the meantime, the diffusion model and parameters derived in this study should be used.

Important lessons regarding the design, execution and evaluation of fuel irradiation tests were learned during this study:

a. The irradiation conditions (temperature, neutron fluxes and burn-up) are important considerations to ensure that realistic core conditions are achieved, and also to produce a range of conditions to evaluate fuel performance through the whole envelope of expected core conditions. It is therefore recommended that fuel spheres are irradiated at temperatures not exceeding 1 200 °C. However, it is also important to evaluate fuel performance at lower temperatures. Therefore irradiation temperatures in the range of 900 -1 100 °C should be considered for some later fuel irradiation tests.

b. The irradiation rig design and placement of irradiation monitors and thermocouples are very important. In all irradiation tests, thermocouple failure is a major problem that influences the accuracy of measurements and even ended some tests prematurely. Only the highest quality thermocouples should be used and the test should be designed to ensure that thermocouple failure remains a minimum.

c. At the end of the German fuel programme, data were not recorded rigorously and a lot of important information from irradiation tests was lost. Similarly, older progress reports and data sets were not stored properly and a lot of information disappeared. For PBMR's own irradiation programme it is vital that all data from irradiation tests are recorded at the end of each irradiation period and evaluated. In this way, discrepancies can be identified and resolved while the current personnel involved are still available.

d. Especially for lower-temperature irradiation tests (mean fuel temperature <1 100 °C) the natural uranium, thorium and silver contamination in the irradiation rig materials dominate the measured ^{110m}Ag activity on rig materials. Determination of transport parameters and evaluation of fuel performance then becomes very complicated and uncertain. Only in one irradiation facility was the natural silver contamination measured for only one of the rig materials. It is therefore critical that all the rig materials are assayed for their uranium, thorium and silver content, as well as any other contamination that might influence the irradiation test results.

e. The natural silver contamination of fuel matrix material is currently not specified. It appears that the natural silver contamination could be the dominant source term for the PBMR core under lower power and temperature conditions. For pre-1980 fuel, German references suggest 2.7 ng/g as a maximum silver contamination level for A3-27 matrix material. For post-1980 fuel a lower value 0.8 ng/g is suggested. For future best estimate analyses it is recommended to use the higher value of 2.7 ng/g. As design limit the actual detection limit results measured on A3-3 matrix material should be used up until such time the actual silver contamination level on PBMR materials can be measured.

Mean fuel irradiation temperatures should not exceed 1 200 °C as subsequent heat-up tests to 1 600 °C may release significant amounts of silver. Should mean fuel temperatures remain below 1 200 °C, 1 600 °C accident events appear feasible. However, accident temperatures above 1 700 °C are not acceptable. All heat-up tests above 1 700 °C show massive SiC degradation failure regarding silver retention. Only one 1 700 °C heat-up test was evaluated in this study, so it cannot be commented if 1 700 °C is an acceptable accident temperature at this stage and should be investigated during PBMR's own fuel qualification programme.

10. References

[1] H Nabielek, P E Brown and P Offerman, "Silver Release from Coated Particle Fuel", Journal of Nuclear Technology, Vol. 35 p. 483-493, September 1977.

[2] K Verfondern *et al*., "Fuel Performance and Fission Product Behaviour in Gas Cooled Reactors", IAEA-TECDOC-978, November 1997.

[3] W Amian and D Stöver, "Diffusion of Silver and Cesium in Silicon-Carbide Coatings of Fuel Particles for High-Temperature Gas-Cooled Reactors", Journal of Nuclear Technology, Vol. 61 p. 475, June 1983.

[4] P E Brown and R L Faircloth, "Metal Fission Product Behavior in High Temperature Reactors – UO2 Coated Particle Fuel", Journal of Nuclear Materials, Vol. 59 pp. 29-41, 1976.

[5] H J Maclean and R G Ballinger, "Silver Ion Implantation and Annealing in CVD Silicon Carbide: The Effect of Temperature on Silver Migration", 2nd International Meeting on High Temperature Reactor Technology, Beijing, China, September 2004.

[6] H J Maclean, "Silver Transport in CVD Silicon Carbide", PhD thesis, MIT, 2004.

[7] J J van der Merwe, "Mitigating the Silver Risk", PBMR report 047585, 2006.

[8] L D Olivier, "PBMR 400 MW Core: Ag-110m MPS Source Term", ESKOM Technical Note 2006/001-ST, October 2006.

[9] G H Lohnert *et al*., "The Fuel Element of the HTR-Module, a Prerequisite of an Inherently Safe Reactor", Nuclear Engineering and Design, Vol 109 pp. 257-263, October 1988.

[10] J H Venter, "Fuel: Design Bases Report" PBMR report 025140, 2005.

[11] J H Venter, "Fuel: Coated Particle Failure Fraction Report" PBMR report 026264, 2005.

[12] J J van der Merwe, "Metallic Fission Product Release Calculation Model", PBMR report T000239, 2008.

[13] K Röllig, "Rechenprogram GETTER", HRB report GBRA 052 477, 2001.

[14] J B Keshaw, "GETTER Theory Description Report", PBMR report 026755, November 2006.

[15] HBK, "HBK Quarterly Report", HBK IV, 1981.

[16] K Hilpert *et al*., "Sorption of Cesium and its Vaporization from Graphitic Materials at High Temperatures", High Temperatures - High Pressures, Vol. 20, pp. 157-164, March 1988.

[17] J Kwasny *et al*., "Cäsium-Sorptionsuntersuchungen an graphitischen Reaktorwerk-stoffen", Jül-2353, April 1990.

[18] E Hoinkis and D Stritzke, "Desorption of Cesium and Silver from a Graphitic Matrix Surface" from "Transport of fission products in matrix and graphite". Hahn-Meitner-Institut für Kernforschung B372, June 1983.

[19] E Hoinkis, "The Determination of Diffusion Coefficients of Cesium and Silver by the Release Method in As-received, Oxidized and Neutron Irradiated Graphitic Matrix" from "Transport of fission products in matrix and graphite". Hahn-Meitner-Institut für Kernforschung B372, June 1983.

[20] E Hoinkis, "The Diffusion of Silver in the Graphitic Matrices of A3-3 and A3-27", Journal of Nuclear Materials, Vol 209, p. 132-147, 1994.

[21] K Röllig, "PBMR Core Release Rates of Metallic Fission Products: Derivation of Design Values", HRB report, GBRA 058 345, 2001.

[22] D Petti *et al*., "Development of Improved Models and Designs for Coated-Particle Gas Reactor Fuels", INEEL/EXT-05-02615, December 2004.

[23] J B Keshaw, "Silver Fission Product Release: Experiments for Model Evaluation", PBMR report 080881, 2008.

[24] J J vd Merwe and L D Olivier, "Modelling Silver: Evaluation of German Experience", 4th International Meeting on High Temperature Reactor Technology, Washington D.C., USA, October 2008.

[25] R Gontard and H Nabielek, "Performance Evaluation of Modern HTR TRISO Fuels", HTA-IB-05/90, July 1990.

[26] R Christ, "Spaltproduktfreisetzung bei HFR-K3", HRB Report GHRA 001343, August 1985.

[27] F Albornoz, "MCNP Neutron Fluxes and Cross Sections for Fission Product Release Calculations", PBMR report T000172, 2007.

[28] H J Hantke, "Performance of High Quality HTR-LEU Fuel Elements with TRISO Coated Particles - A Summary Report", HTA-IB-7/92, December 1992.

[29] R Gontard, B Hürttlen and A W Mehner, "Vorbestrahlungsbericht für die Experimente HFR-K3 und FRJ2-K13", HBK-IB-4/82, June 1982.

[30] R W A Kraakman and W P Voorbraak, "Neutron Metrology in the HFR - D138.03 Irradiation of Fuel Spheres", ECN-84-122, August 1984.

[31] J J van der Merwe, "Development and Validation of Fission Product Release Models and Software at PBMR", 2nd International Meeting on High Temperature Reactor Technology, Beijing, China, September 2004.

[32] J H Venter, "Fuel: HFR-K3 Recalculation Report", PBMR report 100575, January 2007.

[33] A Marmier *et al*., "Preliminary Results of the HFR-EU1 Fuel Irradiation of INET and AVR Pebbles in the HFR Petten", 4th International Meeting on High Temperature Reactor Technology, Washington D.C., USA, October 2008.

[34] J J van der Merwe, "Verification and Validation of the PBMR Models and Codes used to Predict Gaseous Fission Product Releases from Spherical Fuel Elements", MSc Thesis, RAU, February 2004.

[35] G Pott, B Hürttlen and G Borchardt, "Experiment FRJ2-K13: Bestrahlungsbericht", KFA Technical Note IRW-TN-92/85, October 1985.

[36] R Gontard, H Nabielek and L Thöne, "Vorbestrahlungsbericht für das Experiment FRJ2-K15", HBK-IB-10/86, August 1986

[37] H Nabielek *et al*., "Development of Advanced HTR Fuel Elements", Nuclear Engineering and Design, Vol. 121, p199-210, 1990

[38] R Schröder, W Kühnlein and H Dahmen, "FRJ2-K15: Gammaspektrometrie an Brennelementen und Kalotten. Nachrechnung des Spaltproduktinventars", FZJ Technical Note 15/94, 1994.

[39] R Acharya, "Analyses of R2-K12 Irradiation Experiment", GA report 906636, September 1983.

[40] B F Myers and H Nabielek, "Freizetzung fester Spaltprodukte aus HEU-partikeln", HBK-TN-1/83, 1983.

[41] KFA, "PROJEKTBERICHT 1981", KFA-HBK-IB-1/81, 1981.

[42] KFA, " PROJEKTBERICHT 1979", KFA-HBK-IB-1/79, 1979.

[43] KFA, " PROJEKTBERICHT 1980", KFA-HBK-IB-1/80, 1980.

[44] KFA, " PROJEKTBERICHT 1982", KFA-HBK-IB-1/82, 1982.

[45] B Hürttlen, "Bestrahlungsdaten FRJ2-K11", KFA Technical Note, IRW-Vorgang-0534, August 1980.

[46] P E Brown, A J Inns, "Post-Irradiation Examination of Spherical Fuel Elements from Irradiation Experiments FRJ2-K10 and K11", AERE-G.2240, December 1981.

[47] H Nabielek, "Caesium freizetzung bei AVR-brennelementtemperaturen zwisch 1400 un 1600 °C", HBK-IN-4/86, 1986.

[48] W Amian, "Experimental Investigations on the Migrational Behavior of Silver in Coated Particle Fuel for High Temperature Reactors", KFA-Jül-1731, 1981.

[49] E Toscano, "Post-Irradiation Examination of High Temperature Reactor Fuel Elements", HTR-PIE course, NECSA, 2008.

[50] W Schenk, A Naoumidis and H Nickel, "The Behaviour of Spherical HTR Fuel Elements under Accident Conditions", Journal of Nuclear Materials, Vol. 124, pp. 25 - 32, 1984.

[51] J L Martin and H Nabielek, "Modelling of Fuel Element Heating Tests", HBK Technical Note TN-4/88, 1988.

[52] H Nabielek *et al.*, "The Performance of HTR Fuel Particles at Extreme Temperatures", HBK Technical Note TN-3/88, 1988.

[53] C A Baldwin, M J Kania, "Fission Product Retention in TRISO Coated UO2 Particle Fuels Subjected to HTR Simulated Core Heating Tests", IAEA Specialist Meeting on Behaviour of Gas Cooled Reactor Fuel under Accident Conditions, Oak Ridge, Tennessee, 1990.

[54] K Verfondern, "Possible Explanation for HFR-K3/3 IMGA Results", ORNL/M-2248, 1992.

[55] H Nabielek, K Verfondern and M Kania, "Fuel and Fission Products in the Jülich AVR Pebble-Bed Reactor", 4th International Meeting on High Temperature Reactor Technology, Washington D.C., USA, October 2008.

[56] F Reitsma, "Neutronic and Temperature Data for Fission Product Release Analysis during Normal Operation", PBMR report 008310, 2005.

[57] J J van der Merwe and I D Clifford, "Development of the FIPREX-GETTER Calculation Model and its Application at PBMR", 3rd International Meeting on High Temperature Reactor Technology, Johannesburg, South Africa, October 2006.

[58] I D Clifford and J J van der Merwe, "FIPREX Theory Description", PBMR report 032442, July 2006.

[59] J J van der Merwe, "Metallic Fission Product Release from the 400 MW PBMR Core", PBMR report T000140, November 2007.

[60] J J van der Merwe, "Scoping Fission Product Source Term for NGNP", PBMR report T001099, February 2008.